Presynaptic Anchoring of PKA by AKAP7 is Required for Pattern Separation by Dentate Gyrus

Jennifer Dezet Deem

A dissertation
submitted in partial fulfillment of the
requirements for the degree of

Doctor of Philosophy

University of Washington

2016

Reading Committee:
G. Stanley McKnight, Chair
Larry S. Zweifel
Robert Steiner

Program Authorized to Offer Degree:
Pharmacology

University of Washington

Abstract

Presynaptic Anchoring of PKA by AKAP7 is Required for Pattern Separation by Dentate Gyrus

Jennifer Dezet Deem

Chair of the Supervisory Committee:
Professor G. Stanley McKnight
Pharmacology

The intracellular signaling molecule, 3',5'-cyclic adenosine monophosphate (cAMP), is produced by a cell in response to a physiological signal. A derivative of adenosine triphosphate (ATP), cAMP is produced by adenylate cyclases (ACs) localized either to the plasma membrane (insoluble) or cytosol (soluble) and degraded by phosphodiesterases (PDEs) into adenosine monophosphate (AMP) and a phosphate group. Between its production and degradation, cAMP directly activates protein kinase A (PKA), cyclic nucleotide-gated ion channels, and exchange protein directly activated by cAMP (Epac). The activation of PKA is the dominant result of cAMP production. Since the discovery of PKA nearly fifty years ago, phosphorylation provided by PKA has been found to affect protein activity, interaction, localization, and conformation. These PKA mediated events have larger demonstrated roles in cell metabolism, migration, morphology, division, differentiation, activation, transcription and translation. Further, when PKA signaling is impaired, host behavior and health may be affected. The anchoring of PKA and other signaling and structural proteins by A-Kinase anchoring proteins (AKAPs) coordinates precise subcellular and temporally regulated activities while also sequestering aberrant PKA activity.

In the hippocampus, enhanced plasticity between different neuronal populations, or long term potentiation (LTP), is considered the physiological manifestation of memory. The dentate gyrus (DG) receives cortical input from the entorhinal cortex and sends mossy fiber (MF) projections to the CA3 region of the hippocampus. The DG is thought to be responsible for processing and encoding distinct contextual associations in response to highly similar events/experiences, allowing behavioral discrimination. However, the cellular processes underlying this form of learning, known as pattern separation, are poorly understood. Here we demonstrate an essential role for presynaptic AKAP7 in anchoring PKA-RIIβ in MF axons and terminals. Mice with a DG-specific ablation of AKAP7 are selectively deficient in pattern separation but exhibit normal contextual learning and memory, suggesting a link between DG-dependent behaviors and the presynaptic anchoring of PKA by AKAP7. Moreover, genetic ablation of AKAP7 results in a loss of presynaptic and cAMP/PKA-dependent MF-CA3 long-term

potentiation directly initiated by adenylyl cyclase activation without affecting tetanus-induced LTP in this pathway.

DEDICATION

-To the love of my life, Steve, for his unconditional love, friendship, and support.

-To my wonderful kids, who have grown so much over the years, may you continue to be amazing!

-And, to Lisa, the best, happiest, most beautiful person I have ever known.

ACKNOWLEDGEMENTS

I would like to express my sincere appreciation to my advisor, Stan McKnight, and the members of my thesis committee for their guidance and mentoring. I would also like to acknowledge Drs. John Scott, Richard Gardner, and Richard Palmiter, who, although not on my committee, volunteered their time to provide mentoring, guidance, and support. I would also like to thank my fellow lab members including Merle Gilbert, Brian Jones, Linghai Yang, Paul Amieux, and Eli Sanz for their camaraderie over the years. Above all, I would like to thank my family for their patience, love, and support.

TABLE OF CONTENTS

CHAPTER 1: INTRODUCTION

1.1 Historical Perspective

The cell is the building block of life and within it is the capacity to replicate, communicate, and transform. Biology has provided the cell with a coherent and coordinated system for responding to unique environmental cues to induce corresponding cascades of intracellular activity including genetic, metabolic, and morphological changes. The general term used to describe the biochemical chain of events resulting from external effectors is “signal transduction.” Links in this biochemical chain include phosphorylation events provided by protein kinase A (PKA) activated by 3', 5'-cyclic adenosine monophosphate (cAMP). Phosphorylation is the transfer of a phosphate moiety from adenosine triphosphate (ATP) to an amino acid residue. The addition of the phosphate group may alter the activity, interaction, and/or conformation of the substrate. The discovery of the molecule cAMP (Sutherland & Rall 1958) and protein kinase A (PKA) (Walsh et al. 1968)provided critical building blocks for the field of signal transduction and kinase activity.

In the late 1960s, nearly ten years after the discovery of cAMP, the Krebs laboratory found the transfer of a phosphate group from ATP to isolated casein and protamine and another enzyme, phosphorylase kinase, was dependent upon a kinase bound to cAMP (Walsh et al. 1968). The importance of this discovery was made clear as numerous scientific studies began to define PKA as a commonly expressed kinase with broad specificity for protein substrates including enzymes (Kumon et al. 1970). Additional studies separated PKA into two types based upon their elution and their relative requirement for cAMP to induce activity. Type I, named as such because it eluted first, required 3×10^{-8} M cAMP for activation, twice the concentration required to activate Type II (Reimann, Walsh, et al. 1971). By utilizing the relative activation differences of PKA Type I and II (Reimann, Walsh, et al. 1971), it was then possible to characterize Type I as soluble, or associated with the cytoplasm, and Type II as particulate and associated with membrane structures (Corbin et al. 1977).

Further studies by the Krebs lab separated the catalytic (C) and regulatory (R) subunits by affinity chromatography and demonstrated the catalytic subunit for PKA needed to dissociate from the regulatory subunit it was bound to in order to function (Reimann, Brostrom, et al. 1971). Modulation of PKA–mediated activities was further clarified by the separation of PKA into multiple catalytic and regulatory isoforms

(Uhler, Chrivia, et al. 1986; Clegg et al. 1988; Scott et al. 1987). The investigation of each isoform, including their relative importance and contribution, has been advanced by the development of mouse models of PKA isoform-specific gene disruption.

The role of PKA as a modifier of protein localization, interaction, and activity is enhanced when PKA is localized near the proteins it interacts with. A-Kinase anchoring proteins (AKAPs) act to anchor PKA to the cell membrane where they have increased access to other membrane-bound proteins. Discovered in the 1980s, AKAPs were a contaminant in experiments designed to isolate the PKA regulatory subunit,

RIIβ, from brain homogenates. Not surprisingly, the first AKAP identified was microtubule associated protein-2 (MAP2), a highly expressed AKAP localized to dendritic shafts (Theurkauf & Vallee 1982). The significance of anchored PKA has been demonstrated in ion channel potentiation (Fraser & Scott 1999), spindle formation during cell division (Hehnly et al. 2015), excitation-contraction coupling, mitochondrial function, and the regulation of both the actin and microtubule components of cytoskeleton formation and stabilization (Welch et al. 2010). AKAPs also provide anchoring for other signaling enzymes and structural proteins including phosphodiesterases (PDEs), other kinases, phosphatases, actin, microtubules, and ion channels (Langeberg & Scott 2015).

1.2 The Structure of PKA

The PKA holoenzyme exists as a heterotetramer of two regulatory (R) and two catalytic (C) subunits. The catalytic subunit has three isoforms: Cα (Uhler, Carmichael, et al. 1986), Cβ (Uhler, Chrivia, et al. 1986), and Cγ (Beebe et al. 1992), with splice variants thought to provide additional levels of control (Banday et al. 2013). Cα is expressed ubiquitously while Cβ is expressed predominantly in the brain (Uhler, Chrivia, et al. 1986). Very little is known about Cγ and it is thought to be a retrotransposon derived from Cα (Reinton et al. 1998). The regulatory subunit has two isoforms, RI (D. C. Lee et al. 1983) and RII (Scott et al. 1987), divided further into subtypes, α and β. RIα and RIIα are ubiquitously expressed while R1β and RIIβ have preferential expression in the brain. While both RIIα and RIIβ are expressed in the brain, RIIα is expressed ubiquitously while RIIβ demonstrates tissue specific expression patterns (Clegg et al. 1988; Cadd & McKnight 1989).

Each regulatory subunit contains the same complement of domains. The docking and dimerization domain (D/D) is located at the N-terminus and is either 45 (RI isoforms) or 61 (RII isoforms) amino acids in length. The domain resolves into a three-dimensional four helical bundle (Taylor et al. 2013). The domain contains residues important for the dimerization of the two regulatory subunits and the docking of the regulatory subunit to an amphipathic helix found on A-kinase anchoring proteins (AKAPs) (Herberg et al. 2000). These anchoring proteins tether PKA near a specific substrate and/or location, providing tight temporal control over localized PKA kinase activity (Scott et al. 2013).

An inhibitor domain, flanked by two intrinsically disordered regions, the N- and C-linkers, follows the D/D domain. The level of disorder in the linker regions is dependent upon catalytic subunit binding, with order increasing when a catalytic subunit is bound (Taylor et al. 2004). The inhibitor site is remarkably short, five AAs in length. Its role is one of the defining differences between RI and RII isoforms. In inactive RII isoforms, the inhibitor site is a substrate for the catalytic domain at the serine 113 (S113) and is autophosphorylated in the holoenzyme. Alternatively, the RI isoforms contain either an alanine or glycine residue at this position, rendering its inhibitor site a pseudosubstrate for the kinase and having no effect on association (Taylor et al. 2012). Phosphorylation at this site in the RII isoforms enhances dissociation of the holoenzyme, demonstrated by differences in dissociation between RI and RII isoforms (Martin et al. 2007). Two cAMP-binding domains, A and B, follow the inhibitor site and its

linker regions (Figure 4-1).

The catalytic subunit is divided into two lobes, N and C, with disordered N- and C-terminal domains (Figure 4-2). The two lobes interact in an ATP-dependent fashion; when ATP is not bound, the two lobes are spatially separated (Uhler, Carmichael, et al. 1986; Johnson et al. 2001; Johannessen et al. 2004)). The highly conserved catalytic site is located within the larger C lobe, along with substrate-binding sites (Uhler, Chrivia, et al. 1986; Taylor et al. 2013; Woodford et al. 1989). All kinases contain a catalytic domain responsible for catalyzing the covalent addition of a phosphate group to a substrate (Beebe et al. 1992; Ubersax & Ferrell 2007; Herberg et al. 1996). PKA, considered one of the simpler kinases, contains a catalytic domain between the smaller N and larger C-lobe of its catalytic subunits. Within the catalytic domain, magnesium (Mg) and adenosine triphosphate (ATP), providing the source of phosphate, are bound. Once the protein substrate is bound, the γ-phosphate of ATP is transferred to the substrate and the reaction products, ADP-Mg and the phosphorylated substrate, are released (Taylor et al. 2004).

1.3 The Role of PKA in Disease

Aberrant PKA activity has been linked to a number of diseases. In particular, mutations in Cα leading to constitutive kinase activity, possibly due to defective association with regulatory subunits, have a causal role in Cushing's syndrome (Beuschlein et al. 2014) and adrenocortical tumors (Yu et al. 2012). Further, a large (400 Kbp) deletion mutation leading to a Cα and DNAJB1 fusion protein dysregulates Cα activity leading to fibrolamellar hepatocellular carcinoma, a cancer with poor prognosis despite its onset in relatively young patients (Cheung et al. 2015). Finally, impaired inhibition of the catalytic subunit due to mutations in the RIα, gene, which is considered a tumor-suppressor gene in healthy patients, has a causal role in the multiple neoplasia syndrome, Carney complex (Veugelers et al. 2004). The complex is triggered by haploinsufficiency of the RIα subunit due to an inactivating mutation in one allele for RIα. Carney complex patients present with enhanced tumorigenesis, excessive myxomas, endocrinopathy, cardiac function variability, and patchy skin pigmentation. Mutations in RIα also lead to sporadic thyroid cancer and infertility (Veugelers et al. 2004).

1.4 PKA Signaling

cAMP is a derivative of adenosine triphosphate (ATP) that is produced by adenylate cyclases (ACs) localized either to the plasma membrane (insoluble) or cytosol (soluble) (Choi et al. 1993), and is degraded by phosphodiesterases (PDEs) into adenosine monophosphate (AMP) and a phosphate group (Pi) (Bender & Beavo 2006). Activation of ACs is possible by two mechanisms: (1) direct binding by G-alpha g-proteins (Gαs) downstream from Gs-coupled G-protein coupled receptor (GPCR) signaling or (2) binding by calmodulin following its activation downstream from calcium influx through voltage-sensitive Ca^{2+} channels (AC isoforms AC1 and AC8). Although AC isoforms differ in their relative activation by g-proteins and inactivation by calcium, this large family of enzymes is solely responsible for the production of cAMP in a cell, converting ATP to cAMP (Choi et al. 1993).

The dominant result of cAMP production is the activation of PKA. In the absence cAMP, the PKA holoenzyme remains inactive. Upon cAMP binding to the regulatory subunits, two per regulatory subunit, a conformational change releases the catalytic subunits to phosphorylate a range of substrates. Phosphorylation provided by PKA has been found to affect protein activity, interaction, localization, and conformation (Brandon et al. 1997). These small PKA-mediated events have larger demonstrated roles in cell metabolism, migration, morphology, division, differentiation, activation, transcription, and translation (Skålhegg & Taskén 2000; Taskén & Aandahl 2004). When PKA signaling is impaired, behavior (Keil et al. 2016) and health (Veugelers et al. 2004; Cheung et al. 2015) may be affected.

PKA phosphorylates substrates at either a serine or threonine residue within a conserved recognition motif: R-R-X-S/TYY. Considered a molecular switch, phosphorylation by PKA alters the activity of its substrates. PKA substrates include other enzymes (Djouder et al. 2009), ion channels (Langeberg & Scott 2015; Yu et al. 2012; Murphy et al. 2014; Poisbeau et al. 1999; Tavalin et al. 2002; Hall et al. 2007; Tibbs et al. 1998), synaptic proteins (Castillo 2012), GPCRs (Taylor et al. 2012; Veugelers et al. 2004; Martin et al. 2007; Terunuma et al. 2010), and transcription factors (Johnson et al. 2001; Uhler, Carmichael, et al. 1986; Johannessen et al. 2004). Subcellular localization of PKA signaling provided by A-Kinase anchoring proteins (AKAPs) coordinates precise and temporally regulated activities while also sequestering aberrant PKA activity (Langeberg & Scott 2015).

1.5 PKA KO and Mutant Mice

The ability to genetically disrupt a gene was followed closely by the development of mouse models lacking expression of individual PKA subunits. The study of these knock-out (KO) and mutant mice has clarified the relative contribution of individual PKA subunits. The following paragraphs describe studies using KO mice that we developed to investigate each of the individual isoforms of the PKA regulatory subunit.

To produce a RIα KO mouse, a neomycin resistance cassette was targeted to disrupt exon three of the RIα gene (Amieux et al. 2002). As the most highly and ubiquitously expressed regulatory subunit, the loss of RIα is embryonically lethal. The loss of RIα results in developmental irregularities in the formation of organs and tissues derived from mesoderm, including heart, preventing developmental progression from embryo to functional fetus (Amieux & McKnight 2002). RIα serves to sequester excessive catalytic subunit activity. Increases in catalytic subunit expression (Uhler, Carmichael, et al. 1986) or loss of other regulatory subunits, lead to compensatory increases in RIα (Amieux & McKnight 2002). However, a compensatory change by other regulatory subunits and catalytic subunits in the RIα KO embryos was insufficient for rescue. However, further studies reduced catalytic activity by RIαKO to a heterozygous or full KO of the Cα subunit, rescuing the developmental defect phenotype, although still not producing viable offspring (Amieux & McKnight 2002) clarifying aberrant catalytic activity as detrimental.

The type II regulatory subunit of PKA, RIIα, is expressed in most tissues. We disrupted expression of the

RIIα gene by homologous recombination of a neomycin cassette into the transcriptional start site and exon one of the RIα allele (Burton et al. 1997). The loss of RIIα results in viable and fertile offspring with compensatory upregulation of RIα and downregulation of Cα, presumably to control unregulated catalytic activity (Burton et al. 1997; Burton et al. 1999). However, the loss of RIIα reduced long term potentiation (LTP) induced by theta burst stimulation in cortical layers II and III of the visual cortex without affecting synaptic integrity or long term depression (LTD). This reduction in plasticity was phenotypically demonstrable as a loss of activity dependent ocular dominance plasticity (Rao et al. 2004), which requires intact cAMP and PKA signaling (Hensch et al. 1998).

RIβ is neuronal-specific and demonstrates high levels of expression in the cortex and hippocampus (Cadd & McKnight 1989) and its loss results in deficits in both hippocampal and cortical forms of synaptic plasticity (Hensch et al. 1998; Huang et al. 1995; Brandon et al. 1995). The RIβ KO mouse was constructed by disruption of the third exon for RIβ by neomycin cassette insertion. RIα protein demonstrated compensatory upregulation, but deficits in plasticity at the perforant path to dentate gyrus (Brandon et al. 1995) and dentate gyrus to region CA3 (Huang et al. 1995) synapses was impaired by the loss of RIβ .

The type II regulatory subunit of PKA, RIIβ, is highly expressed in brain and brown and white adipose tissue (Cummings et al. 1996). We disrupted the RIIβ gene by targeted insertion of a neomycin resistance cassette into exon 1 of the RIIβ gene (Brandon et al. 1998). The targeted loss of RIIβ results in an enhanced nocturnal locomotion, deficits in PKA mediated gene expression (Brandon et al. 1998), cortical plasticity deficits, reduced fat pads, resistance to diet-induced obesity (DIO) and insulin resistance (Schreyer et al. 2001), and highly reduced serum leptin (Cummings et al. 1996), an adipocyte-derived peripheral hormone known to cross the blood-brain barrier (Williams & Elmquist 2012). Initially, the lean phenotype was thought to be largely due to enhanced energy expenditure and augmented induction of uncoupling protein in fat stores (Nolan, Sikorski, et al. 2004; Planas et al. 1999; Newhall et al. 2005; Cummings et al. 1996). However, additional work by our lab found that selective re-expression of RIIβ in adipose tissue did not rescue any of the body weight phenotypes due to compensation by RIα (Brandon et al. 1998; Cummings et al. 1996) and our focus turned to RIIβ in the brain after determining loss of RIIβ could rescue the obese Agouti yellow mouse, a model of defective melanocortin signaling (Czyzyk et al. 2008). Indeed, further studies found that increasingly selective neuronal re-expression did rescue aspects of the RIIβKO phenotype. The return of RIIβ to medium spiny neurons rescued the enhanced nocturnal locomotion phenotype while re-expression in hypothalamic GABAergic neurons rescued the body weight phenotype (Zheng et al. 2013).

There are two main catalytic subunits of PKA, Cα and Cβ. Cβ is highly expressed in the brain and has been largely investigated for its role in forms of hippocampal plasticity (Qi et al. 1996; Huang et al. 1995). The targeting of a neomycin cassette by homologous recombination to disrupt the first exon and part of the initial intron of the Cβ allele, led to the loss of $C\beta_1$, but not $C\beta_2$ or $C\beta_3$ (Qi et al. 1996). A full Cβ null

mouse was made by inserting a neomycin resistance cassette to replace exon 2, common to all three Cβ isoforms (Howe et al. 2002). The loss of $C\beta_1$ led to deficits in tetanus induced LTP, between the mossy fiber axons of the dentate gyrus and the proximal dendrites of regions CA3 (MF-LTP), without a loss of LTP induced by forskolin, a pharmacological agent that activates adenylate cyclases to produce cAMP (Huang et al. 1995). As this form of LTP does not underlie spatial memory, cued or contextual fear, it is not surprising that $C\beta_1$ KO mice had no deficits in assays of spatial memory or contextual fear and cued fear conditioning. Further studies found deficits in LTP between region CA3 and CA1 and loss of long term depression (LTD) (Qi et al. 1996), known to have a role in spatial memory (Tsien et al. 1996).

The loss of $C\beta_1$ also led to differences in body weight regulation. When placed on a high fat diet, $C\beta_1$ KO mice had enhanced insulin sensitivity by insulin tolerance test, resistance to diet induced obesity, reductions in fat stores, enhanced glucose clearance, and reductions in hepatic steatosis (Enns et al. 2009). The loss of $C\beta_1$ in combination with or without the heterozygous loss of Cα produced offspring with varying defects in neural tube formation and encephalopathy (Huang et al. 2002).

Two Cα KO mice were produced. Inserting a floxed neomycin cassette to replace all three exons of the Cα allele produced a mouse lacking all Cα isoforms. Although the Cα allele produces two splice variants, $C\alpha_1$ and $C\alpha_2$, $C\alpha_2$ is only found in germ cells (Desseyn, 2000). The loss of all Cα isoforms, considering its ubiquitous expression, produces runted offspring with low survival rates past the early postnatal period (Skålhegg et al. 2002). The loss of $C\alpha_2$ was produced by targeted disruption of exon 1(b) of the Cα gene locus. Considering its specificity for germ cells and the importance of cAMP/PKA signaling in sperm motility, the loss of $C\alpha_2$ resulted in poor sperm motility and reduced male fertility (Nolan, Babcock, et al. 2004).

The release of the catalytic subunits from the holoenzyme requires the binding of two cAMP molecules per regulatory subunit. The two cAMP-binding sites are denoted A and B, differing in their relative affinity and retention of bound cAMP (Taylor et al. 2013; Uhler, Chrivia, et al. 1986; Woodford et al. 1989). The B site sterically prevents access to the A site (Ubersax & Ferrell 2007; Beebe et al. 1992; Herberg et al. 1996), has a higher affinity for cAMP (Woodford et al. 1989) and a slower off-rate compared to the A site, giving it a dominant role in kinase activation (Taylor et al. 2004; Uhler, Chrivia, et al. 1986; Taylor et al. 2013; Ogreid et al. 1989). Further, *in vitro* studies found that point mutations within the A site, G200E, or B site, G324D, of RIα resulted in significant reductions in cAMP binding, with the single G324D mutation in the B site reducing cAMP binding more than 100-fold (Choi et al. 1993; Reinton et al. 1998; Woodford et al. 1989; Willis et al. 2011). This single mutation inhibits the dissociation of the catalytic subunit and, because of its dominant role in kinase activation, kinase activity is reduced in a dominant negative fashion. We constructed a mutant mouse expressing this gene in a Cre-dependent manner. Expression of the mutant gene by Cre-mediated excision of an upstream floxed stop codon leads to cell-specific expression of the dominant negative RIα, denoted RIαB.

Our laboratory and others have utilized this mouse to investigate neuronal (Yang & McKnight 2015; Yang et al. 2014), intestinal (Howe et al. 2006), renal (P. E. Gilbert et al. 2001), immune system

(Salmon et al. 2012) and liver function (Willis et al. 2011). Considering the loss of RIα is embryonically lethal, it is not surprising that the phenotypes of mice expressing the mutant allele are robust despite its cell-specific expression. The initial study demonstrating the validity of the mutant mouse utilized a liver-specific Cre driver (*Alb*-Cre) and found that the downregulation of PKA activity in the liver improved glucose clearance (Willis et al. 2011). Utilization of a Cre driver with specific expression for neurons in the paraventricular nucleus of the hypothalamus (PVN) and kidney inhibited urine concentration, resulting in diabetes insipidus. The inhibition of PKA activity impaired proper insertion of the aquaporin channel-2 (Aq-2) into the apical membrane, required for reabsorption of water into the collecting duct (M. L. Gilbert et al. 2015). Expression of the mutant allele in the dopaminergic medium spiny neurons of the striatum using a Darpp-32-Cre, provided a robust phenotype with a syndrome of effects ultimately related back to improper dopamine signaling (Yang et al. 2014). This mouse model is a unique and robust tool for investigating the role of PKA signaling in a specific cell population.

1.6 A-Kinase Anchoring Proteins

AKAPs are a diverse family of proteins without a common evolutionary background that interact with PKA via an amphipathic helix, a 14-18 amino acid motif shared by all AKAPs (Carr et al. 1992). The amphipathic helix interacts with the first twenty-five amino acids of the docking and dimerization (D/D) domain common to all regulatory PKAs (Carr et al. 1992). RII isoforms are typically confined to compartments and associated with subcellular structures while RI isoforms are generally cytosolic (Di Benedetto et al. 2008). However, AKAPs binding RII, RI and RII (dual specific), and only RI isoforms have been described, although they are less common. This difference between RI and RII isoforms is related to the composition of their D/D domains and RI isoforms have a significantly lower affinity for AKAPs (Herberg et al. 2000). AKAPs stabilize PKA near a substrate and, when localized near a subcellular source of cAMP, allow for tight control of the signaling event. This is beneficial for proper cell function when the pool of cAMP produced by a signaling event is small and would otherwise be rapidly degraded by phosphodiesterases (PDEs). In addition, AKAPs provide sequestration of PKA activity, preventing off-target phosphorylation events.

AKAPs associate with a number of subcellular organelles, including the Golgi apparatus, mitochondria, sarcoplasmic reticulum, nucleus, and vesicles
(Pidoux & Taskén 2010; Esseltine & Scott 2013). In fact, most AKAPs have multiple subcellular localization motifs, although their relative import is not understood. Localization motifs have been demonstrated in some AKAPs allowing lipid association, key to lipid raft, plasma, and organelle membrane association. Targeting of AKAPs is also supported by protein interaction motifs. Examples of this include the PIXIT motif in AKAP5 necessary for interaction with calcineurin (CaN or protein phosphatase 2B) (Oliveria et al. 2007).

1.7 AKAPs and plasticity

Plasticity is the ability of a synapse to increase or decrease its synaptic transmission. Enhanced synaptic transmission lasting from minutes to days is known as long-term potentiation (LTP) and reduced synaptic transmission is long-term depression (LTD). It is accepted in the field that, within the hippocampus, LTP is the physiological manifestation of memory (Kandel et al. 2014). PKA has demonstrated roles in presynaptic and postsynaptic forms of LTP and LTD (Castillo 2012). Post-synaptic forms of LTP are dependent upon enhanced glutamate reception at the post-synaptic membrane. The ability to increase reception is possible by the insertion of additional α-amino-3-hydroxy-5-methyl-4-isoxazole propionate receptors (AMPARs) into the post-synaptic membrane, a process that requires PKA phosphorylation provided by AKAP5 (AKAP79/150). The loss of AKAP5 delocalized RIIα and another binding partner of AKAP5, protein phosphatase 2B (PP2B or calcineurin), from post-synaptic densities impacting the expression of LTD.

1.8 AKAP7

The *Akap7* gene is alternatively spliced and regulated by three different promoters giving rise to two short (α and β) and two long isoforms (δ and γ). The long isoforms are typically localized to the cytosol, while the short isoforms are localized to the plasma membrane. Of the seven exons in the AKAP7 allele, only the final exon, is shared by all four isoforms. The two short isoforms contain the same initial 16 amino acids (AAs) required for myristoylation and palmitoylation lipid modifications and allowing membrane association, and end with exon 7. Two important interaction motifs are contained in this final exon, the amphipathic helix that allows interaction with PKA and a modified leucine zipper motif shown to bind with high affinity to voltage-gated $Na_V1.2$ and L-type calcium channels ($Ca_V1.1$ and $Ca_V1.2$) (Catterall 2010; Tian et al. 2003; Hulme et al. 2002). AKAP7 may associate with RI (Brown et al. 2003) or RII regulatory subunits, although there is some contradiction in the literature on this point.

AKAP7α is highly expressed in brain and lung tissue, with lower levels of expression in heart (Jones et al. 2012). AKAP7α was initially discovered in 1997 when co-purified from rabbit skeletal muscle due to its association with L-type calcium channels(Gray et al. 1997). Further studies found the association with L-type calcium channel was required for insulin secretion from pancreatic β-cells in response to glucagon-like peptide-1 (Fraser et al. 1998). Characterization of this interaction with ion channels as a modified leucine zipper motif followed shortly with mutational studies demonstrating its requirement for PKA-mediated potentiation of the CaV1.1 (Hulme et al. 2002). Due to its relatively small size, the ability of AKAP7a to interact with other proteins and PKA may be possible, albeit with some tradeoff. The Dodge-Kafka lab found interactions between AKAP7α and Protein kinase C (PKC) (Redden et al. 2012), although the functional relevance of this *in vivo* has not been determined. Prior studies demonstrating PKA anchored by AKAP7α inhibited sodium epithelial channel activity and involving PKC may corroborate this finding (Bengrine et al. 2007). However, the ability of AKAP7α to bind an ion channel and two kinases is sterically difficult to comprehend and future studies may clarify the association with one kinase or the other as preferential.

AKAP7β is slightly larger than AKAP7α, at 104 compared to 81 AAs. AKAP7β contains an additional 23 amino acid residues between the initial 16 AAs, required for membrane localization, and exon 7. In a model of cells in monolayer, these residues allow segregation of the two short isoforms with AKAP7β demonstrating preferential localization to the apical membrane, whereas AKAP7α localizes to the lateral membrane (Trotter et al. 1999). Very little is known about AKAP7β and its expression is very low.

The two long isoforms of AKAP7 are significantly larger, at 314 (γ) and 353 (δ) AAs in length. The long isoforms of AKAP7 are also expressed in brain and most other tissues (Jones et al. 2012). Lacking the lipid modifications present in the short isoforms, the protein is predominantly localized to the cytosol, although it contains a nuclear localization signal of unclear value near the N-terminus (Brown et al. 2003; Trotter et al. 1999). The long isoforms also contain a phosphoesterase activity domain with sequence homology to viral 2',5'-phosphodiesterases , a domain that degrades 2',5'-oligoadenylate activators of 2'-5' oligoadenylate synthetase-dependent ribonuclease (RNase L), a ribonuclease activated by the interferon pathway, a recognized pathway in RNA viral infection (Gusho et al. 2014). AKAP7γ has been shown to demonstrate interactions with PKC, Inhihbitor-1, phospholamban, and phosphodiesterase 4d (Kritzer et al. 2012).

Our lab has developed a mouse model of selective (CRE-dependent) and whole animal AKAP7 gene disruption. A targeting vector was constructed containing a Neo cassette flanked by FRT sites upstream from exon 7 with the Neo cassette, exon 7, and the majority of the 3'-UTR flanked by loxP sites. Following selection by Neomycin resistance, the chimeric offspring generated were crossed to a germline-expressing Cre recombinase line (Meox2-Cre), removing the entire exon 7. It is possible that the upstream six exons for the long isoforms of AKAP7 may still be expressed (Jones et al. 2012).

1.9 RiboTag Mouse

The ribosome is the molecular machinery responsible for translation, the construction of a protein from its corresponding messenger ribonucleic acid (mRNA). The ribosome complex is composed of ribosomal RNA and approximately 80 proteins that are organized into two subunits, a large and a small. Considering its role in translation, the ribosome is associated with both mRNA, held internally, and the nascent polypeptide strand. Of the many ribosomal proteins, ribosomal protein 22 (RPL22) is a core protein located at the exterior of the ribosome complex, and incorporated into the ribosome complex when tagged with GFP. Production of the RiboTag mouse included the construction of a targeting allele composed of the endogenous fourth exon of the *Rpl22* gene flanked by two loxP sites upstream of neomycin resistance cassette flanked by FLP recombinase sites and a duplicated fourth exon including three hemagglutinin (HA) tags. The neomycin resistance cassette was removed by breeding the resulting mice to a FLP recombinase expressing (FLPeR) mouse line. By crossing the resulting RiboTag mouse with a Cre driver mouse line, the endogenous exon 4 is excised and the HA-tagged exon 4 is expressed in cells expressing Cre recombinase.

Expression of the RiboTag allele is dependent upon the specificity and onset of Cre-recombinase expression. Initiation of Cre-mediated RiboTag expression within a precursor population may lead to confounding results due to reduced specificity of RiboTag expression. Considering the assembly of ribosomes into polysomes, heterozygous expression of both the RiboTag and Cre-recombinase alleles is sufficient for immunoprecipitation. A sufficient number of RiboTag-labeled cells are required to provide a reasonable quantity of isolated RNA for downstream applications such as microarray and qRT-PCR. Between 10-40,000 labeled cells typically provide a yield of 100-200 nanograms (ng) of immunoprecipitated RNA. If smaller populations of neurons are expected, animal tissues may be pooled.

The hypothalamus contains numerous subpopulations with known roles in feeding, thirst, aggression, mating behavior, and sexual development. Prior studies utilizing *in situ* and micro-dissection have defined particular regions of the hypothalamus by their region or cell-specific production of a neuropeptide, i.e. agouti-related protein (*AgRP*) or pro-opiomelanocortin (*Pomc*) to define the arcuate nucleus (Arc), or a transcription factor such as steroidogenic factor 1 (*Sf1* or *Nr5a1*) to define the ventromedial hypothalamus (VMH). However this process is time-consuming and neurons are classified in a manner that may miss further important subpopulations.

1.10 Competing Technologies for RiboTag

A number of techniques have been utilized to isolate the gene expression patterns of specific neuronal populations: laser capture microdissection (Scott et al. 1987; Segal 2005), flow cytometry (Henry et al. 2015), single-cell RT-PCR or RNA-seq, and immunoprecipitation of other ribosomal proteins to isolate associated mRNAs (Ekstrand et al. 2014; Heiman et al. 2008). Each of these techniques has demonstrable attributes and technical limitations.

Laser capture microdissection (LCM) to determine the genetic signature of a group or region of cells from a tissue section has been used for about a decade. Briefly, the technique begins with a tissue section mounted to a common glass slide. The tissue is then sandwiched between a thermoplastic film and the glass slide. Under light microscope, a focused laser beam with microscope optics activates the film over the tissue/cells of interest, adhering the film to the tissue. The film is then removed and the tissue/cells of interest are separated and rapidly processed to isolate RNA (Emmert-Buck et al. 1996; Segal 2005). The isolated RNA is amplified into cDNA and may be run on multiple platforms including qRT-PCR, microarray, or RNA sequencing. Although this technique is a huge improvement compared to the otherwise gross dissection provided by tissue punch, the RNA content of a tissue is rapidly degraded by released RNases following dissection, making the time required to isolate the section a difficult problem to overcome. Pre-treatment with RNase inhibitors and handling of the tissues at 4C or below does reduce RNA degradation. Finally, tissues are rarely homogenous and dissection provides a dominant population contaminated with less common background cell populations. This “background” must be considered when interpreting results of this technique.

To get around the heterogeneous nature of a tissue to isolate a specific population, cell sorting

using Fluorescence-Activated Cell Sorting (FACS)-sorting may be employed (Fulwyler 1965). This technique requires a number of preparatory steps, including tissue dissection and gentle digestion to disperse individual cells. The cells are then labeled by a fluorescent antibody to a particular biomarker of interest or, if already expressing a fluorescent marker, may be directly prepared for cell sorting. The cell sorting procedure relies on the use of a flow cell to organize cells into a single stream that will pass through one or more lasers to measure fluorescence. Cells with the desired fluorescent marker(s) are separated and may then processed for RNA isolation. The technique may also be used to determine population percentages, i.e. how many cells are present with a particular marker compared to a whole population. Considering the amount of processing and time involved in cell sorting and the loss of any cell projections lost by the digestion, determining the genetic signature of the cells is possible. However, the technique is too time intensive to determine cellular changes by a population in response to an intervention.

Moving away from the physical isolation of cell populations from a whole tissue, other techniques similar to RiboTag have been developed. They also allow rapid processing and isolation of polysome-associated transcripts. The Heintz lab developed a bacterial artificial chromosome (Bac)-targeted ribosome affinity purification (TRAP) technique allowing isolation of cell-specific polysome-associated transcripts by isolating ribosomal protein 10a (L10a) tagged with enhanced green fluorescent protein (EGFP) (Heiman et al. 2008). This technique requires the production of a Bac transgenic mouse line expressing the EGFP-tagged ribosomal protein 10a (EGFP-L10a) for each cell type, a daunting task. However, the expression of the EGFP-L10a protein was rapidly adapted by the Friedman lab to be expressed in a Cre-dependent manner (Ekstrand et al. 2014). It has also been combined with the tetracycline transactivator system (tTA) (Eisenhaure 2010). This adaptation still requires the production of a Bac transgenic mouse, but allows for controlling expression of the EGFP-L10a transgene by TetO promoter, which is maintained by providing the mice with a doxycycline supplement. This prevents developmental induction of the tagged L10a until desired, enhancing the specificity of the isolated polysome-associated transcripts according to mature expression of the transgene (Drane et al. 2014).

Determining the entire message complement of an individual cell has recently been made possible by next-generation sequencing (Margulies et al. 2005). The message complement of an individual cell may be extracted following electrophysiology experiments that patch directly on to the cell, allowing extraction of somatic mRNA into the patch needle. Next generation sequencing is then possible by producing amplified cDNA from the extracted RNA by reverse transcription in picoliter reactions. Library generation for RNA sequencing is possible following cDNA amplification if the amplified product is validated for reaction fidelity. The technique excludes any RNA content present in the processes of an extracted cell. In addition, RNA sequencing will still require reads from multiple individual cells to reduce false positives due to sample variations (Schuster 2007; Mardis 2008).

The S6 ribosomal protein is part of the 40S ribosomal subunit. As ribosomes are the machinery of translation, the activation of the S6 by phosphorylation is presumably a marker of active translation

downstream from multiple signaling pathways (Valjent et al. 2011). The protein is phosphorylated on the following serine residues located on the C-terminal: S235, 236, 240, 244, and 247. The phosphorylated ribosome capture technique utilizes an antibody against the S240 and S244 residues to immunoprecipitate the activated S6 ribosomal protein (Knight et al. 2012). For a single immunoprecipitation, 10 to 20 animals are required, depending upon the robustness of the intervention and the size of the population activated. Further, the isolation of an activated translational profile will not isolate a population of cells commonly segregated, i.e. *Pomc* vs. *AgRP*-expressing neurons, if the two populations are both activated by the intervention.

Genetic crosses leading to expression of the RiboTag are dependent upon the fidelity and onset of the Cre recombinase-expressing driver mouse. Induction of RiboTag expression in the mature mouse by viral expression was provided by the production of a viral RiboTag (Sanz et al. 2015). The viral vector is a double inverted cassette containing the HA-tagged *Rpl22* gene. The virus provided much higher fidelity in its expression of the RiboTag, demonstrating de-enrichment for genes that developmental onset of Cre expression might otherwise allow.

1.11 Significance of this work

Long-term changes in synaptic strength are commonly thought to be one of the most important ways that the brain encodes memories. Over the past twenty years, a remarkably diverse array of mechanisms for strengthening and weakening synapses has been discovered (Malenka and Bear, 2004; Nicoll and Roche, 2013) and includes gene transcription, translational regulation, and post-translational protein modification by protein kinases. These events can affect the strength of individual synapses, recruit new synapses, and even promote proliferation and differentiation of neurons in the circuit. Changes in both pre- and postsynaptic compartments can produce long-term potentiation (LTP) of synaptic strength (Zalutsky and Nicoll, 1990). LTP has been most extensively studied in the hippocampus, a region known to be important for many forms of learning and memory. Hippocampal dysfunction in humans or animal models is implicated in a wide range of mood, psychiatric, and cognitive disorders, such as post-traumatic stress disorder (PTSD) and schizophrenia, but the molecular changes that cause these disorders are not well understood (Apfel et al., 2011; Barkus et al., 2010; Dranovsky and Hen, 2006; Dranovsky and Leonardo, 2012; Kheirbek et al., 2012a; Kobayashi, 2009; Snyder et al., 2011).

Perforant path inputs from the entorhinal cortex make excitatory synapses on the hippocampal dentate granule (DG) cells as well as area CA3 pyramidal cells of the hippocampus. DG cells in turn send axons called mossy fibers (MFs) to synapse on dendrites of area CA3 in a region called the stratum lucidum. The CA3 neurons make recurrent connections with other CA3 neurons and also send projections (Schaffer collaterals) to synapse with CA1 pyramidal neurons, which then project back to the entorhinal cortex. Most synapses in the brain, including perforant path-DG synapses, CA3-CA3 recurrent connections, and CA3-CA1 Schaffer collateral synapses in the hippocampus rely on postsynaptic

mechanisms to induce LTP. In contrast, MF-CA3 synapses utilize predominantly presynaptic, NMDA receptor-independent mechanisms to induce and maintain LTP (Nicoll and Schmitz, 2005; Weisskopf et al., 1994). Pharmacological inhibition of PKA (Weisskopf et al., 1994), or genetic deletion of PKA subunits (Huang et al., 1995) impairs MF-LTP.

The role of the dentate gyrus in hippocampus-dependent behaviors has received considerable attention both from a computational perspective (see review by Rolls (Rolls and Kesner, 2006)) and from extensive experimental paradigms to affect DG cell function (Hunsaker and Kesner, 2013). DG neurons contribute to the formation of episodic memories by helping to establish unique representations of highly similar events (pattern separation) and aiding in the recall of these events based on partial cues (pattern completion).

Our work determining the functional value of AKAP7 in the hippocampal dependent memory furthers our understanding of cellular and molecular mechanisms underlying learning and memory. This is critical to our understanding of normal brain function as well as the development of novel therapies targeting mental disorders in which memory and cognition are impaired. Further, the role of presynaptically anchored PKA in plasticity and behavior has not previously been addressed.

CHAPTER 2: PRESYNAPTIC ANCHORING OF PKA BY AKAP7 IS REQUIRED FOR PATTERN SEPARATION BY DENTATE GYRUS

2.1 ABSTRACT

The dentate gyrus (DG) receives cortical input from the entorhinal cortex and sends mossy fiber (MF) projections to the CA3 region of the hippocampus. The DG is thought to be responsible for processing and encoding distinct contextual associations in response to highly similar events/experiences, allowing behavioral discrimination. However, the cellular processes underlying this form of learning, known as pattern separation, are poorly understood. Here we demonstrate an essential role for presynaptic AKAP7 in anchoring protein kinase-A (PKA)-RIIβ in MF axons and terminals. Mice with a DG-specific ablation of AKAP7 are selectively deficient in pattern separation but exhibit normal contextual learning and memory, suggesting a link between DG-dependent behaviors and the presynaptic anchoring of PKA by AKAP7. Moreover, genetic ablation of AKAP7 results in a loss of presynaptic and cAMP/PKA-dependent MF-CA3 long-term potentiation (LTP) directly initiated by adenylyl cyclase activation without affecting tetanus-induced LTP in this pathway.

2.2 INTRODUCTION

The hippocampal formation is an anatomically distinct brain region thought to encode and retrieve episodic and spatial memories (Burgess et al., 2002). Changes in synaptic plasticity (LTP and LTD) within hippocampal circuits are thought to provide a basis for learning and memory (Buzsáki and Moser, 2013; Kandel et al., 2014), but the mechanisms underlying these changes are not fully understood. The DG receives input from the entorhinal cortex and sends its mossy fiber axons to synapse with proximal dendrites in region CA3 (Amaral et al., 2007). Previous theoretical studies predict that the DG accurately separates similar memories by orthogonally encoding discrete non-overlapping input patterns onto the CA3 field (Lee and Solivan, 2010; Rolls, 2013; Schmidt et al., 2012). This precise form of encoding is known as pattern separation (Gilbert et al., 2001; Kesner and Rolls, 2015; Leutgeb et al., 2007; Nakashiba et al., 2012). Behavioral studies have helped to clarify the role of the circuit between the DG and region CA3 in modulating spatial and contextual pattern separation (Aimone et al., 2011a; Myers and Scharfman, 2011; Treves et al., 2008). However, the molecular mechanisms underlying synaptic plasticity at the mossy fiber-CA3 (MF-CA3) synapse and their role in pattern separation are incompletely understood.

Long-term plasticity (LTP) at the MF-CA3 synapse is a presynaptic, protein kinase A (PKA)-dependent, and NMDA receptor-independent form of LTP (herein referred to as MF-LTP) (Harris and Cotman, 1986; Huang et al., 1994; Nguyen and Woo, 2003; Weisskopf et al., 1994). The molecular nature of this presynaptic LTP is not fully understood, although several molecular players have been identified (Castillo, 2012; Kaeser-Woo et al., 2013). A possible model for MF-LTP suggests that presynaptic calcium influx during MF repetitive firing activates calcium-sensitive adenylyl cyclases (ACs) that produce cyclic AMP (cAMP) leading to PKA activation and the phosphorylation of substrates (Huang

et al., 1994; Villacres et al., 1998; Wang et al., 2003; Weisskopf et al., 1994; Zalutsky and Nicoll, 1990). MF-LTP can be induced either by repeated high frequency stimulation (tetanus) or by direct application of the adenylyl cyclase activator, forskolin (FSK). Genetic deletion of calcium-activated ACs (Villacres et al., 1998; Wang et al., 2003) decreased tetanus induced MF-LTP without affecting FSK induced LTP. Functional studies into the role of PKA in MF-CA3 plasticity in mice demonstrated that deletion of either the Cβ1 isoform of the catalytic subunit or the RIβ regulatory subunit selectively inhibited tetanus induced LTP without blocking FSK induced LTP (Huang et al., 1995). These results suggest that FSK and tetanus-induced LTP function by distinct pathways although both appear to require cAMP and PKA activation. The role of sub-cellular localization of the cAMP/PKA signaling pathway has not been addressed in DG neurons and could play a critical role in both synaptic plasticity and contextual discrimination.

A Kinase Anchoring Proteins (AKAPs) are multi-domain scaffolding proteins that localize PKA and other proteins to discrete subcellular domains and spatially restrict intracellular signaling events that are required for neuroplasticity (Dell'Acqua et al., 2006; Scott et al., 2013). We, and others, have shown that genetic deletion of a dendritic AKAP (AKAP5) results in delocalization of PKA from the postsynaptic dendrites of CA1 and CA3 hippocampal neurons and leads to behavioral defects in memory and learning (Lu et al., 2007; Tunquist et al., 2008; Weisenhaus et al., 2010). Previous studies have shown localization of PKA-RIIβ to MF projections (Glantz et al., 1992; Weisenhaus et al., 2010) suggesting the presence of a presynaptic anchoring protein but no presynaptic AKAP has been previously reported in adult neurons.
We report that AKAP7 (also referred to as AKAP15/18) is expressed in many regions of the brain including the hippocampus. In the hippocampal formation, AKAP7 is selectively expressed in DG neurons and localizes to both dendrites and the MF presynaptic projections. Loss of AKAP7 results in delocalization of PKA-RIIβ from the MF projections back to the soma and dendrites . AKAP7 global KO mice demonstrate deficits in non-cued spatial and contextual pattern separation. Slice electrophysiology revealed that AKAP7 KO animals lost sensitivity to FSK-induced MF-LTP but retained PKA dependent tetanus-induced MF-LTP. We specifically deleted AKAP7 from DG neurons and found that the behavioral deficits seen in the global KO are specific to the DG-CA3 pathway. Our results identify AKAP7 as a unique AKAP that localizes PKA to axons and terminals of adult neurons and we demonstrate that AKAP7 functions to regulate both synaptic plasticity and behavior.

2.3 RESULTS

AKAP7 is highly expressed in dentate granule cells

Previous work from our lab and others has shown preferential staining for PKA-RIIβ in the MF projection field, also known as the stratum lucidum, of the hippocampus (Glantz et al., 1992, Weisenhaus et al., 2010). Since genetic deletion of AKAP5 from the hippocampus did not disrupt PKA-RIIβ staining in

MFs (Weisenhaus et al., 2010), we hypothesized another AKAP targets PKA to presynaptic MF projections.

The *Akap7* gene encodes multiple isoforms using two separate promoters to generate either long (γ/δ) or short (α) isoforms (Figure 1A). Only the final exon, containing the PKA-binding domain characteristic of AKAPs, is shared by all AKAP7 isoforms. The long isoforms are expressed in all tissues examined including brain but the short isoform has prevalent neuronal expression (Jones et al., 2012). Similar to the dominant staining in DG neurons within the hippocampus, staining in other brain regions also demonstrates preference for distinct neuronal populations (Figure S2). Long and short AKAP7 isoforms differ in subcellular localization. Long isoforms, γ/δ, are predominantly cytosolic, though they contain a potential nuclear localization sequence. The short α isoform contains N-terminal myristoylation and palmitoylation sites, facilitating membrane association (Trotter et al., 1999). Western immunoblotting of hippocampal extracts demonstrated that the α isoform was much more abundant than γ/δ isoforms in the hippocampus (Figure 1B) as well as other brain regions (Figure S2).

By immunohistochemistry, we found intense staining for AKAP7 in the MF projections (Figure 1D). However, considering the structural and subcellular localization differences of AKAP7 isoforms and how they might differentially impact DG function (Trotter et al., 1999), we then set out to determine which AKAP7 isoforms are expressed in DG neurons. By crossing a DG-specific Cre driver mouse (*Pomc*-Cre) (Mchugh et al., 2007) to the RiboTag mouse {Sanz, 2009 #197}, we were able to immunoprecipitate DG-specific polysomes and their associated transcripts from heterogeneous homogenates. Comparison between DG-specific transcripts (IP) and total hippocampal transcripts (Input) revealed strong enrichment for *Akap7α* (Figure 1C) and DG-specific transcripts, *Dsp* and *Prox1* (Figure S1), validating the fidelity of the Cre-mediated expression of the RiboTag for dentate granule neurons. *Akap7γ* and *Akap5* transcripts (Figure 1C) were comparable to CA3 and oligodendrocyte-specific transcripts (Figure S1). Thus, nearly all *Akap7* transcript expressed in DG neurons is the short, membrane-associated *Akap7α* isoform (Figure 1C). Considering the presynaptic and PKA-dependent nature of MF-LTP, we chose to expand our investigation of AKAP7 anchoring of PKA in the MF projections and how this might impact properties of the DG-CA3 circuit.

AKAP7 is presynaptic at the MF-CA3 synapse

The stratum lucidum includes the proximal CA3 dendrites and the mossy fiber axons and boutons projecting from the dentate gyrus. To determine the specificity of AKAP7 for the MF projections, we colocalized AKAP7 staining with pre- and post-synaptic markers. We found co-localization of AKAP7 with neurofilament-M (NF-M), a protein that labels axons, and with zinc transporter-3 (ZNT3) and synaptophysin (SYP), which are present in MF boutons. We saw no co-localization of AKAP7 with post-synaptic markers; either for the dendritic shaft, microtubule-associated protein-2 (MAP-2), or the post-synaptic density-95 protein (PSD-95), suggesting AKAP7 was in MF projections (Figure 2). Together, our

data indicate that AKAP7 is expressed throughout the MF projections but is not present in post-synaptic CA3 dendrites.

Presynaptic AKAP7 is the sole anchor for PKA-RIIβ in MF projections

The defining characteristic of AKAPs is their affinity for PKA. Utilizing our previously developed global AKAP7 KO mouse (Jones et al., 2012), we then sought to determine whether AKAP7 was anchoring PKA-RIIβ in the MF projections. Deletion of AKAP7 resulted in complete delocalization of PKA-RIIβ from the MF projections (Figure 3A and 3B) back to the soma and dendrites (Figure 3A), although, this delocalization did not lead to reductions in PKA-RIIβ protein (Figure 1B). Furthermore, although the catalytic subunit PKA-Cα was also absent from MF projections in AKAP7 KO mice (Figure 3C). Thus, AKAP7 is required for localization of PKA to MF projections.

Loss of AKAP7 results in uncoupled MF-CA3 LTP

Since the AKAP7 KO mice revealed a dramatic delocalization of PKA from the MF projections (Figure 3), we reasoned that presynaptic PKA-dependent forms of long-term plasticity would be disrupted. To examine this, we performed extracellular field excitatory postsynaptic potential (fEPSP) recordings of MF-CA3 synaptic transmission in acute hippocampal slices acquired from AKAP7 wild-type (WT) and KO mice (Figure 4). FSK-induced MF-LTP was nearly abolished in the AKAP7 KO mice when compared to WT littermate controls both by field and whole cell recordings (Figure 4B). We repeated these findings using a different electrophysiological recording configuration designed to reliably measure presynaptic function at the MF-CA3 synapse. Whole-cell recordings of NMDA receptor (NMDAR)-mediated excitatory postsynaptic currents (EPSCs) were performed under experimental conditions designed to reduce polysynaptic contamination generated by associational-commissural inputs onto the CA3 pyramidal cells (Nicoll and Schmitz, 2005, Kwon and Castillo, 2008). Consistent with the results shown in Figure 4, FSK-induced MF-LTP measured by whole cell recordings was also abolished in AKAP7 KO mice compared with WT controls whereas tetanus-induced MF-LTP remained intact (Figure 4C).

Impairment of basal synaptic transmission at the MF-CA3 synapse might underlie the effects we are seeing in FSK-induced MF-LTP. To ascertain intact basal transmission, measures of short-term plasticity in AKAP7 WT and KO mice were tested. We monitored the NMDAR component under conditions that limit CA3 network activity. All measured short-term plasticity dynamics, paired pulse facilitation and frequency facilitation, were comparable to WT controls (Figure 4D-F). A previous report found that presynaptic long-term depression (LTD) at MF-CA3 synapses relies on cAMP/PKA signaling (Tzounopoulos et al., 1998). We therefore examined the AKAP7 KO and found that LTD was preserved in the AKAP7 KO mice compared with WT controls (Figure 4G). Collectively, these results suggest the loss of AKAP7 has uncoupled the two forms of MF-LTP, FSK/PKA-dependent and tetanus-induced. Remarkably, tetanus-induced MF-LTP remained intact in the AKAP7 KO mice compared with WT controls (Figure 4H). We then investigated whether the tetanus-induced MF-LTP in AKAP7 KO mice remains

dependent on PKA despite the delocalization of RIIβ and the Cα subunit from the MF projections. To test this, we inhibited PKA pharmacologically in AKAP7 KO slices with H89 and found that tetanus-induced MF-LTP still relied on intact PKA signaling (Figure 4I). This may demonstrate a differential regulation of PKA between the soma/dendrites and the presynaptic regions.

Impaired contextual pattern separation in AKAP7 KO mice

Similar to previous studies showing that disruption of DG integrity, either by lesion or loss of circuit integrity between the perforant path and the DG (McHugh et al. 2007) could impact DG-specific behaviors, we reasoned DG-mediated behaviors might also be impaired by the loss of presynaptic PKA. To test for alterations in DG-dependent contextual pattern separation in the AKAP7 KO mice, we used a contextual fear discrimination paradigm (Figure 5A), used in previous studies (Mchugh et al., 2007, Nakashiba et al., 2012). WT and KO animals received a foot-shock in “context A” but not in “context B,” where the two contexts differed only in the flooring and wallpaper. WT mice rapidly reduced their level of freezing (time immobile) in the no-shock “context B” while retaining a robust freezing response in “context A” demonstrating intact contextual pattern separation. However, AKAP7 KO mice took significantly longer to distinguish safe from unsafe contexts and continued to demonstrate comparable enhanced freezing in both contexts for 8 days (Figure 4B-D). In contrast to this substantial delay in pattern separation, KO animals displayed no significant delay in fear extinction (Figure 4E). This deficit was not related to deficits in motor function or anxiety (Figure S4 C-I).

Pattern separation behavior has been directly linked to the process of ongoing neurogenesis that occurs in the subgranular zone of the DG leading to a continuous integration of adult born DG neurons into the dentate granule cell layer (Clelland et al., 2009, Scobie et al., 2009, Sahay et al., 2011, Nakashiba et al., 2012, Tronel et al., 2012). To determine whether reduced adult hippocampal neurogenesis contributes to the behavioral deficiency in AKAP7 KO mice, we quantified neurogenesis by BrdU incorporation into dividing cells. BrdU-positive neurons at multiple stages of DG cell differentiation in WT and KO mice were counted. We found no differences in neurogenesis either under basal conditions or when enhanced by running wheel access and environmental enrichment at multiple time points classically defined for neurogenesis (Ming and Song, 2011) (Figure S5). These results demonstrate that neurogenesis is not affected by loss of AKAP7 and therefore does not underlie the deficits in contextual pattern separation behavior that we observe in the AKAP7 KO mice. Taken together, these results suggest presynaptically anchored AKAP7 is important for DG-mediated contextual pattern separation.

Targeted deletion of AKAP7 in DGCs

Results from global AKAP7 KO mice demonstrate a critical role for AKAP7 in FSK-induced MF-LTP but the effects on behavior could be influenced by the substantial expression of AKAP7 in other brain regions (Figure S2). To address this question, we specifically deleted *Akap7* from DG neurons using the same *Pomc*-Cre driver mouse line used in our RiboTag experiments (Mchugh et al., 2007) crossed with

Akap7$^{Lox/Lox}$ mice (Jones et al., 2012). Specificity of Cre recombinase expression was determined by TdTomato reporter (*ROSA26Sor*-Lox-STOP-TdTomato x *Pomc*-Cre) (Figure 6A-B). TdTomato expression was tightly restricted to DG neurons and the arcuate nucleus, consistent with previous reports (Mchugh et al., 2007, Sanz et al., 2015). We then bred *Pomc*-Cre mice onto an *Akap7* KO background and crossed the resulting *Pomc*$^{Cre/+}$;*Akap7*$^{+/-}$ mice to *Akap7*$^{Lox/Lox}$ mice to generate *Pomc*$^{Cre/+}$;*Akap7*$^{Lox/-}$ (DG-KO) mice. DG-KO animals are heterozygous for *Akap7* in all tissues except those that are Cre-positive, where *Akap7* is completely absent. This cross also produced appropriate control mice: i.e., Cre-negative Akap7$^{Lox/-}$ (Het) and Cre-negative Akap7$^{+/Lox}$ (WT). Immunofluorescence microscopy showed delocalization of PKA-RIIβ and loss of AKAP7 in the DG of DG-KO animals, whereas localization and expression in Het animals were normal (Figure 6C). Expression of AKAP7 in the thalamus (Figure 6C) and other brain regions (not shown) was unaffected in the DG-KO. The delocalization was not as complete as in the global AKAP7 KO probably due to incomplete Cre recombination (Figure 6D).

We also examined whether DG-KO animals would recapitulate the electrophysiological and behavioral deficits seen in the global AKAP7 KO. MF-CA3 synaptic transmission was monitored using extracellular field recordings in acute hippocampal slices. DG-KO mice exhibited impaired FSK-induced MF-LTP (Figure 6D), although not as severely as the global KO, likely due to incomplete Cre recombination. As in the global KO, the tetanus-induced MF-LTP remained intact (Figure 6E). These results confirm that presynaptically localized PKA is essential for FSK-induced MF-LTP.

Non-cued spatial pattern separation is also impaired by loss of AKAP7 from DG neurons

We next examined whether AKAP7 deletion specifically in DG neurons impaired pattern separation. To complement our previous findings with the contextual pattern separation assay, we utilized the delayed non-matching-to-place 8-arm radial arm maze (DNMP-RAM) to determine alterations in non-cued spatial pattern separation (Clelland et al., 2009, Nakashiba et al., 2012, Guo et al., 2012). All four genotypes: WT, global KO, DG-KO, and Het were tested. The assay determines the ability of an animal to recognize spatial differences to locate food reward without relying on visual cues. Animals were placed at the end of a start arm and were trained to locate a food reward at the end of a separate open arm. After finding the reward, mice were returned to their home cage and a new arm was opened and baited. Mice were then returned to the maze to test whether they could correctly differentiate between the previous reward arm, believing it now empty, and the new reward arm (Figure 7A). The spatial separation (2 or 4-arm) between the previous reward arm and the new reward arm provides a discrimination feature, such that, arms closer together (2-arm) are more difficult to discriminate between spatially, compared to arms that are further apart (4-arm). After three days of training, WT and Het animals avoided the previously explored arm and favored the new arm while AKAP7 KO and DG-KO animals committed significantly more errors in the 2-arm configuration (Figure 7B). Therefore, further separating the new reward arm from the previous reward arm (4-arm) facilitated spatial discrimination and resulted in fewer errors for both AKAP7 KO and DG-KO animals and their performance became more similar to WT and Het animals. The

loss of AKAP7 from DG neurons is sufficient to disrupt non-cued spatial pattern separation to the same degree as the global KO (Figure 7B). These results strengthen our contextual pattern separation results linking anchored PKA in MF projections to DG-mediated behaviors.

2.4 DISCUSSION

The postsynaptic localization of PKA in the dendrites and spines of neurons has been shown to depend on specific AKAPs. Disruption of that anchoring results in behavioral deficits as well as alterations in synaptic plasticity (Havekes et al., 2012; Sanderson and Dell'acqua, 2011; Tunquist et al., 2008; Weisenhaus et al., 2010). However, there are multiple circuits in which presynaptic PKA has been shown to play an important functional role in synaptic plasticity including the hippocampal MF-CA3 synapses (Nicoll and Schmitz, 2005), the hippocampal CA3-CA1 synapse (Park et al., 2014), corticothalamic synapses (Castro-Alamancos and Calcagnotto, 1999), corticostriatal synapses (Spencer and Murphy, 2002), and the parallel fiber synapses in the cerebellum (Linden and Ahn, 1999). Our study has identified the first presynaptic AKAP involved in anchoring PKA in axonal projections in adult neurons. AKAP7α localizes PKA-RIIβ presynaptically in the axons and terminals of MF projections to the CA3 pyramidal cells of the hippocampus. We have used genetic disruption of AKAP7 first globally and then specifically in DG neurons to explore the function of this presynaptic AKAP and it's colocalized PKA. We find that loss of AKAP7 prevents PKA from migrating into the MF projections and this leads to a defect in pattern separation behaviors that have been shown to depend specifically on DG neurons (McHugh et al., 2007). In addition we find that the AKAP7 KO displays a unique loss of FSK-induced LTP at the MF-CA3 synapse.

AKAP7α is primarily restricted to DG neurons in the hippocampus although it is widely expressed in other brain regions including the cortex, striatum, thalamus, and cerebellum (Figure S2). The AKAP7 α-helical amphoteric binding site for the R subunits of PKA is adjacent to a modified leucine zipper domain which interacts with brain Na^{2+} and L-type Ca^{2+} channels and facilitates PKA modulation of ion conductance through these channels (Marshall et al., 2011; Tibbs et al., 1998). AKAP7α is also both N-terminally myristylated and palmitoylated and these fatty acid modifications target it to membranes (Gray et al., 1998). In MF axons, AKAP7 is apparently the only anchor for PKA-RIIβ since the two proteins colocalize throughout the axons and terminals and the loss of AKAP7 results in complete delocalization of PKA-RIIβ from these presynaptic projections. In contrast, dendritic AKAP7 shares anchoring duties with other AKAPs including AKAP5 (Sanderson and Dell'acqua, 2011; Tunquist et al., 2008; Weisenhaus et al., 2010), AKAP12 (gravin) (Havekes et al., 2012) and MAP2 (Zhong et al., 2009) . We do not know to what degree AKAP7 plays a specific role in dendrites that cannot be compensated for by other AKAPs but our results demonstrate that PKA-RIIβ continues to localize in the DG dendrites even in the absence of AKAP7.

Our understanding of the role of the DG in memory and learning has developed significantly over the past 15 years. Early studies investigating the role of the DG in contextual discrimination found that

colchicine induced lesions in the DG but not CA1 regions of the hippocampus in rats produced deficits in spatial discrimination (Gilbert et al., 2001). Genetic disruption of the NR1 subunit of the NMDA receptor specifically in DG neurons results in a defect in discrimination between similar contexts (pattern separation) in mice (McHugh et al., 2007). The DG and the olfactory bulb are the only brain regions in the mouse where neurogenesis has been shown to occur throughout adult life (Aimone et al., 2011b). Adult born DG neurons are constantly integrating into the DG circuits and this has led to efforts to determine whether these adult born DG neurons play a distinct role in contextual discrimination (Aimone et al., 2011b; Sahay et al., 2011). Although the mechanisms are not resolved the conclusions from a number of studies indicate that adult born DG neurons are preferentially involved in accurate pattern separation and the mature DG neurons play a more significant role in pattern completion or generalization (Danielson et al., 2016; Nakashiba et al., 2012). Although deleting AKAP7 did not affect adult neurogenesis it is likely that the role of AKAP7 in pattern separation preferentially involves these adult born DG neurons.

The earliest efforts to understand the signaling mechanisms that regulate MF-LTP relied on pharmacological tools that affect Ca^{2+} or PKA throughout the DG neuron. Chelating intracellular Ca^{2+} (Zalutsky and Nicoll, 1990) or removing extracellular Ca^{2+} (Castillo et al., 1994) during tetanus blocks the induction of MF-LTP as does bath application of PKA inhibitors (Weisskopf et al., 1994). The role of adenylyl cyclases was demonstrated by genetic deletion of the calcium stimulated cyclases, AC8 and AC1. Deletion of AC1 or AC8 reduced tetanus induced MF-LTP and the double KO completely eliminated tetanus induced LTP. It is interesting to note that the LTP induced by direct cyclase activation with FSK was unaffected in the AC1/AC8 double KO suggesting that FSK is capable of acting on another cyclase in the DG neuron (Wong et al., 1999). Targeted disruption of either the Cβ or RIβ subunit gene of PKA inhibited tetanus-induced LTP at MF-CA3 synapses without decreasing FSK-induced LTP (Huang et al., 1995). These approaches clearly establish a role for cAMP and PKA in MF-LTP, but do not provide an understanding of the importance of subcellular localization of PKA in axons, soma, or dendrites of DG neurons. Our study demonstrates that AKAP7 anchors PKA in the axonal projections of DG neurons and coordinates the FSK-sensitive LTP pathway without affecting the PKA dependent tetanus-induced MF-LTP. This surprising result suggests that localization of PKA could play a discrete role in these two different modes of eliciting LTP. We know that RI and RII isoforms of PKA have different anchoring characteristics (Di Benedetto et al., 2008) with PKA-RI often concentrated in the soma of neurons (Yang et al., 2014) while PKA-RIIβ is usually tightly anchored to AKAPs in dendrites and, in this study, axonal projections. We speculate that tetanus-induced LTP is more dependent on PKA activation in the soma and forskolin induced LTP may depend on PKA-RIIβ in the MF projections. The expression of AKAP7 in other brain regions suggests a possible PKA anchoring role in other presynaptic pathways where PKA dependent LTP has been observed and our $Akap7^{lox/lox}$ mouse line will facilitate these future studies.

Experience-induced changes in synaptic plasticity (LTP and LTD) are the most attractive substrates to explain learning, memory, and forgetting but it has been exceedingly difficult to make causal connections between synaptic plasticity and behavior. However, a recent report using optogenetic

generation of LTP and LTD in an auditory input to activate or inhibit cued fear conditioning provides compelling evidence for a causal relationship between LTP and memory (Nabavi et al., 2014). The function of the LTP mechanism that can be directly engaged by FSK and is disrupted in the AKAP7 KO is unknown. One possibility is that direct activation of localized Gs-coupled receptors, cyclases and PKA in the axons and presynaptic terminals could alter the excitability of those MF projections and might act either alone or synergistically with perforant path induced DG excitation. Extrinsic neuromodulatory projections from the locus coeruleus (LC) terminate in the stratum lucidum (Amaral et al., 2007) and may provide noradrenergic modulation of MF-LTP (Huang and Kandel, 1996). In addition, the pituitary adenylate cyclase activating peptide (PACAP) receptor is highly expressed in DG neurons and is localized to MF projections (Otto et al., 1999). Targeted disruption of the PACAP receptor (*Adcyap1r1*) in neocortex and hippocampus led to deficits in both MF-LTP and contextual fear conditioning (Otto et al., 2001). There is considerable evidence for synergism between the β-adrenergic receptor agonist, isoproterenol, and repetitive synaptic stimulation of MF-LTP in slice culture (Huang and Kandel, 1996). More recently it has been observed that a weak tetanic stimulation of the MF-CA3 pathway *in vivo* can synergize with lateral ventricle administration of isoproterenol to elicit LTP lasting more than 24 hours (Hagena and Manahan-Vaughan, 2012). We propose that AKAP7 localized PKA provides an intracellular signaling mechanism to potentiate the actions of neuromodulators targeting G-protein coupled receptors expressed specifically on the MF projections. DG dysfunction has been implicated in a wide range of psychiatric disorders including post-traumatic stress disorder, depression, and addictive behavior (Garcia-Fuster et al., 2013; Kheirbek et al., 2012). Our studies suggest that alterations in presynaptically anchored PKA can disrupt specific aspects of DG function and could play a role in these disorders.

2.5 EXPERIMENTAL PROCEDURES

Generation of Akap7 mutant mice*:* Generation of AKAP7 KO and floxed AKAP7 mouse lines was described previously (Jones et al., 2012). We generated tissue-specific DG-KO animals by crossing *Akap7*$^{lox/lox}$ to *Pomc*-Cre^{+};Akap7$^{+/-}$ animals, which express Cre recombinase primarily in the hypothalamus and dentate gyrus. This cross generates four genotypes: *Pomc*-Cre^{+};*Akap7*$^{lox/-}$ (global Het, DG-KO), Cre^{-};*Akap7*$^{lox/-}$ (global Het), Cre;*Akap7*$^{+/lox}$ (WT), and *Pomc*-Cre^{+};*Akap7*$^{+/lox}$ (DG-Het; not used). Mice were given access to food pellets and water ad libitum, and maintained on a 12:12-hr light/dark cycle. All procedures were approved by the Institutional Animal Care and Use Committee of the University of Washington and conformed to NIH guidelines. For all experiments, the experimenter was blind to genotype and un-blinded after completing data analysis.

Immunoblotting: Hippocampi were rapidly dissected and homogenized for immunoblotting following previously described methods (Jones et al., 2012). Antibodies used were as follows: rabbit anti-AKAP7 (Proteintech), mouse anti-PKA-RIIβ (BD Biosciences), and mouse anti-SP1 (07-645, Millipore).

Immunohistochemistry and Imaging: Brains were fixed and processed for standard

immunohistochemistry. Neuron subregions were identified using antibodies specific for each: dendrites, anti-MAP2 (Thermo Scientific); Axons, anti-Neurofilament-M (Developmental Studies Hybridoma Bank); Pre-synaptic boutons, anti-Znt3 (Synaptic Systems) and anti-synaptophysin (Millipore); Post-synaptic densities, anti-PSD-95 (Alomone). Citrate buffer antigen retrieval was required to recover AKAP7 (Proteintech) immunostaining. PKA subunits were visualized using anti-PKA-RIIβ (BD Biosciences) and anti-PKA-Cα (laboratory of Susan Taylor). Fluorescent secondary antibodies were utilized (Molecular Probes). Coverslips were mounted with ProLong Gold (Molecular Probes) or Fluoromount G (Electron Microscopy Sciences) with or without DAPI. Slides were imaged in the University of Washington Keck Microscopy Center on a Nikon Eclipse E600, Zeiss 510 META, or Leica SL confocal microscopes.

Contextual Fear Discrimination and Extinction: Assay was performed according to previous reports (Mchugh et al., 2007, Nakashiba et al., 2012). Briefly, mice were placed in a shock chamber (Colbourn Instruments, Whitehall, PA) placed inside a fume hood to provide background noise. Animals were acclimated to handling and transportation prior to testing. Trials consisted of two types: context A (shock) and context B (non-shock). The two chambers differed only in the floor (white plastic versus shock grid) and wallpaper (striped wallpaper versus white). For context A, animals were placed in the chamber and allowed to explore for 3 min, given a 2-s, 0.65 mA foot shock, and removed 1 min after foot shock. Context B followed the same procedure, except that animals received no foot shock. Testing in A occurred once daily for 3 days. Between every trial, the chamber was cleaned with 5% NaOH and the floor scented with 1% Acetic Acid. On day 4, animals experienced only context B. On day 5, animals experienced context A without a foot shock. On the remaining days 6-17, animals were each context once daily, presented in pseudorandom order. Video recordings were analyzed by Noldus EthoVision software. Contextual fear extinction was carried out similarly, except that animals only received foot shocks on days 1-3 and were never introduced to a second context.

Delayed Non-Matching-to-Place Radial 8-Arm Maze (DNMP-RAM): We followed the behavioral assay procedure as previously described (Clelland et al., 2009). Briefly, mice were singly housed and food restricted to 85–90% of initial body weight. Testing included 4 trials per day over 5 consecutive days. Each trial included two phases, a sample phase and a choice phase. For the sample phase, only the sample and start arms were open, separated by 90-degrees, with a food reward placed at the end of the sample arm (Froot Loops, Kellogg's, Battle Creek, MI). Mice were placed in the maze facing the end of the start arm and allowed 3 min to find the food reward, after which they were removed and returned to their home cage. The maze then rotated 90 degrees and cleaned with 1% acetic acid. New start and sample arms were opened in the same relative locations as during the sample phase. A third arm, the baited choice arm, was also opened, separated from the sample arm by 1 (2-arm separation) or 3 (4-arm separation) closed arms. 2- and 4-arm separations were presented in random sequence each day. An observer blinded to genotypes scored correct or incorrect choices. Data were analyzed by comparing the combined test days 4 and 5. Data were analyzed by Fisher's exact test.

***Electrophysiology*:** Experiments were carried out as in previous work (Kaeser-Woo et al., 2013). Briefly, mice were deeply anaesthetized with isoflurane, decapitated, and acute, transverse hippocampal slices (400 mm) were prepared with a VT1200S microtome (Leica). Experiments were carried out at 25 ± 0.5°C. To monitor synaptic transmission and plasticity, conventional field and whole-cell recordings were made with a Multi-Clamp 700B amplifier (Molecular Devices). Stimulation and acquisition were controlled by custom software. Output signals from recordings were acquired at 5 kHz, filtered at 2.4 kHz, and stored in IgorPro (Wavemetrics). Summary data are expressed as mean ±SEM. Statistics were performed using OriginPro (Origin Lab), and statistical significance was determined by the Student's t test. Only statistically significant differences are indicated. To elicit long-term plasticity, two trains containing 125 pulses at 25 Hz, 20 s inter-train interval, were delivered via the stimulating pipette. Alternatively, 10 μM forskolin, an activator of adenylyl cyclase, was bath applied for 10 min and then washed out. The magnitude of long-term plasticity was determined by comparing baseline-averaged responses before induction with the last 10 min of the experiment. Example traces are averages of at least 30 consecutive sweeps taken from a single representative experiment.

RiboTag isolation and analysis of mRNA transcripts: RiboTag experiments were performed as described (Sanz et al., 2009). Briefly, mice were bred to selectively express a floxed HA-tagged ribosomal protein, RPL22, by crossing the RiboTag mouse with a dentate gyrus-specific Cre driver mouse, *Pomc*-Cre (Mchugh et al., 2007). To isolate DG-specific transcripts, mice were sacrificed and the hippocampi were rapidly dissected and flash frozen. Individual tissue samples were dounce homogenized in a buffer supplemented with RNase inhibitors. Polysomes were immunoprecipitated using antibodies to HA (Covance) and protein A/G-coupled magnetic beads (Pierce BioTechnologies). Input and immunoprecipitated (IP) RNA were quantified by Quant-It RiboGreen (Life Technologies). Quantitative reverse transcriptase-PCR was performed using SYBR green One-Step (Agilent). Oligonucleotides selected using the PrimerBank database: Desmoplakin (*Dsp)*: For: 5'-GGATTCTTCTAGGGAGACTCAGT-3', Rev: 5'-CCACTCGTATTCCGTCTGGG-3', Proximal 1 (*Prox1*): For: 5' AGAAGGGTTGACATTGGAGTGA-3', Rev: 5'-TGCGTGTTGCACCACAGAATA-3', Glutaminase (*Gls*): For: 5'-CTACAGGATTGCGAACATCTGAT-3', Rev: 5'- ACACCATCTGACGTTGTCTGA-3', Phosphodiesterase 1a (*Pde1a*): For: 5'-CCGGGATTGGTTGGCTTCAA-3', Rev: 5'-AATGCTGCGAAACTTTGGTTTT-3', CNPase (*Cnp*): For: 5'-TTTACCCGCAAAAGCCACACA-3', Rev: 5'-CACCGTGTCCTCATCTTGAAG-3', Transferrin (*Trf*): For: 3'-GCTGTCCCTGACAAAACGGT-3', Rev: 5'-CGGAAGGACGGTCTTCATGTG-3'. *Akap7* isoform-specific primers as described previously (Jones et al., 2012).

CHAPTER 2: FIGURES

Figure 2-1:

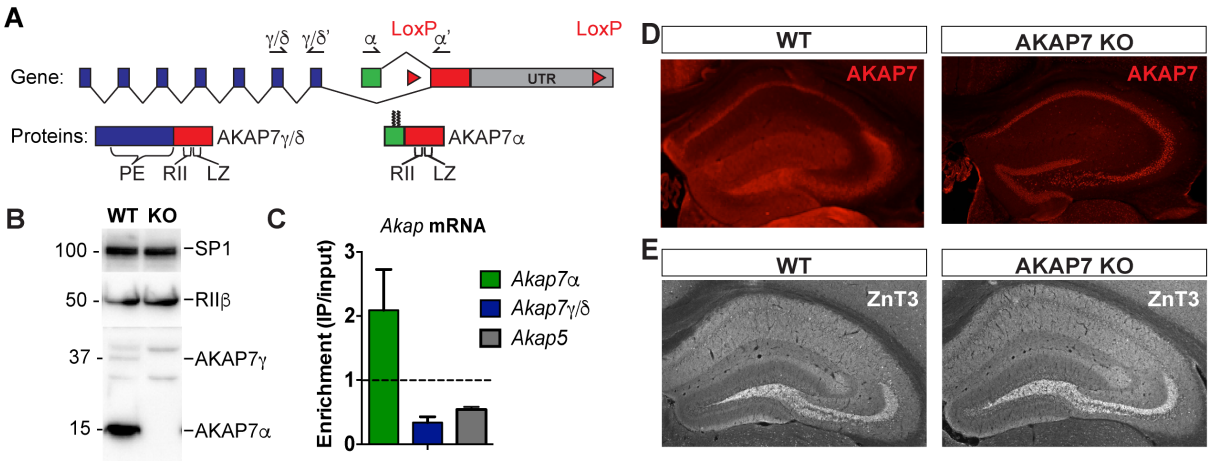

Figure 2-1 Legend: AKAP7 is highly expressed in the dentate gyrus.
(A) Map of *Akap7* gene (introns not to scale) showing engineered LoxP sites and location of primer sets to distinguish between long and short isoforms. AKAP7 proteins resulting from alternate splicing showing phosphoesterase (PE), PKA-RII–binding (RII), and modified leucine zipper (LZ) domains and N-terminal lipid modifications on AKAP7α. (B) Immunoblot of hippocampal lysates shows that the AKAP7α protein at much higher levels than AKAP7γ and protein level of PKA-RIIβ is not reduced in AKAP7 KO. Transcription factor SP1 was used as a loading control. (C) RiboTag immunoprecipitation comparison of DG-specific transcripts compared to total hippocampal transcripts found enrichment for AKAP7α and de-enrichment of AKAP7γ/δ and AKAP5. (D) Immunofluorescence microscopy of WT or KO hippocampus with an antibody against AKAP7 reveals expression in dentate granule neurons but not areas CA1 or CA3. There is some retention of non-specific staining retained in the nuclei in the AKAP7 KO (E) Immunofluorescence microscopy with an antibody against zinc transporter ZNT3 shows normal size of mossy fiber field and hippocampal layering in KO compared to WT.

Figure 2-2:

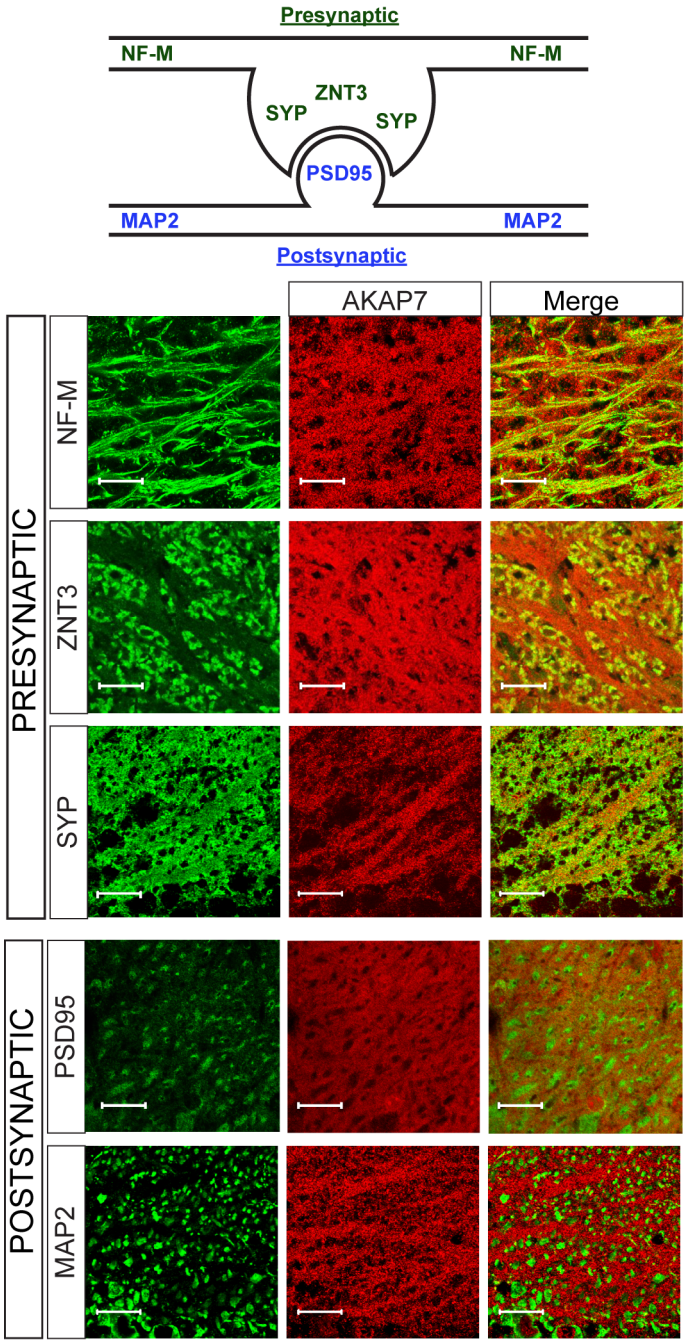

Figure 2-2 Legend: AKAP7 anchors throughout the mossy fiber axon.
Diagram: Model of the localization of pre- and postsynaptic proteins. Scale bars, 20 µm. Confocal images of stratum lucidum show AKAP7 distributed throughout mossy fiber axons but not in postsynaptic compartments. Top: AKAP7 in red, Presynaptic markers: neurofilament-M (NF-M), zinc transporter 3 (ZnT3), synaptophysin (SYP). Bottom: Post-synaptic markers: post-synaptic density protein-95 (PSD95), or microtubule-associated protein 2 (MAP2) in green.

Figure 2-3:

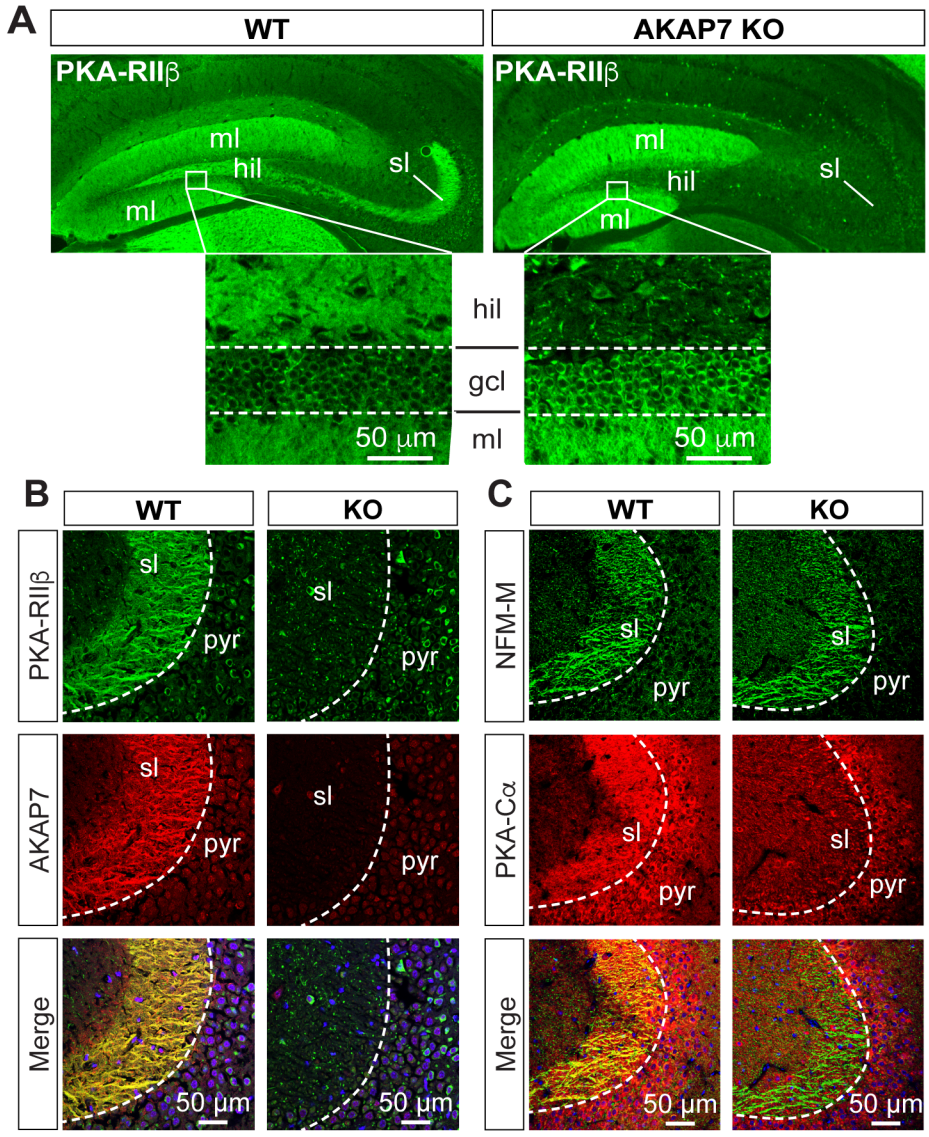

Figure 2-3 Legend: AKAP7 anchors PKA in the mossy fiber axons of dentate granule cells. (A) PKA-RIIβ is lost from mossy fibers (hil and sl) but increased in soma (gcl) and dendrites (ml) in AKAP7 KO. (B),Confocal images of stratum lucidum (sl) showing PKA-RIIβ (green) colocalized with AKAP7 (red) in mossy fibers in WT but not KO animals. Nuclei are stained with DAPI (blue); CA3 pyramidal cell layer (pyr). (C) Confocal images as in *C* showing neurofilament-M (green) colocalized with PKA-Cα (red) in mossy fibers in WT but not KO animals. Nuclei are stained with DAPI (blue).

Figure 2-4:

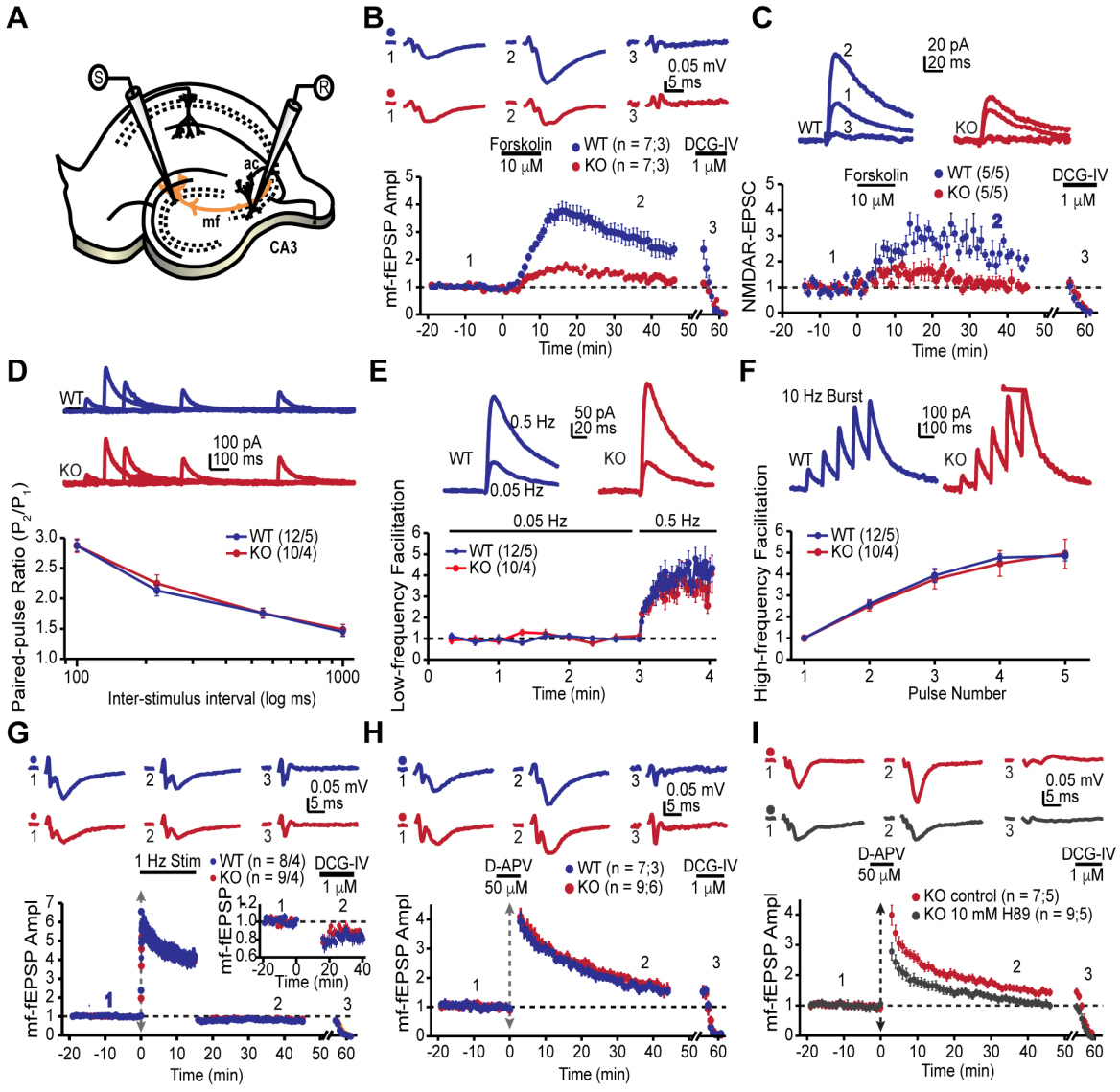
A
S
R
ac
mf
CA3
B
0.05 mV
5 ms
Forskolin
10 μM
WT (n = 7;3)
KO (n = 7;3)
DCG-IV
1 μM
mf-fEPSP Ampl
Time (min)
C
20 pA
20 ms
WT
KO
Forskolin
10 μM
WT (5/5)
KO (5/5)
DCG-IV
1 μM
NMDAR-EPSC
Time (min)
D
WT
KO
100 pA
100 ms
WT (12/5)
KO (10/4)
Paired-pulse Ratio (P2/P1)
Inter-stimulus interval (log ms)
E
0.5 Hz
0.05 Hz
50 pA
20 ms
WT
KO
0.05 Hz
0.5 Hz
WT (12/5)
KO (10/4)
Low-frequency Facilitation
Time (min)
F
10 Hz Burst
100 pA
100 ms
WT
KO
WT (12/5)
KO (10/4)
High-frequency Facilitation
Pulse Number
G
0.05 mV
5 ms
1 Hz Stim
WT (n = 8/4)
KO (n = 9/4)
DCG-IV
1 μM
mf-fEPSP Ampl
mf-fEPSP
Time (min)
H
0.05 mV
5 ms
D-APV
50 μM
WT (n = 7;3)
KO (n = 9;6)
DCG-IV
1 μM
mf-fEPSP Ampl
Time (min)
I
0.05 mV
5 ms
D-APV
50 μM
DCG-IV
1 μM
KO control (n = 7;5)
KO 10 mM H89 (n = 9;5)
mf-fEPSP Ampl
Time (min)

Figure 2-4 Legend: AKAP7 is required for forskolin-induced LTP at MF-to-CA3 pyramidal cell synapses.
(A) Schematic of hippocampal slice, stimulating (S, placed in dentate gyrus) and recording (R, placed in CA3) pipettes used to measure long-term and short-term plasticity at MF-CA3 synapses in vitro. (B) Extracellular field potential recordings reveal cAMP/PKA-induced LTP was abolished in the AKAP7 KO mice. WT: 2.42924 ± 0.29963 of baseline vs. KO: 1.28436 ± 0.07305 of baseline; p = 0.00297; Student's unpaired t-test. LTP was triggered chemically with bath-applied forskolin. For this and all remaining electrophysiology experiments, DCG-IV was bath applied at the end of each experiment to confirm mossy fiber synaptic transmission. Since DCG-IV application time was slightly different between experiments, a break in the x-axis was introduced and the DCG-IV effect was time-aligned. Representative traces are shown above with numbers corresponding to the summary time course plot below, and "n" in parentheses reflects number of slices and animals, respectively. (C) Intracellular whole-cell voltage-clamp recordings of isolated NMDAR-EPSCs also show impaired LTP triggered with forskolin. WT: 2.12649 ± 0.16448 of baseline vs. KO: 1.09268 ± 0.178 of baseline; p = 0.00274; Student's unpaired t-test. Magnitude of LTP was assessed 35-45 min post forskolin application. (D-F) Basal synaptic transmission and short-term plasticity were intact in the AKAP7 KO mice compared to WT controls: (D) Paired-pulse ratio (inversely related to release probability) was calculated by dividing the second of two successive pulses by the first; (E) Low-frequency facilitation triggered by increasing the baseline stimulation frequency; (F) High-frequency facilitation triggered with a 10 Hz burst. Each pulse in the burst was normalized to the amplitude of the first pulse. (G) LTD was normal in AKAP7 KO mice. LTD was induced with a 1 Hz, 15 min protocol. Inset shows expanded view of the summary data to highlight the magnitude of LTD in the AKAP7 animals. (H) Tetanus-induced LTP between AKAP7 WT and KO mice was comparable. Experimental conditions were identical to panel B, except that the NMDA receptor antagonist D-APV was bath applied before and washed out immediately after the tetanus to block postsynaptic NMDA receptor-mediated LTP. LTP was induced with a tetanus (vertical double arrow) consisting of 2 bursts (each with 125 pulses at 25 Hz) spaced by 20s. (I) Tetanus-induced MF-LTP still relied on intact PKA signaling because it was reduced in AKAP7 KO mice. Slices were pre-incubated (>1hr) and continuously perfused with the PKA inhibitor H89. Control: 1.4755 ± 0.07594 of baseline vs. H89: 1.07987 ± 0.06457; p=0.00135 (Student's unpaired t-test).

Figure 2-5:

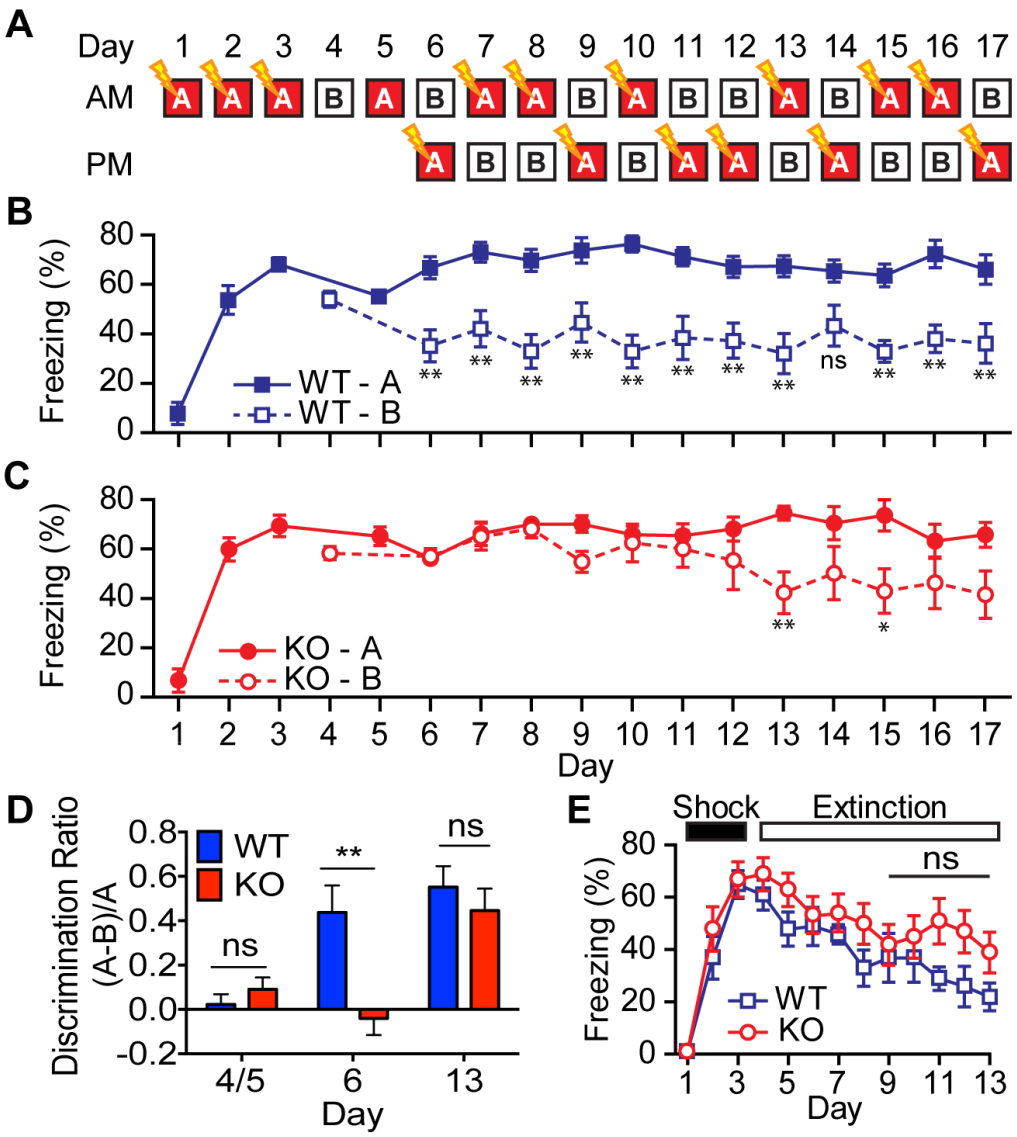

Figure 2-5 Legend: AKAP7 KO animals show impaired contextual discrimination. (A) Experimental protocol to test contextual fear discrimination. Animals were probed for freezing (% time immobile) in either "context A" where they received a single footshock (0.65 mA, 2 sec) (except Day 5, when there was no footshock) or the no-shock "context B", which had a different floor and a striped pattern on one wall. (B) WT animals exhibited a comparable duration of freezing behavior in both contexts on Days 4 and 5, respectively, but by Day 6 and thereafter demonstrated reduced freezing behavior in "context B". (C) KO animals did not begin to discriminate between contexts A and B until Day 13. (D) Discrimination ratio for days 5, 6, and 13 demonstrate differences between WT and KO animals on key days (n=7 animals per group); data are presented as mean ± SEM (Student's unpaired t-test). (E) Following 3 days of footshock delivery only in "context A", AKAP7 KO animals demonstrated only a slight but not significant deficit in contextual fear extinction compared to WT animals (n=6-8 animals per group). Animals were never introduced to "context B."

Figure 2-6:

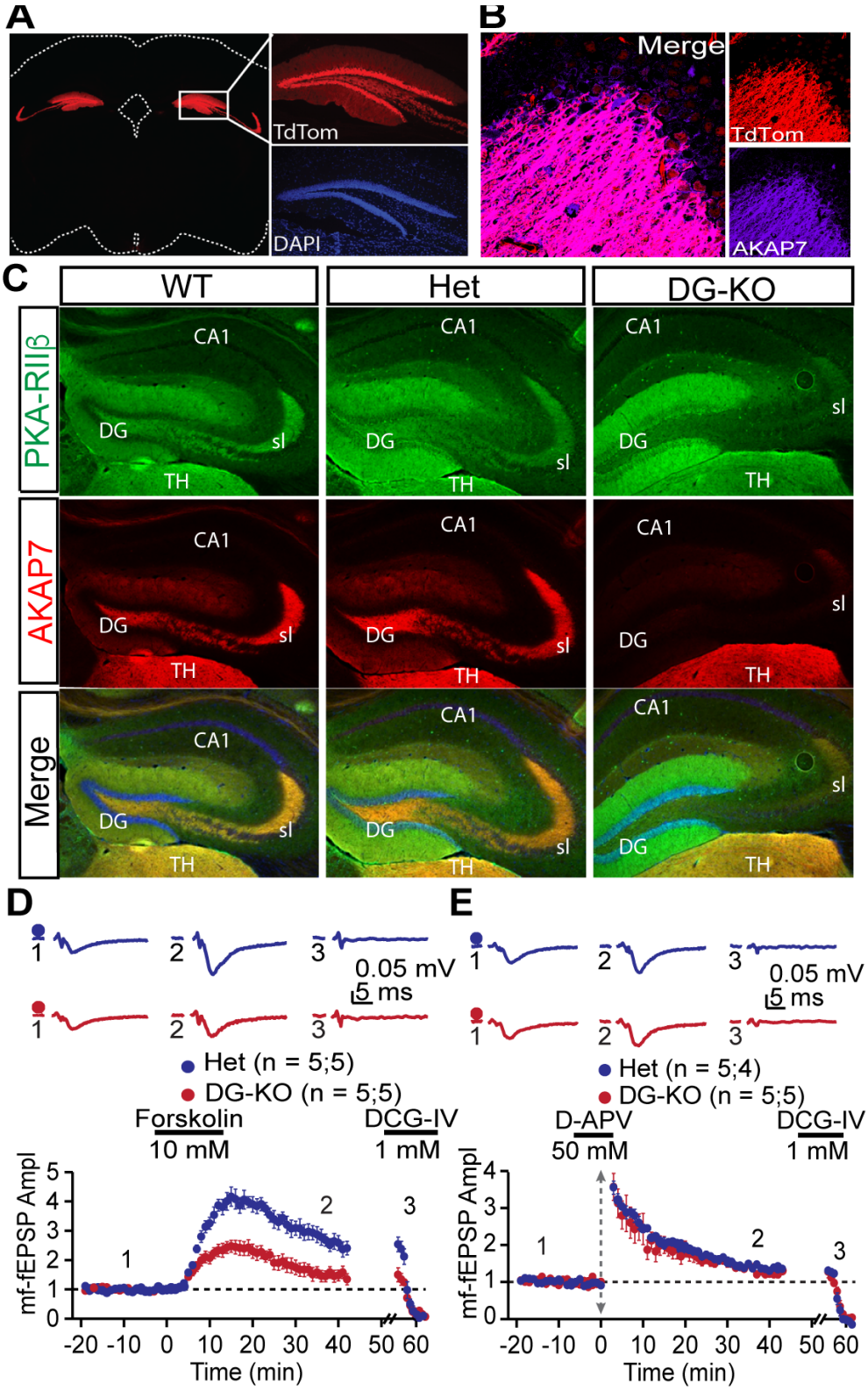
A
TdTom
DAPI
B
Merge
TdTom
AKAP7
C
WT
Het
DG-KO
PKA-RIIβ3
AKAP7
Merge
CA1
DG
sl
TH
D
E
0.05 mV
5 ms
Het (n = 5;5)
DG-KO (n = 5;5)
Forskolin
10 mM
DCG-IV
1 mM
D-APV
50 mM
mf-fEPSP Ampl
Time (min)

Figure 2-6 Legend: DG-KO shows plasticity deficits similar to global KO.
(A) Fluorescent protein TdTomato expression in the hippocampus of *Pomc*$^{+/Cre}$ crossed to TdTomato reporter mice is restricted to dentate granule neurons. (B) Merged image of TdTomato expression and AKAP7 staining show that *Pomc*-Cre was active in the majority of AKAP7-expressing DG neurons. (C) *Pomc*$^{+/Cre}$;*Akap7*$^{Lox/-}$ (DG-KO) animals lose AKAP7 in the dentate gyrus but not the neighboring thalamus (or other brain regions; not shown). PKA-RIIβ is likewise displaced from mossy fibers in DG-KO animals, although some staining is still present in stratum lucidum due to incomplete Cre recombination. *Akap7*$^{Lox/-}$ (Het) animals show AKAP7 expression and PKA-RIIβ distribution comparable to WT (D) FSK-induced MF-LTP is impaired in DG-KO animals, similar to global AKAP7 KO. Het (control): 2.73231 ± 0.24576 of baseline vs. DG-KO: 1.54051 ± 0.1953 of baseline; p = 0.00526 (Student's unpaired t-test). Experimental conditions are as in Figure 6A. (E) Similar to global AKAP7 KO, the DG-KO shows no difference in tetanus-induced MF-LTP compared with Het control. Experimental conditions are as in Figure 4.

Figure 2-7:

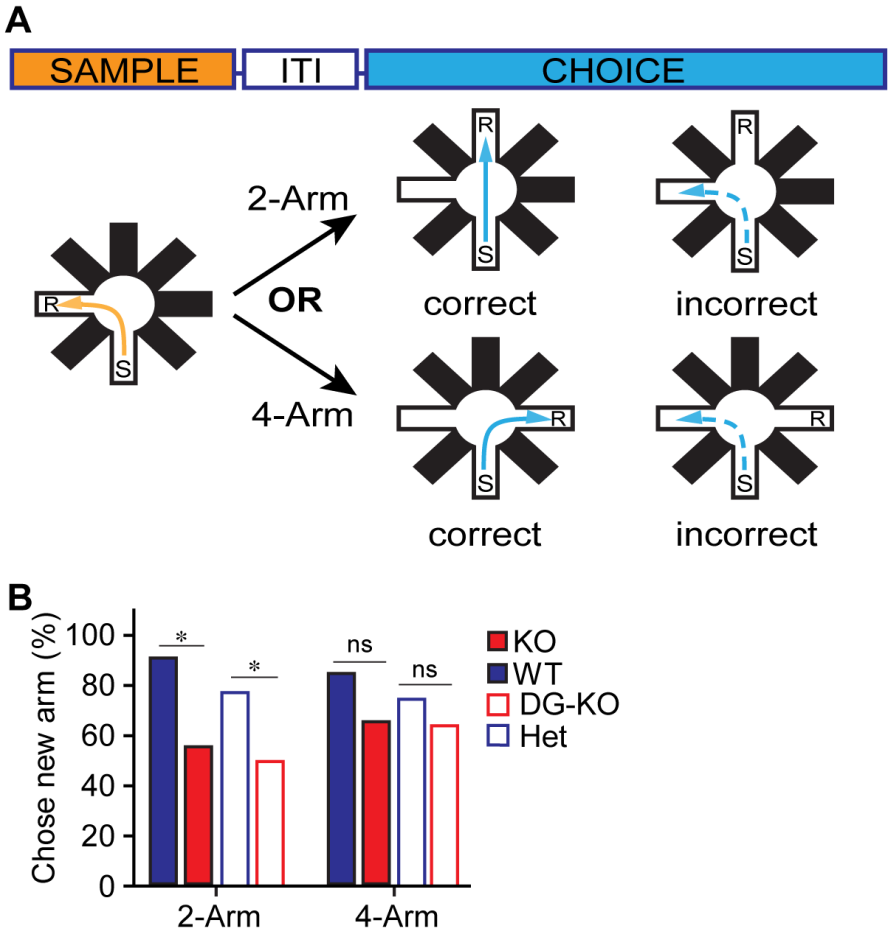

Figure 2-7 Legend: AKAP7KO and DGKO animals demonstrate impaired non-cued spatial pattern separation.
(A) Experimental protocol to test non-cued spatial discrimination by delayed non-matching-to-place using an 8-arm radial arm maze (DNMP-RAM). (B) AKAP7 KO and DG-KO animals discriminate poorly, compared to their respective controls between 2-arm separation, but not the less difficult 4-arm separation, in the DNMP-RAM. (n=7-11 animals per group) (Fisher's Exact test). * $p<0.05$; ** $p<0.01$.

Supplemental Figure 2-1:

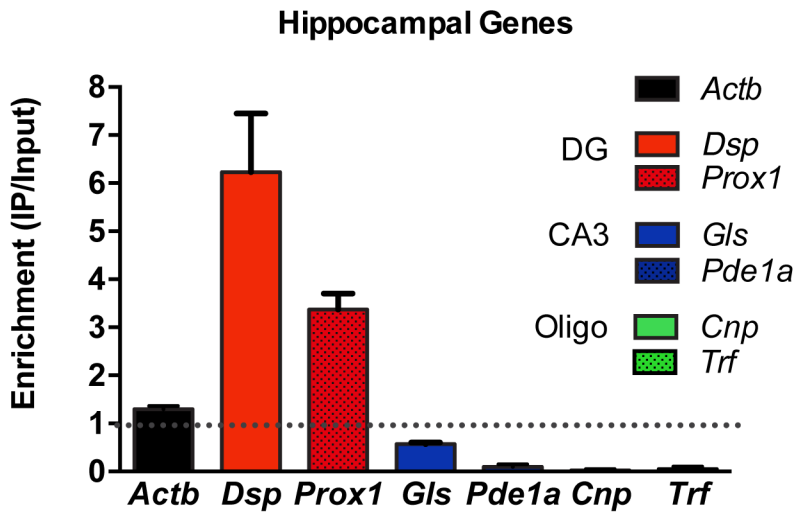

S Figure 2-1 Legend: Validation of DG-specificity of RiboTag Immunoprecipitation (*Related to Figure 2-1*).
RiboTag analysis of actively transcribed mRNA transcripts immunoprecipitated from the DG neurons of *Pomc*-Cre;*Rpl22*$^{ha+/-}$ mice were quantified by qRT-PCR (n=4, mean +/- SEM). Demonstration of enrichment of genes known to be specific to DG neurons compared to de-enrichment of CA3- or Oligodendrocyte-specific transcripts. DG-specific: Desmoplakin (*Dsp)*, Proximal 1 (*Prox1*). CA3-specific: Glutaminase (*Gls*), Phosphodiesterase 1a (*Pde1a*). Oligodendrocyte-specific: CNPase (*Cnp*), Transferrin (*Trf*).

Supplemental Figure 2-2:

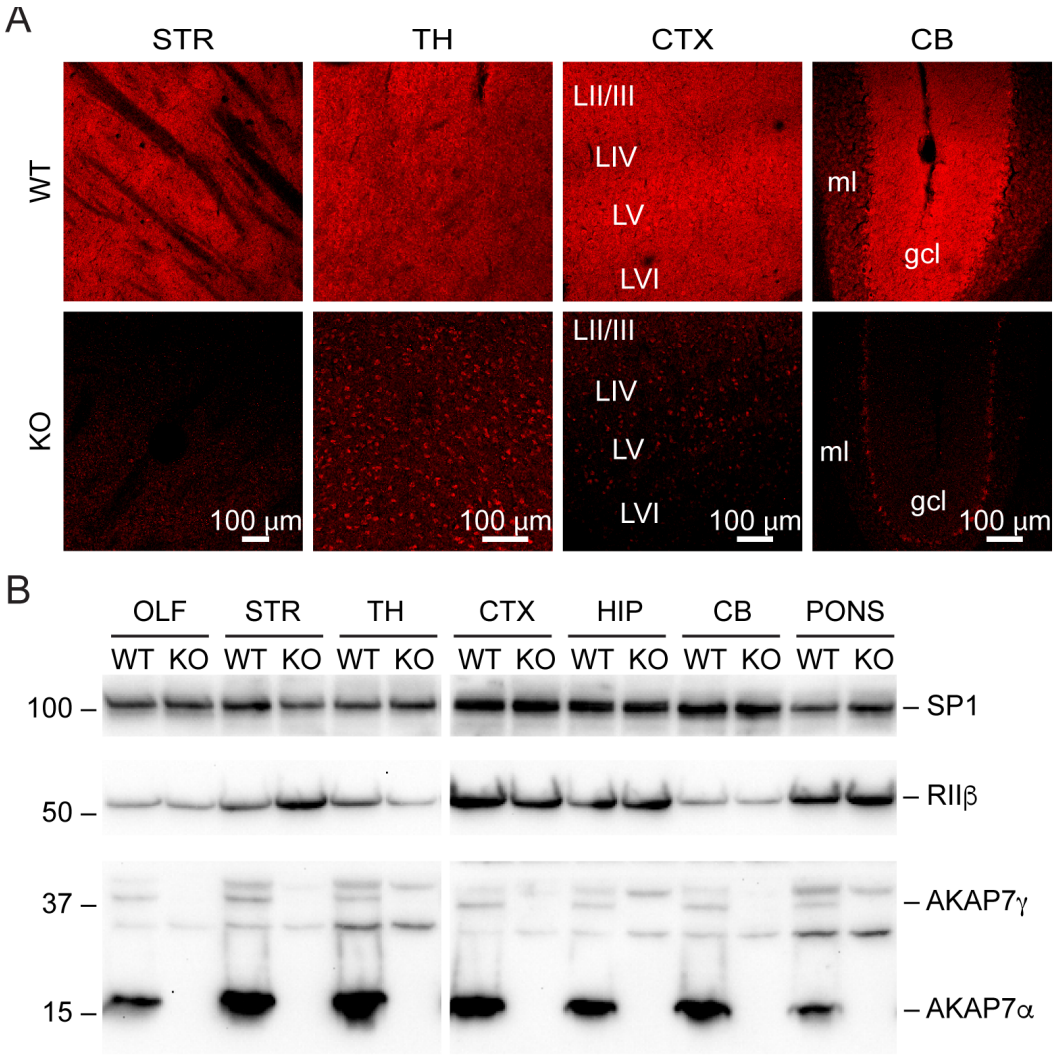

S Figure 2-2 Legend: AKAP7 is widely expressed throughout the brain and in some regions appears restricted to specific neurons. ***(Related to Figures 2-1 and 2-2)*** (A) Immunofluorescence microscopy of AKAP7 as in Figure 1C shows strong, diffuse expression in striatum (STR), thalamus (TH), and cortex (CTX). Expression in cerebellum (CB) is restricted to the granule cell layer (gcl). Non-specific staining is seen in nuclei in KO sections. LII-LVI, cortical layers; ml, molecular layer. (B) Immunoblot of brain region lysates as in Figure 1B showing expression of AKAP7 throughout the brain.

Supplemental Figure 2-3:

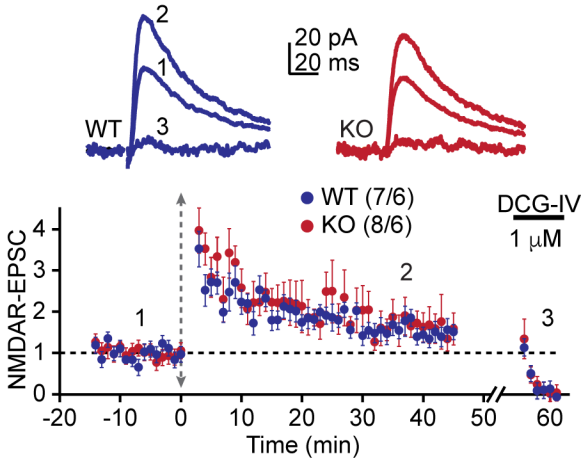

S Figure 2-3 Legend: Whole-cell voltage clamp recordings confirm intact tetanus-induced MF-LTP *(Related to Figure 2-4).*
LTP was induced with a tetanus as in Figure 4. Consistent with the fEPSP recordings, there was also no significant difference in tetanus-induced LTP between AKAP7 WT and KO mice under this recording configuration. Experimental conditions identical to Figure 4.

Supplemental Figure 2-4:

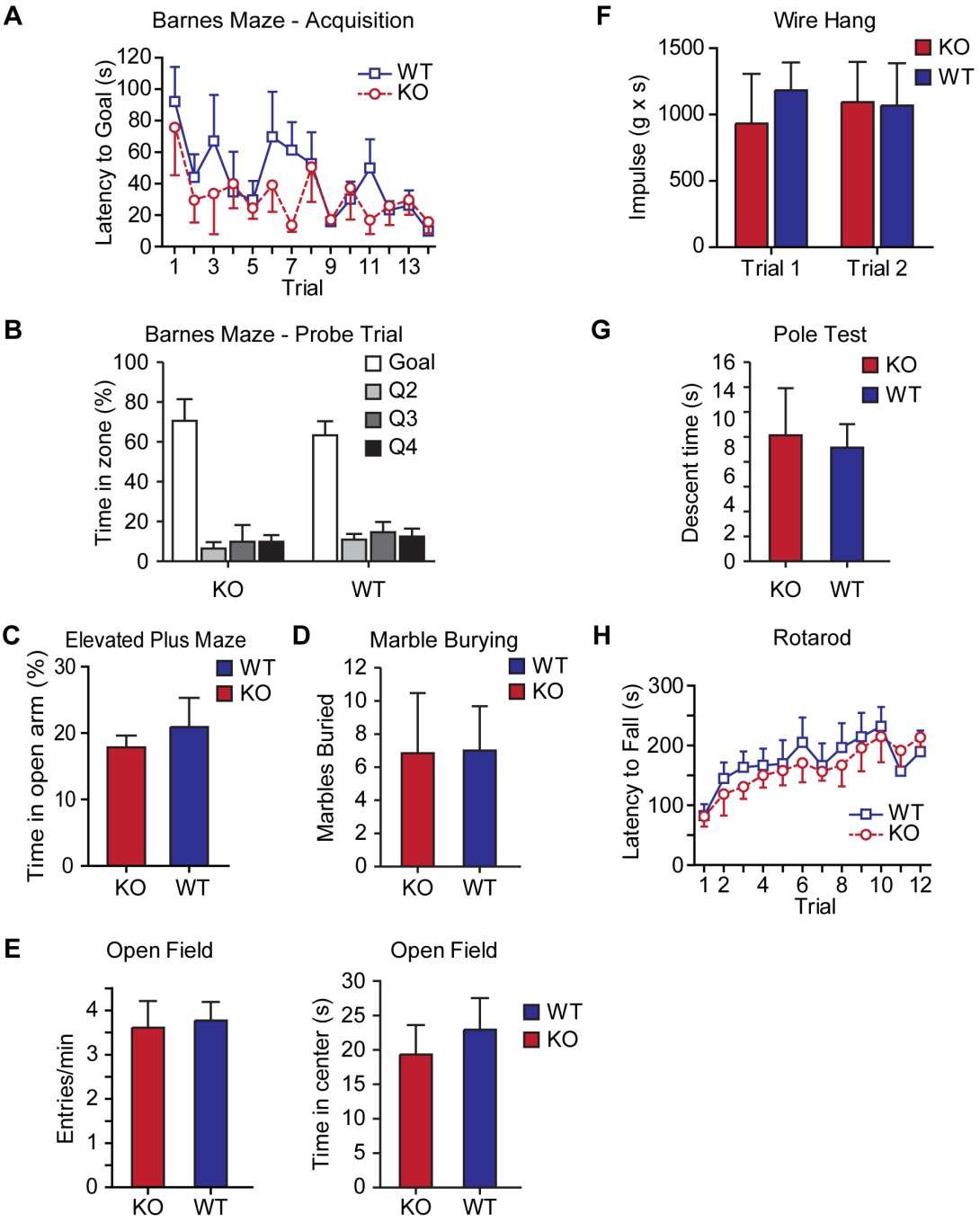

S Figure 2-4 Legend: AKAP7 KO mice show normal spatial learning, anxiety, and motor behaviors *(Related to Figure 5).*

AKAP7 KO mice behave similarly to WT on spatial learning (A-B) Barnes maze (n=4-6 per group), measures of anxiety (C) elevated plus maze (n=12 per group), (D) marble burying (n=13 per group), (E) open field (n=11-13 per group), and motor coordination (F) wire hang (n=13 per group), (G) vertical pole descending (n=9-11 per group), and (H-I) slow- and fast-accelerating rotarod (n=8 per group).

Supplemental Figure 2-5:

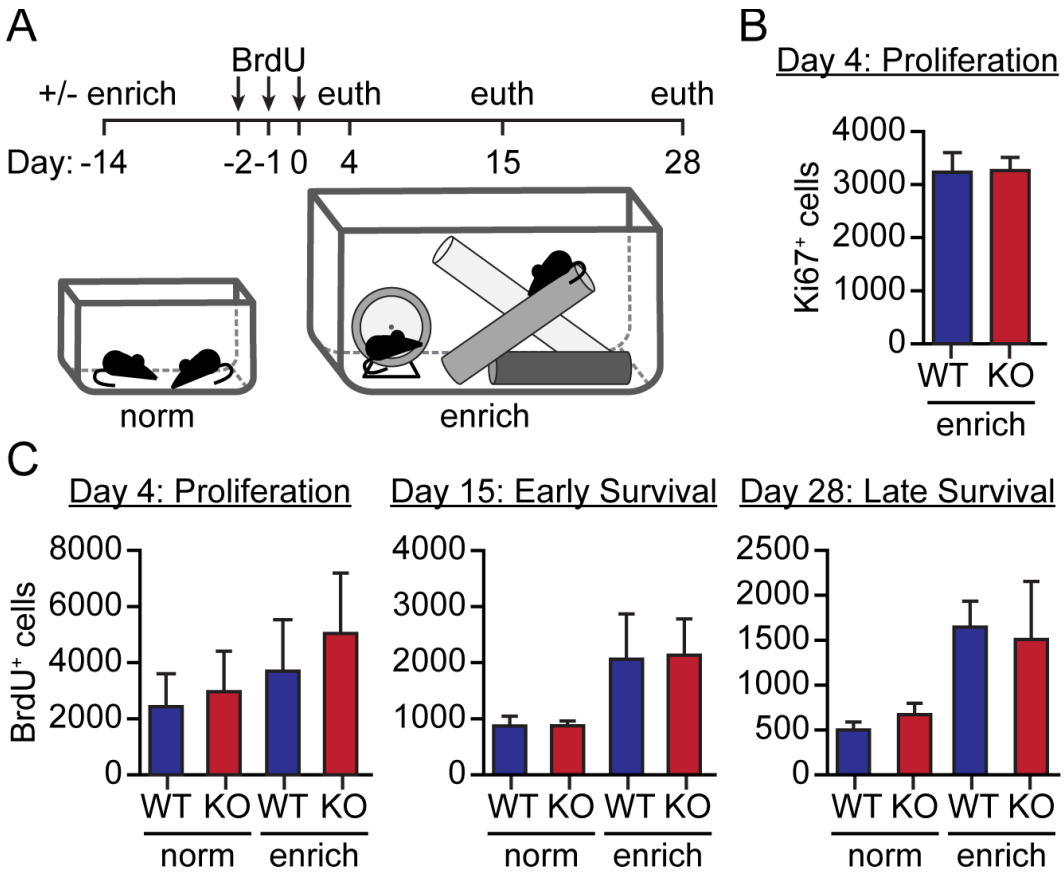

S Figure 2-5 Legend: Adult neurogenesis is normal in AKAP7 KO animals (*Related to Figure 5*). (A) Cartoon of experimental protocol. (B) As a measure of proliferating adult neurogenesis, we stained for Ki67, a protein expressed only in the nuclei of proliferating neurons. We saw no differences in the number of Ki67-positive cells between WT and KO. Cell counts were made for every eighth 35µm section across the entire hippocampus (total cells counts = total count from every 8th section x 8) (n=5 per group). (C) We quantified BrdU-positive neurons in WT and KO mice that had been housed in normal or in enriched cages at multiple timepoints to demonstrate proliferation and maturation of adult born neurons. We found no differences in the number of BrdU-positive cells within the subgranular zone of WT versus KO at any time point (Days 4, 15, 28). Environmental enrichment and exercise promoted neurogenesis equally in both genotypes. These results suggest that adult neurogenesis is not affected by loss of AKAP7 and therefore does not underlie the deficits in discrimination behavior. Cell counts were made for every eighth 35µm section across the entire hippocampus (total cells counts =total count from every 8th section x 8) (n=3-5 per group).

CHAPTER 3: CRTC1 MAY COMPENSATE FOR LOSS OF PHOSPHORYLATED CREB IN A MODEL OF REDUCED PKA ACTIVITY

3.1 ABSTRACT

In the arcuate nucleus of the hypothalamus (ARC), fasting activates PKA in multiple neuronal populations, leading to the phosphorylation of the transcription factor cAMP response element binding protein (CREB). Loss of hypothalamic PKA enhances sensitivity for the "satiety hormone", leptin. Agouti-related peptide (AgRP) expressing neurons of the hypothalamus are first order neurons, receiving peripheral and central hormonal cues; their activation is sufficient to drive the feeding response. The role of PKA signaling in AgRP neuron function is not fully understood. When we specifically inhibit PKA in AgRP neurons by genetic expression of a mutated dominant negative PKA, denoted RIαB, mice lose more weight during a fast and are resistant to diet induced obesity (DIO), without significant differences in feeding behavior. Not surprisingly, AgRP neuron-specific inhibition of PKA leads to deficits in fasting-induced phosphorylation of CREB by PKA (pCREB). There is increasing evidence for a role for CREB-regulated transcriptional co-activator-1 (CRTC1) in central leptin signaling. CREB-regulated transcriptional co-activator-1 (CRTC1) interacts with and enhances CREB mediated gene transcription when CREB is not phosphorylated. Genetic deletion of CRTC1 results in a leptin resistant, obese phenotype. Further, in models of leptin resistance, the nuclear translocation of CRTC1 is impaired. During a fast, CRTC1 is sequestered outside of the nucleus moving to the nucleus when the animal is fed or dosed with leptin. Considering the movement of CRTC1 to the nucleus during the fed state, previous studies have focused on the importance of CRTC1 in pro-opiomelanocortin-expressing (Pomc) neurons, which are active during the fed state. However, we have found CRTC1 also translocates to the nucleus of AgRP neurons during the fed state, when AgRP neurons are less active. In our model of PKA inhibition specifically within AgRP neurons, we have found CRTC1 in the nucleus during both fed and fasted states possibly providing a compensatory role in maintaining CREB-mediated gene transcription. However, after an extended high fat diet (HFD), when leptin resistance is likely, the attenuation of fasting-induced PKA-mediated phosphorylation of CREB in our model is restored. We hypothesize a compensatory role for CRTC1 in maintaining pCREB-regulated gene transcription when PKA is inhibited in the AgRP neuron. Further, we hypothesize that the restoration of pCREB induction on a HFD is due to the onset of leptin resistance and sequestration of CRTC1, leaving CREB open to phosphorylation by other kinases.

3.2 INTRODUCTION

The hypothalamus is a relatively small, evolutionarily conserved region of the brain with highly specialized neuronal populations controlling essential functions such as thermoregulation, fertility, and feeding (Patel et al. 2006; Saper & Lowell 2014). Within the ARC, peripheral nutritional status is sensed by two first order neuronal populations: AgRP and Pomc neurons via the median eminence, a circumventricular organ located immediately proximal to the ARC (Saper & Lowell 2014; Belgardt et al. 2009). The gabaergic AgRP neurons have receptors for hormones with known roles in feeding and body weight regulation including the gut-derived hormone ghrelin (Kohno et al. 2003), which activates the

neuron (Kojima et al. 1999), and leptin, the adipocyte-derived hormone, which inactivates the neuron (Varela & T. L. Horvath 2012; Baver et al. 2014). When leptin signaling is reduced, AgRP neurons drive feeding (Wang et al. 2014; Aponte et al. 2010; Sternson & Atasoy 2014; Baver et al. 2014) and reduce energy expenditure (Tong et al. 2008), by inhibiting downstream afferent targets that induce feelings of satiety (Atasoy et al. 2012). Leptin signaling within gabaergic hypothalamic neurons is dominant despite leptin receptor expression on glutamatergic populations within the paraventricular nucleus (PVH), ventromedial hypothalamus (VMH), and other ARC populations (Vong et al. 2011).

There is consensus in the literature: central leptin signaling counters obesity. If leptin signaling is impaired, obesity is likely to occur. Accompanying this understanding, there is growing evidence that enhanced leptin sensitivity resists diet-induced obesity. We, and others, are finding that cAMP/PKA signaling impacts leptin sensitivity. Increases in cAMP reduce leptin sensitivity (Zhan et al. 2013; Fukuda et al. 2011) and leptin sensitivity is enhanced by the loss of a PKA regulatory subunit (Yang & McKnight 2015), leading to sustained STAT3-mediated gene transcription and a deficit in PKA-mediated phosphorylation of the transcription factor CREB. This evidence leads us to hypothesize reciprocal or antagonistic cross talk between the two signaling pathways. Recent literature supporting this hypothesis found that a supraphysiological increase in cAMP/PKA signaling by a Gs-coupled DREADD receptor, specifically within AgRP neurons, led to a sustained augmentation of the feeding drive (Nakajima et al. 2016) possibly by countering leptin-mediated inhibition of the feeding drive. However, how the two signaling pathways mechanistically counter each other is unclear. This led us to further investigate the mechanistic interaction between PKA and leptin signaling within the AgRP neuron. Specifically, if we impair PKA signaling in AgRP neurons, how will this affect leptin sensitivity and gene expression?

CREB-regulated transcriptional co-activator-1 (CRTC1) appears to be a central player between cAMP/PKA and leptin signaling. CREB-mediated gene transcription commonly requires phosphorylation at serine 133. However, CRTC1 binds CREB lacking this phosphorylation and induces gene transcription. Indeed, when two key pCREB interacting proteins are genetically deleted, preventing pCREB-mediated gene transcription, CRTC1 compensates for the loss and maintains CREB-regulated gene transcription (Kasper et al. 2010). CRTC1 is typically sequestered out in the processes and translocates to the nucleus when intracellular calcium concentrations increase. Leptin leads to CRTC1 translocation to the nucleus and this process is impaired in models of leptin resistance (Altarejos et al. 2008). Further, genetic deletion of CRTC1 leads to leptin resistance and obesity (Altarejos et al. 2008). If CRTC1 can compensate for the loss of pCREB, it may be detected as enhanced leptin sensitivity/signaling.

We have previously investigated the role of PKA in gabaergic AgRP neurons.

Mice with PKA inhibited specifically in these neurons,by genetic expression of a mutated dominant negative PKA (denoted AgRP:RIαB) became resistant to diet induced obesity (DIO) accompanied by an attenuation of fasting-induced CREB phosphorylation specifically within AgRP neurons (Yang & McKnight 2015). In the basal state, the AgRP:RIαB mouse is phenotypically comparable to wild-type (WT), demonstrating equivalent glucose tolerance, serum leptin, and feeding behaviors. However, when

stressed by a fast, AgRP:RIαB mice lose more weight than wild-type controls. Further, despite their resistance to DIO, AgRP:RIαB mice have restored fasting-induced CREB phosphorylation. Considering our hypothesis that CRTC1 might be providing a point of cross talk between leptin and PKA signaling, we found CRTC1 localized to the nucleus during the fasted state in the AgRP:RIαB mouse, possibly providing a compensatory role for the loss of fasting-induced CREB phosphorylation. Further, gene expression changes did not find a clear deficit in CREB-mediated gene transcription, although further analysis is required.

Although this study was not completed, further study could include the following: (1) a demonstration of enhanced leptin sensitivity/signaling in the AgRP:RIαB mouse, (2) the induction of leptin resistance and (3) sequestration of hypothalamic CRTC1 in the AgRP:RIαB mouse following an extended HFD and finally, (4) *in silico* analysis of gene expression changes demonstrating a compensatory role for CRTC1 in maintaining CREB-mediated gene transcription in the AgRP:RIaB mouse.

3.3 RESULTS

PKA-RIαB is expressed and stabilized in AgRP neurons

The activation of PKA requires the binding of two cAMP molecules per regulatory subunit, leading to the release of the catalytic subunits. The dominant cAMP-binding site (B-site) demonstrates greater affinity and retention of bound cAMP
(Woodford et al. 1989; Ogreid et al. 1989) and sterically prevents access to the A-site (Herberg et al. 1996). By mutating a single amino acid within the B-site of PKA-RIα, cAMP binding is reduced by 100-fold (Woodford et al. 1989), inhibiting the dissociation of the catalytic subunit and, because of the dominant role of the B-site in kinase activation, the effect is a dominant negative. We constructed a mutant mouse expressing this gene in a Cre-mediated manner (Willis et al. 2011). Expression of the mutant gene, denoted RIαB, by Cre-mediated excision of an upstream floxed stop codon, leads to cell-specific expression of a dominant negative RIα. We, and others, have utilized this mouse to investigate the role of PKA-mediated signaling in neuronal (Yang & McKnight 2015; Yang et al. 2014), intestinal (Howe et al. 2006), renal (P. E. Gilbert et al. 2001), immune (Salmon et al. 2012), and liver function (Willis et al. 2011).

By crossing a AgRP-Cre-EGFP driver mouse (Padilla et al. 2016) to the RIαB mouse, we were able to express RIαB specifically in AgRP neurons. Comparable to previous work by our lab (Yang et al. 2014), expression of the mutated PKA-RIα led to stabilization of the PKA holoenzyme due to lack of cAMP-induced catalytic subunit dissociation and degradation, visualized as enhanced somatic RIα staining (Figure 3-1).

AgRP:RIαB mice demonstrate normal feeding behavior

The breeding of AgRP-Cre-EGFP mice to RIαB mice produces the $AgRP^{Cre/+;}RI\alpha B^{+/-}$ mice (RIαB ON), and the appropriate control mice: $RI\alpha B^{+/-}$ (RIαB OFF), which are heterozygous for RIα, and

AgRP$^{Cre/+}$ (AgRP-Cre), which are heterozygous for AgRP (Figure 3-2A). To determine differences in food intake and meal patterning, mice were singly housed in BioDaq chambers, capable of providing accurate food consumption measurements every few seconds. All three groups demonstrated normal and comparable feeding parameters on a chow diet, although the number of animals per group was small and combined sexes (Figure 3-2B).

Lack of inhibition by AgRP neurons on populations known to drive satiety in the paraventricular nucleus and parabrachial nucleus (Atasoy et al. 2012) may be demonstrated by alterations in meal patterning; in particular, meal initiation and termination. Our data was insufficient to demonstrate differences in meal patterning or alterations in lights on/lights off food intake (bout number) (Figure 3-3).

AgRP:RIαB mice demonstrate a normal response to ghrelin

Ghrelin is produced by the stomach fundus and signals via the growth hormone secretagogue receptor (GHSR or ghrelin receptor) (Kojima et al. 1999) to activate AgRP neurons, inducing a robust feeding response (Cowley et al. 2003; Wang et al. 2014). The ghrelin receptor is a constitutively active Gq-coupled G-protein coupled receptor (GPCR) (Mear et al. 2013) whose activity is enhanced further by the binding of ghrelin. Receptor activation leads to the release of Gαq/11, stimulating production of phospholipase C (PLC), cleavage of the membrane associated phosphoinositol 4,5 diphosphate (PIP2) and production of inositol-3-phosphate (IP3) and diacylglycerol (DAG). This allows for two mechanisms of calcium release: (1) binding of IP3 to the IP3 receptor on the endoplasmic reticulum (ER) releases intracellular calcium stores, and (2) DAG-mediated activation of protein kinase C (PKC), inhibits potassium channel activity and activates N-type calcium channels, presumably via cAMP/PKA signaling pathways (López Soto et al. 2015; Yin et al. 2014). However, there is a lack of consensus in the literature on this point. To test for attenuation of ghrelin-induced feeding drive, mice were fed overnight and dosed with IP ghrelin during early morning hours when mice are satiated and unlikely to initiate a meal. AgRP:RIαB mice demonstrate comparable induction of feeding in response to ghrelin (Figure 3-4). Therefore, reductions in PKA activity in AgRP neurons do not impact ghrelin-induced feeding.

AgRP:RIαB mice lose more weight following a fast

We were able to recapitulate previous work by our lab demonstrating reductions in fasting-induced phosphorylated CREB (pCREB), a transcription factor and direct target of cAMP/PKA signaling, specifically within AgRP neurons of AgRP:RIαB mice (Yang & McKnight 2015) (Figure 3-5A). Although the AgRP:RIαB mice were comparably induced to feeding by ghrelin, ghrelin receptors are found in other neuronal populations and alterations in AgRP neuron-mediated effects during a fast may still be altered. Previous work has demonstrated enhanced weight loss and delayed weight rebound following a fast in a model of neuropeptide Y (NPY) loss (Patel et al. 2006). We hypothesized that AgRP:RIαB mice might also demonstrate enhanced weight loss and attenuated weight rebound following a fast. Following a 24 hour fast, AgRP:RIαB mice demonstrate enhanced weight loss when singly- or group-housed (Figure 3-

5B), although the time required for them to rebound to pre-fast weight, despite their greater weight loss, was comparable to controls (Figure 3-5C) and immediate post-fast refeeding was comparable to controls (Figure 3-5D). Interestingly, when singly housed, AgRP-RIαB mice demonstrate reduced weight loss compared to group-housed, although still trending toward significantly greater weight loss in both. This is likely due to greater weight reserves in group housed mice as a result of huddling behavior that reduces the energy requirements of body temperature maintenance (Ellacott et al. 2010).

Transcription factors are misregulated in fasted AgRP:RIαB mice

Fasting activates AgRP neurons, inducing the immediate early gene, cFOS (Liu et al. 2012). Considering the deficits in pCREB, we hypothesized comparable reductions in cFOS induction following a fast. However, cFOS induction, both across the arcuate and specifically within AgRP neurons was intact in fasted AgRP:RIαB mice (Figure 3-6).

In neurons, the CREB-regulated transcription co-activator-1 (CRTC1) is localized out in the processes and synapses, anchored to 14-3-3 proteins in an inactive, phosphorylated state (Atasoy et al. 2012; Ch'ng et al. 2012). Upon calcium influx, the phosphatase, calcineurin, removes the phosphate group, releasing CRTC1 to go to the nucleus and enhance CREB-mediated transcription. Importantly, the association of CRTC1 with CREB is dependent upon CREB lacking phosphorylation at Serine-133(Altarejos & Montminy 2011), the site phosphorylated by PKA, among others, and lacking in AgRP:RIαB mice during a fast. Others have shown CRTC1 to act in a compensatory manner in models of inhibited pCREB-mediated transcription (Kasper et al. 2010). This led us to hypothesize a compensatory role for CRTC1 in maintaining CREB-mediated gene transcription in a model of impaired CREB phosphorylation. Interestingly, in wild type mice, we found that CRTC1 is localized in the nucleus of AgRP neurons in the fed state, but not the fasted state, when AgRP neurons are activated (Belgardt et al. 2009) (Figure 3-7). Importantly, in the AgRP:RIαB mouse, CRTC1 is maintained in the nucleus of AgRP neurons during both fasted and fed states (Figure 3-8), providing initial support for our hypothesis that it is compensating for reduced pCREB-mediated gene transcription.

Fasting induction of pCREB is restored following high fat diet

Previous work by our lab found that the AgRP:RIαB mouse was resistant to diet-induced obesity (Yang & McKnight 2015). We were able to recapitulate this and found significant differences in weight gain by 10 weeks of exposure to a high fat diet (HFD) (Figure 3-9A). However, when we repeated our immunohistochemistry for pCREB in fasted WT and AgRP:RIαB mice after 12 weeks on the HFD, we found that fasting-induced increases in pCREB were restored in the AgRP:RIαB mice (Figure 3-9B) without any differences in normal feeding parameters (Figure 3-9C). This led us to consider previous work demonstrating impaired CRTC1 nuclear translocation in models of impaired leptin signaling (Kasper et al. 2010; Altarejos et al. 2008). After 12 weeks on a HFD, WT mice demonstrate central leptin resistance (Altarejos et al. 2008; Balland & Cowley 2015). If leptin resistance is present in the AgRP:RIαB mice after

12 weeks on a HFD, CRTC1 may be sequestered at the membrane, exposing Serine 133 on CREB to other kinases known to also phosphorylate this site (Altarejos et al. 2008; Xing et al. 1998). Future experiments to test this would include immunohistochemistry for CRTC1 in both fed and fasted mice on HFD, complemented by immunoblotting of hypothalamic extracts from corresponding groups demonstrating sequestration of CRTC1 in its phosphorylated state.

Gene expression differences in AgRP neurons expressing RIαB

Considering the alterations in pCREB and CRTC1 during both fed and fasted states, we hypothesized differences in gene expression in AgRP neurons expressing the dominant negative PKA in response to feeding related cues. A breeding schema produced triple cross AgRP-Cre$^{+/-}$;RiboTag$^{+/-}$;RIαB$^{+/-}$ mice expressing RiboTag and RIaB specifically within AgRP neurons. The cross also produced AgRP-Cre$^{+/-}$;RiboTag$^{+/-}$ controls (Figure 3-10A). By expressing the RiboTag allele specifically within AgRP neurons, we were able to immunoprecipitate AgRP-specific, polysome-associated transcripts (Sanz et al. 2009) from our mutant and control mice and compare them to total hypothalamic RNA (Input). A scatterplot of microarray data demonstrates intact *AgRP* and *Npy* expression and enrichment in both mutant and WT AgRP-specific IP samples vs. Input (Figure 3-10B).

Analysis of microarray data demonstrates differences in enriched genes between WT and mutant mice during both fasted and fed states (IP/Input enrichment) (Tables 3-1 thru 4). We next queried which genes demonstrated the greatest difference in fasting-induced genes between WT and mutant mice. By comparing the genes induced by fasting between WT and mutant mice, we found five genes (*Cited1, Foxq1, Rrad, Sdk2, Rbp2*, and *Ghsr*) which were highly induced by fasting in WT AgRP neurons that were not induced in mutant AgRP neurons and three genes (*Serpina3n, Bclaf1*, and *Lrrc29*) that were more highly induced by fasting in mutant AgRP neurons (Figure 3-10C and Tables 3-5 and 3-6). However, validation of differences by immunoblotting found confirmation of differences in CITED1, but not the ghrelin (GHSR) or Pacap receptor (Pac1R) (Figure 3-11). Cited1 was highly induced in WT mice by fasting and this was reversed in both gene expression and protein, although this must be validated by further study. Previous literature has found that Cited1 enhances CBP/p300 interactions with phosphorylated CREB (Shi et al. 2006). However, a role for Cited1 in body weight regulation has not been described.

3.4 DISCUSSION

The adipocyte-derived hormone, leptin, signals peripherally and centrally to promote body weight homeostasis. Central leptin signaling reduces food intake and increases energy expenditure, regulating energy balance. Reduced leptin sensitivity and, ultimately, central resistance to leptin are well-characterized symptoms of metabolic disorders. Targets of central leptin signaling include populations in the ARC, PVH, VMH, DMH, and lateral hypothalamus. Recent studies have demonstrated a dominant

role for leptin signaling in gabaergic hypothalamic neurons (Vong et al. 2011; Yang & McKnight 2015). Recent work by our lab has demonstrated a role for cAMP/PKA signaling as counter to leptin signaling, with the loss or inhibition of PKA signaling enhancing leptin sensitivity and reducing adiposity, particularly in gabaergic hypothalamic neurons in the lateral hypothalamus and ARC (Yang & McKnight 2015). As part of this previous work, we published a model of PKA inhibition in AgRP neurons and found a deficit in fasting-induced phosphorylation of CREB (pCREB), a PKA substrate, and a resistance to diet-induced obesity (DIO) (Yang & McKnight 2015). The goal of the current study was to add to this previous work and to validate the specificity of our finding by using an AgRP-Cre with less ectopic expression (Padilla et al. 2016). Indeed, our current study validated the model's resistance to DIO and attenuated fasting-induced pCREB. However, differences in cFOS induction presented in our previous study could not be recapitulated and were intact.

A more in-depth study of food intake found no significant differences in meal patterning, although animal numbers were low and not separated by sex. Further phenotyping found retention of ghrelin-induced feeding and comparable glucose tolerance and serum leptin. Despite these similarities, we found that the loss of PKA signaling in AgRP neurons enhances weight loss during a fast, without impacting rebounding weight gain or feeding. Interestingly, when placed on an extended HFD, fasting-induced pCREB was restored in the AgRP:RIaB mouse and the enhanced fast-induced weight loss during a fast was ameliorated. We also found significant differences in fasting-induced gene expression between the mutant and wild-type (WT).

There is growing support for a link between leptin sensitivity in the arcuate nucleus (ARC) and coactivator of CREB-mediated transcription-1 (CRTC1). Increases in serum leptin, either during the fed state or following a leptin injection, induce CRTC1 nuclear localization. In addition, in a model of defective leptin signaling, the *ob/ob* mouse, CRTC1 is sequestered outside of the nucleus in both fed and fasted states. However, a leptin injection induces nuclear translocation. (Altarejos et al. 2008). Linking CRTC1 to PKA signaling, CRTC1 is also a co-activator of CREB-mediated gene transcription, enhancing the association of CREB with the TFIID transcriptional machinery when CREB is not phosphorylated (Willis et al. 2011; Altarejos & Montminy 2011; Okuno 2011).

We have found CRTC1 is localized to the nucleus of AgRP neurons, and other ARC populations in the fed state, and is sequestered outside of the nucleus during the fasted state, in conflict with previous characterization as activity-dependent (Altarejos & Montminy 2011). Phosphorylated CRTC1 is associated/anchored/sequestered by 14-3-3 proteins outside of the nucleus (Screaton et al. 2004). When intracellular calcium increases, the calcium-activated phosphatase calcineurin, is activated, removing the phosphate group from CRTC1 and leading to its nuclear translocation. cAMP/PKA complement calcium/calcineurin activation of CRTC1 by inhibiting the kinase responsible for phosphorylating CRTC1, salt-inducible kinase-1 (Ch'ng et al. 2012). Considering cAMP and calcium increase when a cell is in an "active" state, previous studies demonstrating nuclear localization of CRTC1 (Altarejos et al. 2008) and CRTC2 (Lerner et al. 2009) in the arcuate nucleus (ARC) during the fed state focused on Pomc neurons,

expected to be active during the fed state. Looking at their work critically, their labeling of Pomc neurons by *in situ* histology was not as definitive as our AgRP-Cre-EGFP expression, although we do see CRTC1 movement to the nucleus in populations other than AgRP neurons.

Just as we saw CRTC1 movement to the nucleus of ARC neurons in the fed state, we also see pCREB induction in the fasted state in the majority of ARC neurons, further muddying the on/off activity states for ARC populations. How then should we think about the "activity" states of ARC neurons and the relative activation/movement of CREB and CRTC1? Perhaps CREB and CRTC1 are reciprocal partners? Further studies may provide clarity on this subject. Indeed, recent work found AgRP neuron activity, as measured by calcium signaling, does not correlate with a temporally delayed upswing of leptin following a meal, but rather, terminates upon presentation of food and is restored shortly after removal of presented but inaccessible food (Chen et al. 2015).

Finally, in our model of PKA inhibition and attenuated fasting-induced pCREB, CRTC1 is retained in the nucleus during the fasted state. This led us to hypothesize a compensatory role for CRTC1 in maintaining CREB-mediated gene transcription, considering the reductions in pCREB present in our model and previous studies demonstrating CRTC1 compensation for deficits in pCREB-mediated gene transcription (Kasper et al. 2010). Indeed, when we knock out another regulatory subunit of PKA, RIIβ, we see strong upregulation of activated CRTC1 in hypothalamic extracts during a fast (data not shown).

As a further point of interest, despite the significant reductions in fasting-induced CREB activation in the AgRP:RIαB mouse when on a normal chow diet, after consuming a HFD for an amount of time capable of inducing leptin resistance in WT mice (Townsend et al. 2008), fasting-induced activation of CREB was restored. It is possible that AgRP:RIαB mice have also developed leptin resistance and CRTC1 is now sequestered outside of the nucleus. This might leave CREB open to phosphorylation by other kinases.

How leptin and PKA signaling pathways cross talk and if it is truly reciprocal requires further study. Clarification of the relationship between leptin, CRTC1, and CREB signaling may provide a pharmacological target in models of obesity and leptin resistance.

3.5 EXPERIMENTAL PROCEDURES

Animal Care: All procedures were approved by the Institutional Animal Care and Use Committee of the University of Washington and conformed to NIH guidelines. Mice were given access to food pellets and water ad libitum, and maintained on a 12:12-hr light/dark cycle. Generation of RIαB and RiboTag mice were described previously (Willis et al. 2011; Sanz et al. 2009). AgRP-Cre mice were generously donated by the laboratory of Richard Palmiter (Padilla et al. 2016). We generated AgRP-specific expression of RIαB by crossing AgRP-Cre$^{+/-}$ to RIαB$^{+/-}$ animals to obtain AgRP-Cre$^{+/-}$, RIαB$^{+/-}$ (RIaB OFF) and AgRP-Cre$^{+/-}$;RIαB$^{+/-}$ (RIaB ON) offspring. Triple cross AgRP-Cre$^{+/-}$;RiboTag$^{+/-}$;RIαB$^{+/-}$ mice were generated by crossing RIαB+/- mice to RiboTag+/+ mice to generate RiboTag$^{+/+}$;RIαB$^{+/-}$ mice after two crosses. The offspring of this cross were then mated to AgRP-Cre$^{+/+}$ mice to generate appropriate offspring and

controls in 50:50 ratio.

Feeding Behavior: To determine differences in food intake parameters, normal feeding and re-feeding responses, meal patterning, and alterations in sensitivity to the hormones leptin and ghrelin, mice were singly housed in BioDaq chambers (Research Diets, Inc.). Body weights were measured weekly. Mice were fasted for 36 hours or fed ad lib. Acylated ghrelin peptide (Tocris) was dissolved in sterile 0.9% saline for injection (Hospira) and dosed at 500 mg/kg, i.p For experimental measurements, mice were habituated to BioDaq cages for at least seven days. Data output from BioDaq Feeding records were analyzed using BioDAQ Viewer Software. A feeding bout (>0.01g minimum) was defined as a meal if 0.06 g of food was ingested and if it was separated from another meal by an intermeal interval (IMI) >300s.

Serum leptin and blood glucose measurements: To measure basal blood glucose, mice were rehoused in a clean cage. After five hours in the clean cage, blood glucose measurements were taken by tail bleed. On the following day, mice were again rehoused for five hours and then dosed with an IP dextrose bolus and blood glucose measurements were taken by tail bleed at t=15, 30, 60, 90, and 120 min. Blood glucose values were determined by Accu-Chek glucometer (Aviva). Serum leptin measurements were made by ELISA assay kit (Abcam).

Immunohistochemistry and Imaging: Brains were fixed and processed for standard immunohistochemistry. Primary antibodies included goat anti-cFOS (Santa Cruz, 1:1000), chicken anti-GFP (1:10,000), rabbit anti-pCREB (1:300), and rabbit anti-CRTC1 (Bethyl Laboratories, 1:200). Fluorescent secondary antibodies were utilized to visualize primary antibodies (Molecular Probes). Coverslips were mounted with Fluoromount G with DAPI (Electron Microscopy Sciences). Slides were imaged in the University of Washington Keck Microscopy Center on a Leica SL confocal microscope.

RiboTag isolation and analysis of mRNA transcripts: RiboTag experiments were performed as described (Sanz et al., 2009). To isolate AgRP-specific transcripts, mice were sacrificed and the hypothalamic were rapidly dissected and flash frozen. In order to provide a reasonable amount of RNA, dissected hypothalami were pooled into groups of two females and two males, to obscure sex differences. Tissue samples were dounce homogenized in a buffer supplemented with RNase inhibitors. Polysomes were immunoprecipitated using antibodies to HA (Covance) and protein A/G-coupled magnetic beads (Pierce BioTechnologies). Total hypothalamic (Input) and immunoprecipitated (IP) RNA were quantified by Quant-It RiboGreen (Life Technologies). Isolated RNA was then amplified and hybridized to a microarray chip for analysis. Gene expression analysis was done will be done *in silico* (Genome Studio, Gene Ontology databases). Quantitative reverse transcriptase-PCR was performed using SYBR green One-Step (Agilent). Oligonucleotides for the validation of the microarray hits were selected using the PrimerBank database (https://pga.mgh.harvard.edu/primerbank/): BCL2-associated transcription factor 1 (*Bclaf1)*: For: 5'- ACTCACCACGAGATGAAAGACT -3', Rev: 5'-TGTCCCAGCAAAAACTCCTCT-3', Cbp/p300-interacting transactivator with Glu/Asp-rich carboxy-terminal domain 1 (*Cited1*): For: 5' AACCTTGGAGTGAAGGATCGC -3', Rev: 5'-GTAGGAGAGCCTATTGGAGATGT -3', Pleiomorphic Adenoma Gene-Like 1 (*Plagl1*): For: 5'-

ATGGCTCCATTCCGCTGTC -3', Rev: 5'- CTCAGCCTTCGAGCACTTGAA -3', Cyclin-Dependent Kinase Inhibitor 1A (*Cdkn1a*): For: 5'- CCTGGTGATGTCCGACCTG -3', Rev: 5'- CCATGAGCGCATCGCAATC -3', CNPase (*Cnp*): For: 5'-TTTACCCGCAAAAGCCACACA-3', Rev: 5'- CACCGTGTCCTCATCTTGAAG-3', Pituitary adenylate cyclase activating peptide receptor 1 (*Adcyap1r1*): For: 3'-TACTGTGTGTGTAACTGTGTGGG -3', Rev: 5'- GCCAGCCGTAAGTAGATGCTC -3', Agouti-related peptide (*AgRP*): For: 5'-TAGATCCACAGAACCGCGAGT-3' Rev: 5'-GAAGCGGCAGTAGCACGTA-3'

Immunoblotting: Hypothalami were rapidly dissected and homogenized directly in 1X NuPage LDS solution (ThermoFisher Scientific). Blotting was performed according to standard methods. Antibodies used were as follows: rabbit anti Pac1R (Alomone laboratories), Rabbit anti Rgs2 (Santa Cruz), rabbit anti-Cited1 (Santa Cruz), rabbit anti-pCREB (BD Biosciences), mouse anti-pPKA-RIIβ (BD Biosciences), rabbit anti-GHSR (Alomone laboratories), rabbit anti-Foxq1 (Santa Cruz), rabbit anti-RIa (Santa Cruz), mouse anti-dynamin1 (Abcam), and rabbit anti-CRTC1 (Torc1) (Bethyl Laboratories). Immunoblots were developed using SuperSignal West Pico Chemiluminescent Substrate (Thermo Fisher Scientific) and imaged using a ChemiDoc Touch Imaging System (BioRad).

CHAPTER 3: FIGURES

Figure 3-1

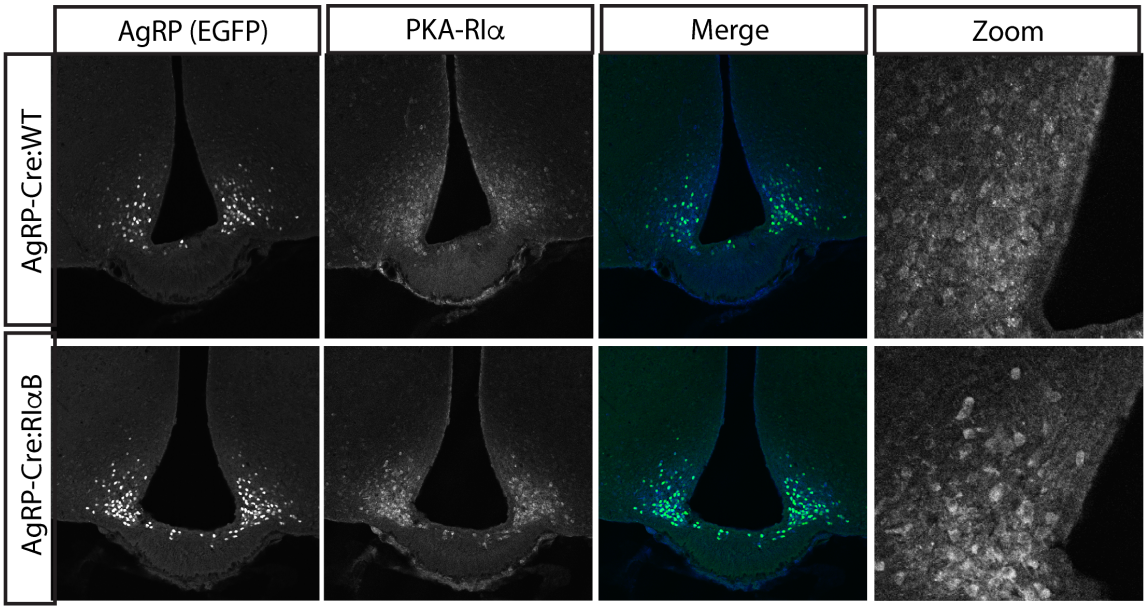

Figure 3-1 Legend: PKA-RIαB is expressed and stabilized in AgRP neurons
Low magnification of arcuate nucleus AgRP neurons shows labeling by expression of EGFP. Immunohistochemistry of PKA-RIα reactivity demonstrates localization to arcuate neurons. Zoomed image of PKA-RIα staining demonstrates expected increases in RIα protein.

Figure 3-2:

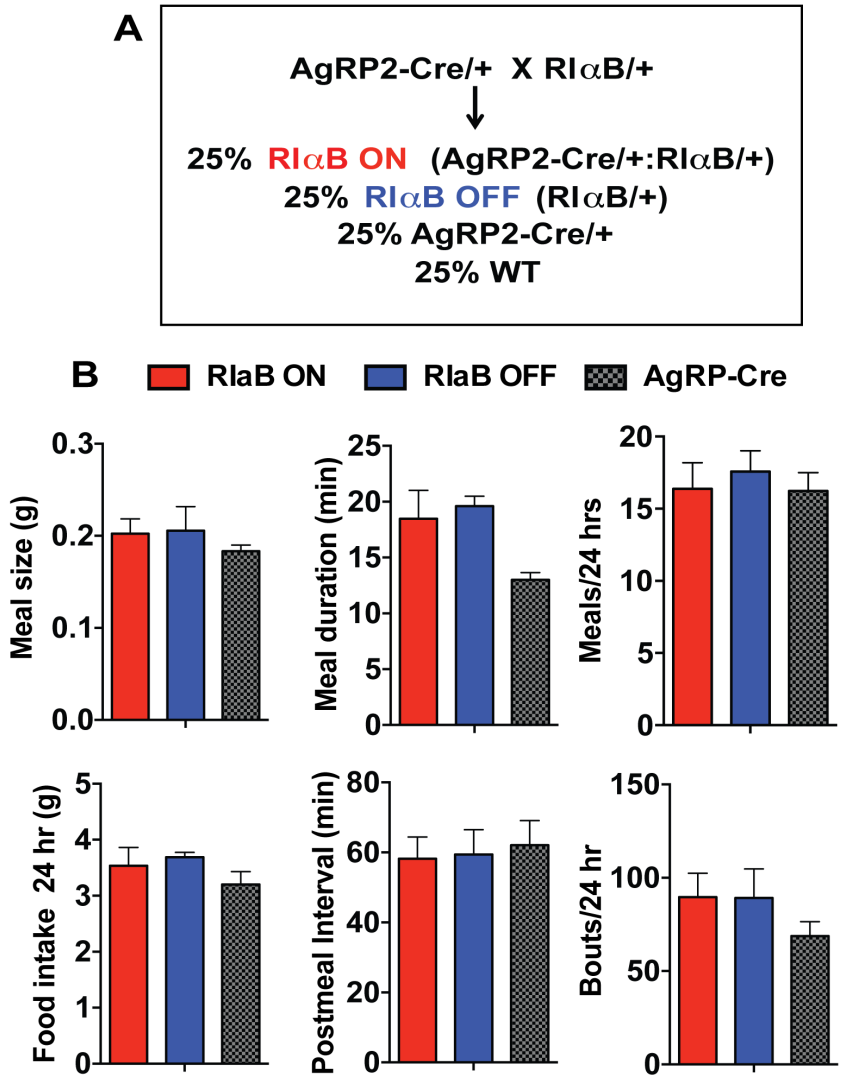

Figure 3-2 Legend: Breeding scheme and Chow diet food intake parameters.
(A) Diagram of breeding scheme to clarify nomenclature of animals utilized in this study. Wild-type mice were not included. (B) Food intake parameters measured across a 72-hour period were comparable between three groups of mice. (RIαB ON, n=5; RIαB OFF, n=4; AgRP-Cre, n=3)

Figure 3-3:

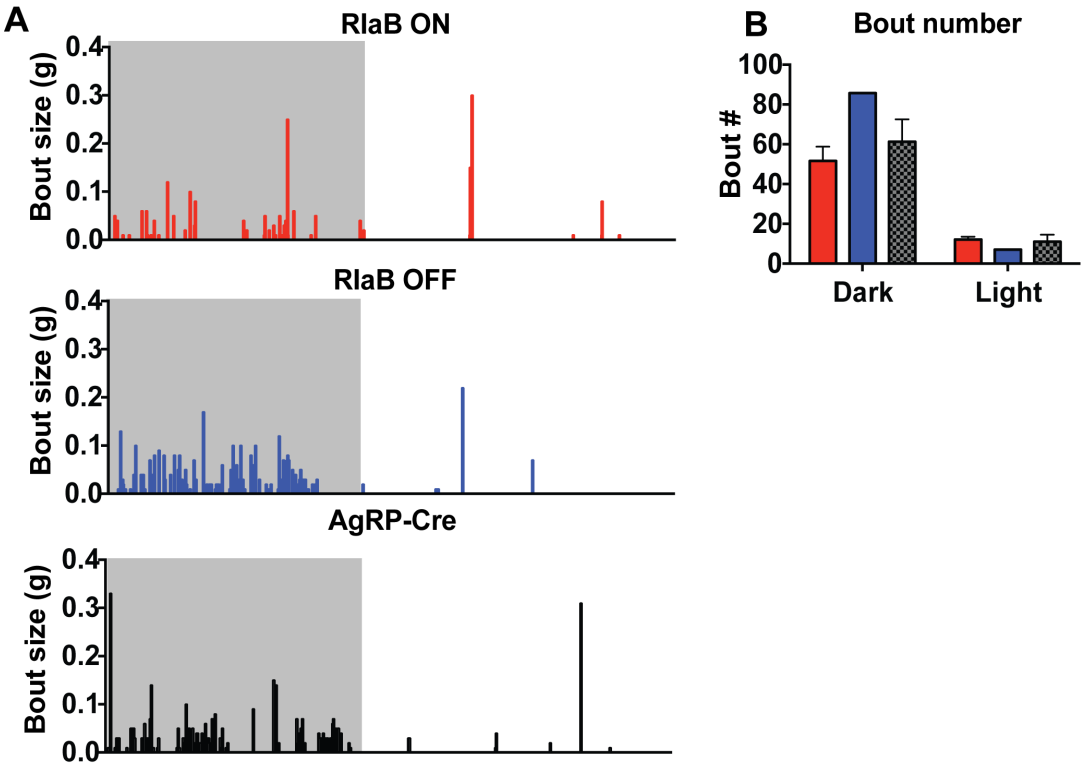

Figure 3-3 Legend: Meal patterning
(A) Meal-pattern analysis was obtained from bout size recordings using set meal parameters. (B) Separation of bout number into light and dark phases for males only (RIαB ON, n=3; RIαB OFF, n=1; AgRP-Cre, n=2).

Figure 3-4:

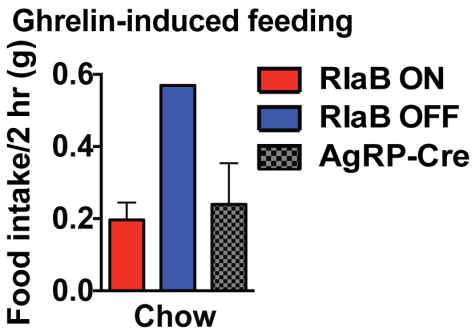

Figure 3-4 Legend: Ghrelin-induced feeding
Mice were dosed with IP ghrelin within one hour of start of light phase to determine ghrelin responsiveness while in a satiated state (RIαB ON, n=6; RIαB OFF, n=1; AgRP-Cre, n=5).

Figure 3-5:

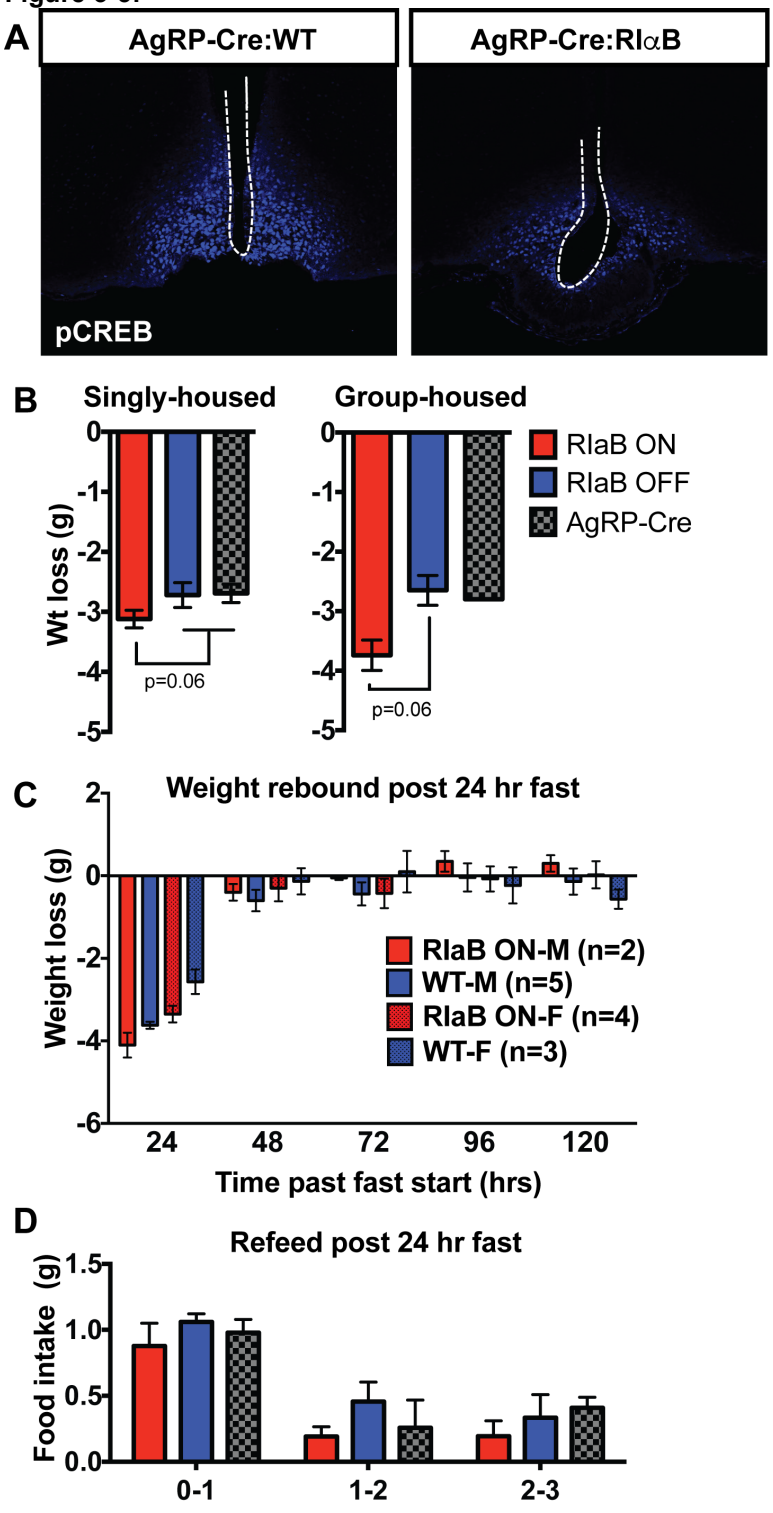
A
AgRP-Cre:WT
AgRP-Cre:RIαB
pCREB
B
Singly-housed
Group-housed
Wt loss (g)
0
-1
-2
-3
-4
-5
p=0.06
p=0.06
RIaB ON
RIaB OFF
AgRP-Cre
C
Weight rebound post 24 hr fast
Weight loss (g)
2
0
-2
-4
-6
RIaB ON-M (n=2)
WT-M (n=5)
RIaB ON-F (n=4)
WT-F (n=3)
24
48
72
96
120
Time past fast start (hrs)
D
Refeed post 24 hr fast
Food intake (g)
1.5
1.0
0.5
0.0
0-1
1-2
2-3

Figure 3-5 Legend: Phenotyping of behaviors related to fasting response on Chow diet.
(A) Immohistochemistry of arcuate nucleus of fasted AgRP-Cre:WT and AgRP-Cre:RIαB mice (RIαB ON) for induction of phosphorylated CREB (pCREB). (B) Fasting-induced weight loss between groups when singly housed for at least ten days (RIαB ON, n=10; RIαB OFF, n=5; AgRP-Cre, n=11; Student's t-test) or when group housed (RIαB ON, n=5; RIαB OFF, n=2; AgRP-Cre, n=1; Student's t-test). (C) Animals were weighed daily for five days following a 24 hour fast to test for a delay in weight rebound and separated by sex (Males: RIαB ON, n=2, WT/AgRP-Cre, n=5; Females: RIαB ON, n=4, WT/AgRP-Cre, n=3). (D) Food intake separated into 1-hour bins following reintroduction of food following a 24 hour fast (RIαB ON, n=5; RIαB OFF, n=3; AgRP-Cre, n=3; Student's t-test).

Figure 3-6:

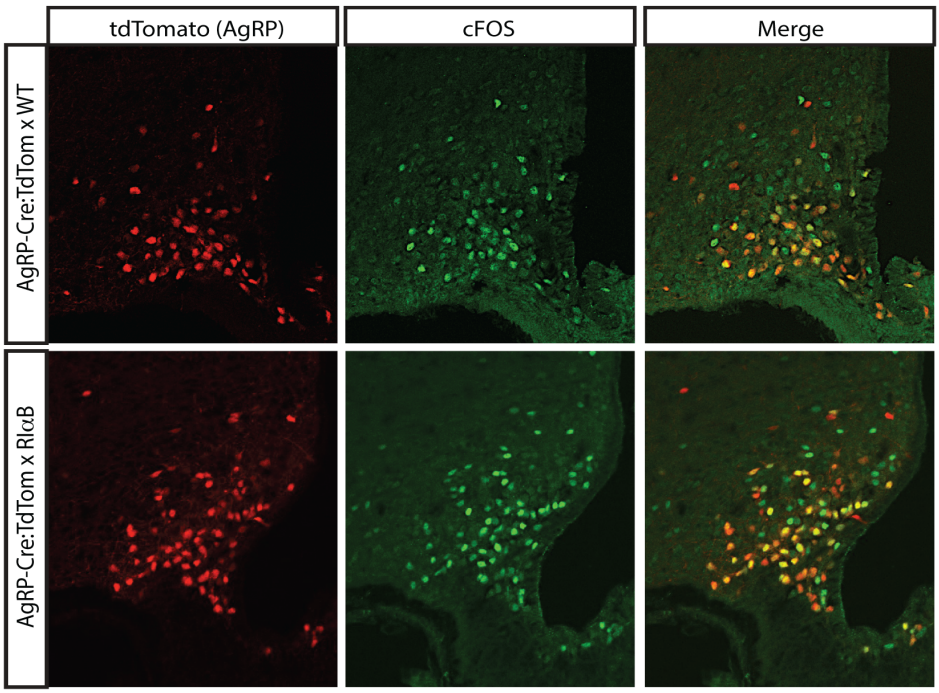

Figure 3-6 Legend: Fasting induction of cFOS in arcuate nucleus.
Immunohistochemical analysis of arcuate nucleus sections from AgRP-Cre:TdTom:WT and AgRP-Cre:TdTom:RIαB mice for cFOS reactivity following a 24 hour fast.

Figure 3-7:

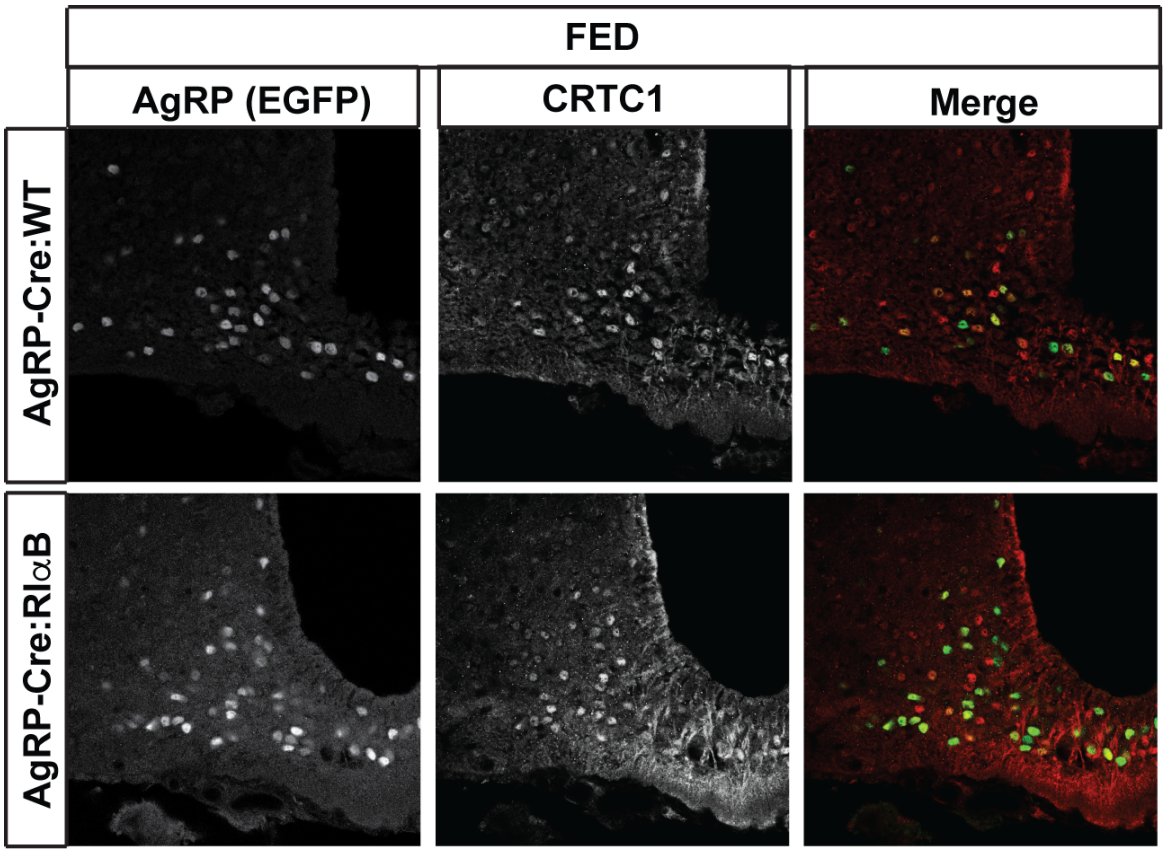

Figure 3-7 Legend: CRTC1 colocalization during FED state.
Immunohistochemical analysis of arcuate nucleus sections from AgRP-Cre:WT and AgRP-Cre:RIαB mice for CRTC1 and EGFP reactivity (AgRP neuron) within 20 minutes of start of light phase. CRTC1 is localized to nucleus of multiple arcuate populations including AgRP neurons.

Figure 3-8:

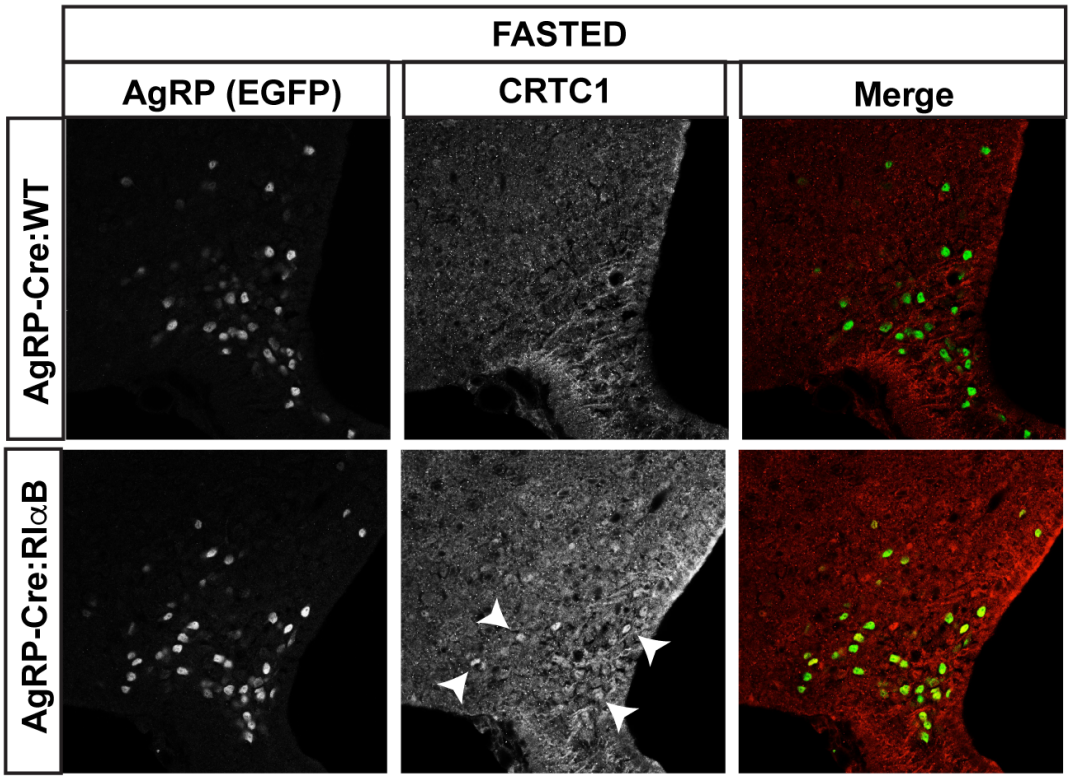

Figure 3-8 Legend: CRTC1 colocalization during FED state.
Immunohistochemical analysis of arcuate nucleus sections from AgRP-Cre:WT and AgRP-Cre:RIαB mice for CRTC1 and EGFP reactivity (AgRP neuron) following a 24 hour fast. CRTC1 nuclear localization in multiple neuronal populations of the arcuate nucleus including AgRP neurons in AgRP-Cre:RIαB mice.

Figure 3-9:

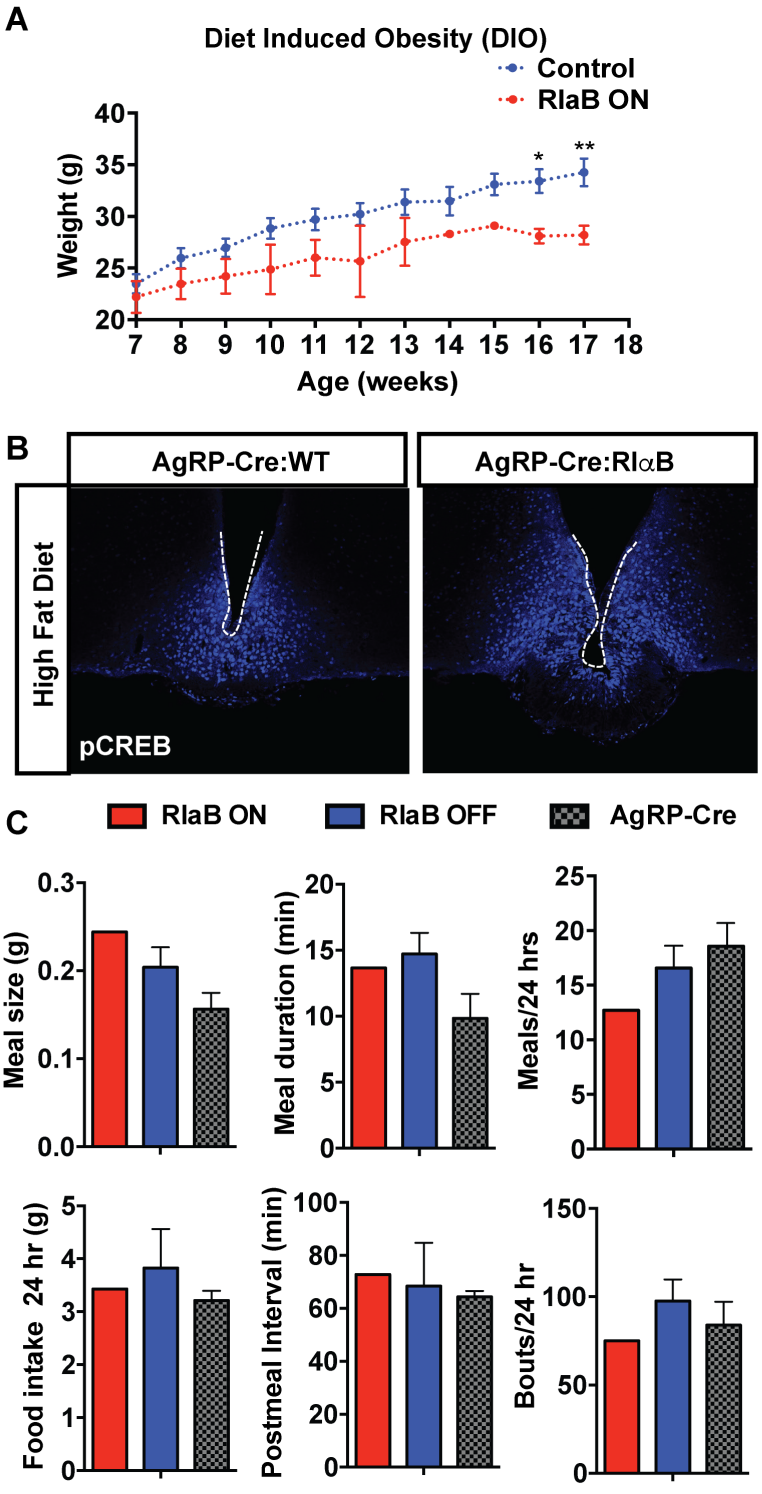
A
Diet Induced Obesity (DIO)
Control
RIaB ON
Weight (g)
Age (weeks)
*
**
B
AgRP-Cre:WT
AgRP-Cre:RIαB
High Fat Diet
pCREB
C
RIaB ON
RIaB OFF
AgRP-Cre
Meal size (g)
Meal duration (min)
Meals/24 hrs
Food intake 24 hr (g)
Postmeal Interval (min)
Bouts/24 hr

Figure 3-9 Legend: Phenotyping of behaviors related to fasting response on High Fat Diet (HFD). (A) Weight curves of control (AgRP-Cre and RIaB OFF) and RIaB ON male mice over a ten week period (7 to 17 weeks of age). HFD was introduced at six weeks of age. (control, n=6; RIaB On, n=3). (B) Immohistochemistry of arcuate nucleus of fasted AgRP-Cre:WT and AgRP-Cre:RIαB mice (RIαB ON) for induction of phosphorylated CREB (pCREB) after twelve weeks on a HFD. (C) Food intake parameters measured across a 72-hour period were comparable between three groups of mice. (RIαB ON, n=1; RIαB OFF, n=4; AgRP-Cre, n=3)

Figure 3-10:

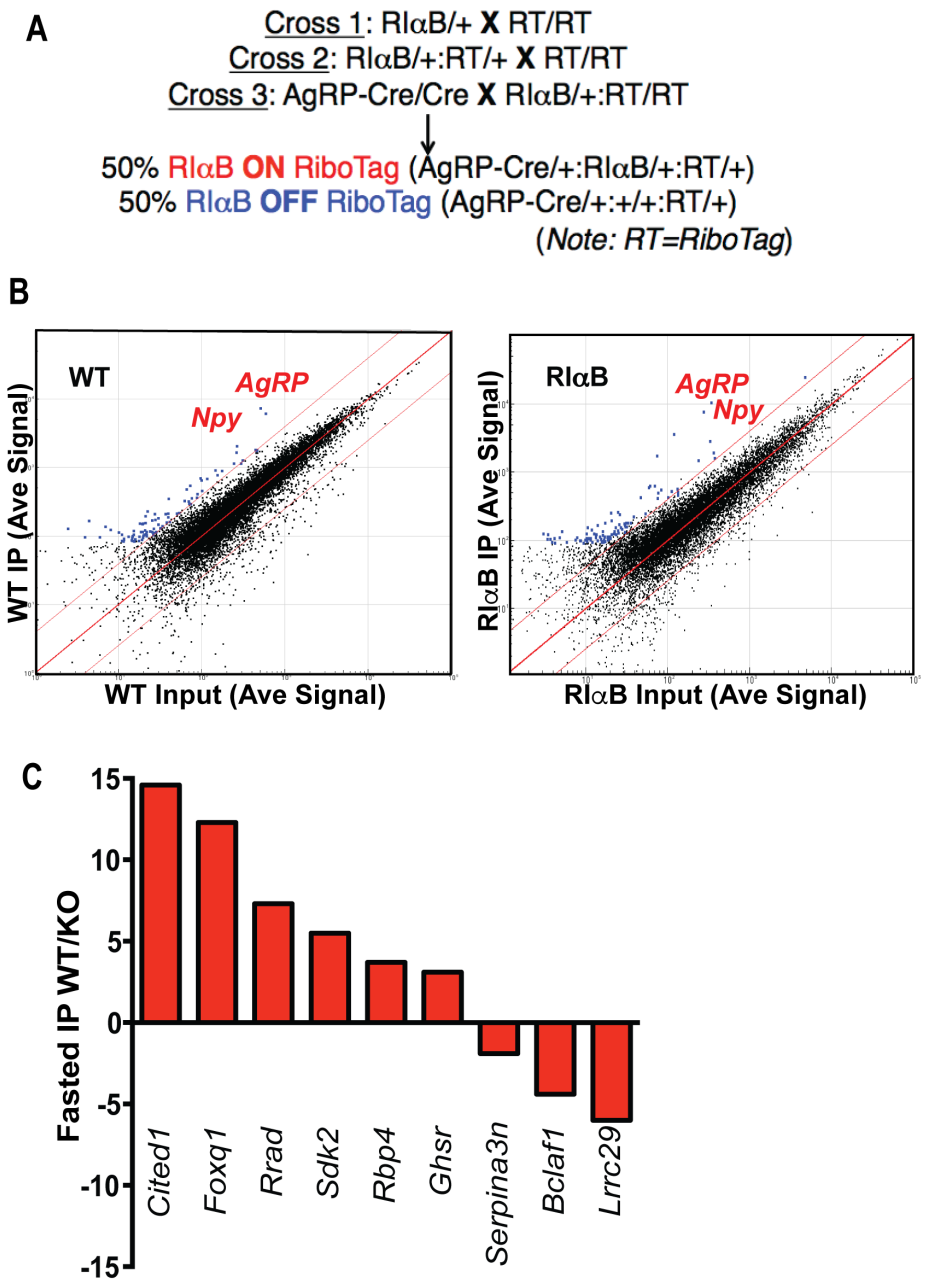

Figure 3-10 Legend: Microarray Results
(A) Diagram of breeding scheme to clarify nomenclature of animals utilized in RiboTag immunoprecipitation study. RIαB OFF animals were AgRP-Cre:RiboTag unlike previous experiments labeling RIα het mice as RIαB OFF. (B) Scatter plots of microarray results demonstrating enrichment (IP/Input average signal value) for *AgRP* and *Npy* in both wild-type and mutant arrays. (C) IP/IP analysis of array results for enriched genes induced by fasting showing the greatest difference between groups (Calculated as IP WT signal / IP RIaB signal). See Table 1 for gene names.

Figure 3-11:

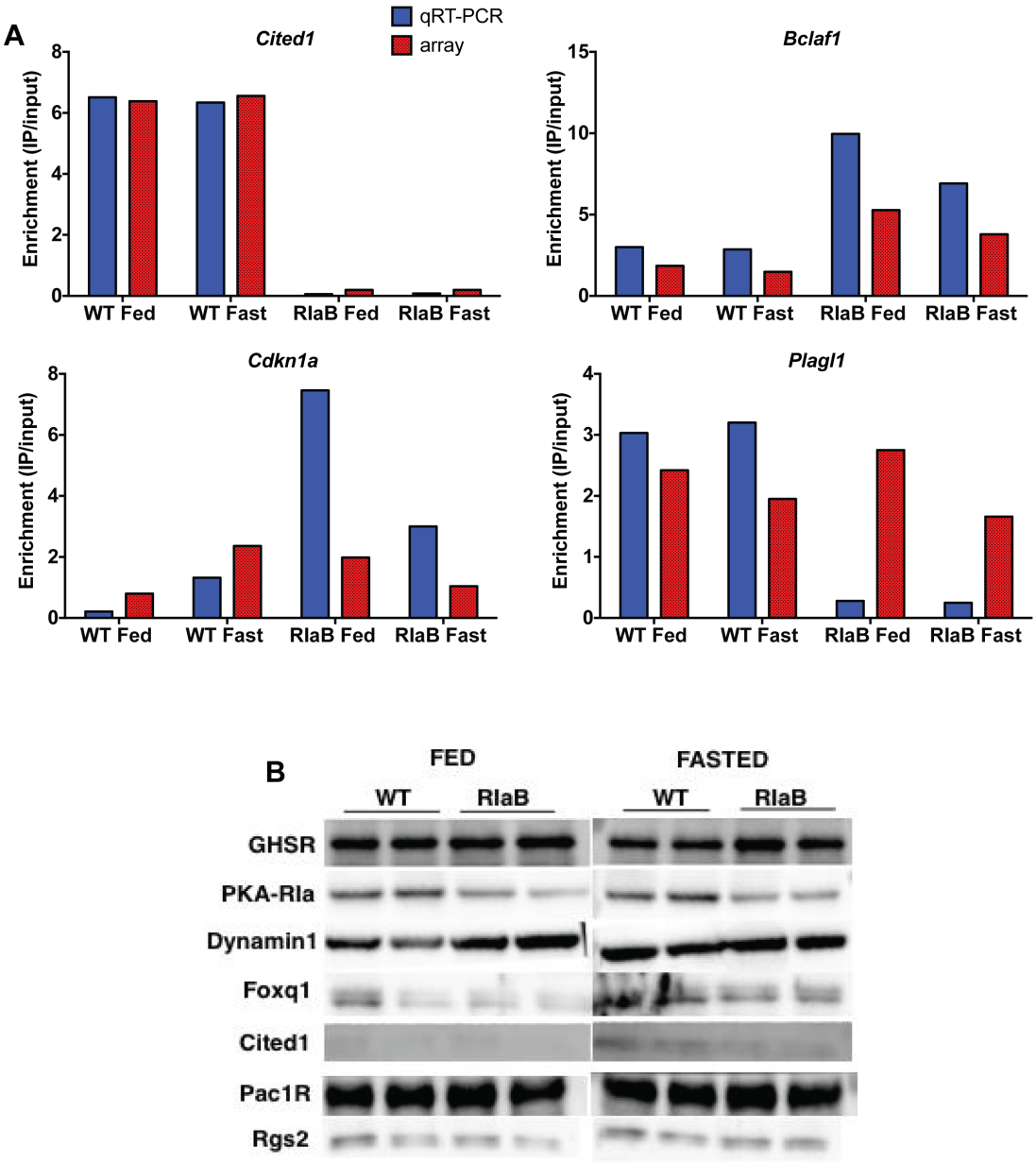

Figure 3-11 Legend: Validation of microarray key genes by qRT-PCR and immunoblotting.
(A) qRT-PCR validation of enrichment and changes in gene expression for key genes: *Cited1*: Cbp/p300-interacting transactivator with Glu/Asp-rich carboxy-terminal domain 1, *Bclaf1*: BCL2-associated transcription factor 1, transcript variant 2, *Cdkn1a*: Cyclin-dependent kinase inhibitor 1A, *Plagl1*: Pleiomorphic adenoma gene-like 1.
(B) Immunoblots of hypothalamic homogenates from either wild-type or AgRP-Cre:RIaB Fed or Fasted animals (Individual samples run on each lane, n=2/group). Animals were sacrificed following a 24-hr fast or within 20 minutes of lights on.

Table 3-1: Enriched in WT during Fed state

Enrich Fed WT	SYMBOL	DEFINITION
14.7	***Agrp***	Agouti related protein (Agrp), mRNA.
10.8	***Npy***	Neuropeptide Y (Npy), mRNA.
9.0	*Tnfaip8l3*	Tumor necrosis factor, alpha-induced protein 8-like 3 (Tnfaip8l3), mRNA.
8.0	***4732456N10Rik***	RIKEN cDNA 4732456N10 gene (4732456N10Rik), mRNA.
7.8	*Stat3*	Signal transducer and activator of transcription 3 (Stat3), transcript variant 3, mRNA.
7.5	*Gbp10*	Guanylate-binding protein 10 (Gbp10), mRNA.
7.4	*Acvr1c*	Mus musculus activin A receptor, type IC (Acvr1c), mRNA.
6.7	*Calcr*	Calcitonin receptor (Calcr), transcript variant a, mRNA.
6.5	*Unc13b*	Unc-13 homolog B (C. elegans) (Unc13b), mRNA.
6.4	*Cited1*	Cbp/p300-interacting transactivator with Glu/Asp-rich carboxy-terminal domain 1 (Cited1), mRNA.
6.0	*Npy2r*	Neuropeptide Y receptor Y2 (Npy2r), mRNA.
5.4	*Snrk*	SNF related kinase (Snrk), mRNA.
5.2	*LOC100047200*	PREDICTED: Mus musculus similar to T-box 3 protein (LOC100047200), mRNA.
5.1	*Rasgrp1*	Mus musculus RAS guanyl releasing protein 1 (Rasgrp1), mRNA.

Table 3-2: Enriched in mutant during Fed state

Enrich Fed KO	SYMBOL	DEFINITION
30.6	***Agrp***	Agouti related protein (Agrp), mRNA.
30.3	*Serpina3n*	Serine (or cysteine) peptidase inhibitor, clade A, member 3N (Serpina3n), mRNA.
27.5	***Npy***	Neuropeptide Y (Npy), mRNA.
23.7	***4732456N10Rik***	RIKEN cDNA 4732456N10 gene (4732456N10Rik), mRNA.
12.4	*Nr5a2*	Nuclear receptor subfamily 5, group A, member 2 (Nr5a2), mRNA.
10.4	*Tgfbi*	Transforming growth factor, beta induced (Tgfbi), mRNA.
10.2	*Acvr1c*	Activin A receptor, type IC (Acvr1c), mRNA.
10.1	*Calcr*	Calcitonin receptor (Calcr), transcript variant a, mRNA.
9.2	*Rgs2*	
9.0	*Npy2r*	Neuropeptide Y receptor Y2 (Npy2r), mRNA.
8.6	*Bclaf1*	BCL2-associated transcription factor 1 (Bclaf1), transcript variant 2, mRNA.
8.2	*Bclaf1*	BCL2-associated transcription factor 1 (Bclaf1), transcript variant 2, mRNA.
6.6	*LOC100047200*	Similar to T-box 3 protein (LOC100047200), mRNA.
6.5	*Gpc4*	Glypican 4 (Gpc4), mRNA.
6.3	*Lrrc29*	Leucine rich repeat containing 29 (Lrrc29), mRNA.
5.4	*Ghsr*	Growth hormone secretagogue receptor (Ghsr), mRNA.
5.3	*Bclaf1*	BCL2-associated transcription factor 1 (Bclaf1), transcript variant 3, mRNA.
5.3	*Ghr*	Growth hormone receptor (Ghr), transcript variant 1, mRNA.
5.2	*Plagl1*	Pleiomorphic adenoma gene-like 1 (Plagl1), mRNA.

Table 3-3: Enrich in WT during Fasted state

Enrich Fast WT	SYMBOL	DEFINITION
31.6	*Ghsr*	Growth hormone secretagogue receptor (Ghsr), mRNA.
11.1	*Rbp4*	Retinol binding protein 4, plasma (Rbp4), mRNA.
8.4	*Acvr1c*	Activin A receptor, type IC (Acvr1c), mRNA.
8.1	*Vgf*	VGF nerve growth factor inducible (Vgf), mRNA.
7.7	***4732456N10Rik***	RIKEN cDNA 4732456N10 gene (4732456N10Rik), mRNA.
7.6	*Ghsr*	Growth hormone secretagogue receptor (Ghsr), mRNA.
7.6	*Npy2r*	Neuropeptide Y receptor Y2 (Npy2r), mRNA.
7.3	*Ghsr*	Growth hormone secretagogue receptor (Ghsr), mRNA.
7.2	*Sdk2*	Sidekick homolog 2 (chicken) (Sdk2), mRNA.
6.7	*Foxq1*	Forkhead box Q1 (Foxq1), mRNA.
6.6	*Cited1*	Cbp/p300-interacting transactivator with Glu/Asp-rich carboxy-terminal domain 1 (Cited1), mRNA.
6.1	*Rrad*	Ras-related associated with diabetes
6.0	***Npy***	Neuropeptide Y (Npy), mRNA.
5.9	*Cish*	Cytokine inducible SH2-containing protein (Cish), mRNA.
5.8	*Ap3b1*	Adaptor-related protein complex 3, beta 1 subunit (Ap3b1), mRNA.
5.7	*Elmo1*	Engulfment and cell motility 1, ced-12 homolog (C. elegans) (Elmo1), transcript variant 1, mRNA.
5.5	*Tgfbi*	Transforming growth factor, beta induced (Tgfbi), mRNA.
5.4	***Agrp***	Agouti related protein (Agrp), mRNA.
5.4	*Rplp0*	Ribosomal protein, large, P0 (Rplp0), mRNA.
5.4	*Ghr*	Growth hormone receptor (Ghr), transcript variant 1, mRNA.
5.2	*Zdhhc14*	Zinc finger, DHHC domain containing 14 (Zdhhc14), mRNA.
5.2	*Spnb1*	Spectrin beta 1 (Spnb1), mRNA.
5.0	*Calcr*	Calcitonin receptor (Calcr), transcript variant a, mRNA.

Table 3-4: Enrich in Mutant during Fasted state

Enrich Fast KO	SYMBOL	DEFINITION
56.4	*Acvr1c*	Activin A receptor, type IC (Acvr1c), mRNA.
55.0	***4732456N10Rik***	RIKEN cDNA 4732456N10 gene (4732456N10Rik), mRNA.
30.9	*Lrrc9*	Leucine rich repeat containing 9 (Lrrc9), mRNA.
23.3	***Npy***	Neuropeptide Y (Npy), mRNA.
18.5	***Agrp***	Agouti related protein (Agrp), mRNA.
17.0	*Serpina3n*	Serine (or cysteine) peptidase inhibitor, clade A, member 3N (Serpina3n), mRNA.
14.1	***Ghsr***	Growth hormone secretagogue receptor (Ghsr), mRNA.
12.6	*Elmo1*	Engulfment and cell motility 1, ced-12 homolog (C. elegans) (Elmo1), transcript variant 1, mRNA.
11.7	*Mkl2*	MKL/myocardin-like 2 (Mkl2), transcript variant 2, mRNA.
9.7	*Bclaf1*	BCL2-associated transcription factor 1 (Bclaf1), transcript variant 2, mRNA.
9.7	*Dlk1*	Delta-like 1 homolog (Drosophila) (Dlk1), mRNA.
8.2	*LOC100047200*	Similar to T-box 3 protein (LOC100047200), mRNA.
7.6	*Vgf*	VGF nerve growth factor inducible (Vgf), mRNA.
6.8	*Gpc4*	Glypican 4 (Gpc4), mRNA.
6.4	*Tnrc18*	Trinucleotide repeat containing 18 (Tnrc18), transcript variant B, mRNA.
6.4	*Bclaf1*	BCL2-associated transcription factor 1 (Bclaf1), transcript variant 2, mRNA.
6.2	*Trpm3*	Transient receptor potential cation channel, subfamily M, member 3 (Trpm3), transcript variant 7, mRNA.
6.2	*Ptprn*	Protein tyrosine phosphatase, receptor type, N
6.1	*Rev3l*	REV3-like, catalytic subunit of DNA polymerase zeta RAD54 like (S. cerevisiae) (Rev3l), mRNA.
6.0	*Syncrip*	Synaptotagmin binding, cytoplasmic RNA interacting protein (Syncrip), transcript variant 1, mRNA.
6.0	*Zfp318*	Zinc finger protein 318 (Zfp318), transcript variant 1, mRNA.
5.9	***Ghsr***	Growth hormone secretagogue receptor (Ghsr), mRNA.
5.8	*Med23*	Mediator complex subunit 23 (Med23), mRNA.
5.7	*Lrrc29*	Leucine rich repeat containing 29 (Lrrc29), mRNA.
5.5	*Calcr*	Calcitonin receptor (Calcr), transcript variant a, mRNA.
5.5	*Prkch*	Pprotein kinase C, eta (Prkch), mRNA.
5.4	*Dgka*	Diacylglycerol kinase, alpha (Dgka), mRNA.
5.4	*Lepr*	Leptin receptor (Lepr), transcript variant 1, mRNA.
5.3	*Spnb1*	Spectrin beta 1 (Spnb1), mRNA.
5.2	*Ghr*	Growth hormone receptor (Ghr), transcript variant 1, mRNA.
5.2	*Trpc4*	Transient receptor potential cation channel, subfamily C, member 4 (Trpc4), mRNA.
5.0	*Nfkbiz*	Nuclear factor of kappa light polypeptide gene enhancer in B-cells inhibitor, zeta (Nfkbiz), mRNA.

Table 3-5: WT vs. Mutant FED state

FED GENE EXPRESSION DIFFERENCES		
Fed IP WT/KO	**SYMBOL**	DEFINITION
9.3	Cited1	Cbp/p300-interacting transactivator with Glu/Asp-rich carboxy-terminal domain 1 (Cited1), mRNA.
7.7	Stat3	Signal transducer and activator of transcription 3 (Stat3), transcript variant 3, mRNA.
2.1	Unc13b	Unc-13 homolog B (C. elegans) (Unc13b), mRNA.
2.0	Rasgrp1	RAS guanyl releasing protein 1 (Rasgrp1), mRNA.
1.6	LOC100047200	PREDICTED: Similar to T-box 3 protein (LOC100047200), mRNA.
1.2	**4732456N10Rik**	RIKEN cDNA 4732456N10 gene (4732456N10Rik), mRNA.
1.1	Acvr1c	A receptor, type IC (Acvr1c), mRNA.
1.1	Calcr	Calcitonin receptor (Calcr), transcript variant a, mRNA.
1.1	Npy2r	Mus musculus neuropeptide Y receptor Y2 (Npy2r), mRNA.
0.8	**Npy**	Neuropeptide Y (Npy), mRNA.
0.7	**Agrp**	Agouti related protein (Agrp), mRNA.
Fed IP KO/WT	**SYMBOL**	DEFINITION
6.7	Lrrc29	Leucine rich repeat containing 29 (Lrrc29), mRNA.
4.0	Bclaf1	BCL2-associated transcription factor 1 (Bclaf1), transcript variant 2, mRNA.
3.8	Bclaf1	BCL2-associated transcription factor 1 (Bclaf1), transcript variant 2, mRNA.
3.5	Bclaf1	BCL2-associated transcription factor 1 (Bclaf1), transcript variant 2, mRNA.
1.8	Serpina3n	Mus musculus serine (or cysteine) peptidase inhibitor, clade A, member 3N (Serpina3n), mRNA.
1.4	**Agrp**	Agouti related protein (Agrp), mRNA.
1.2	**Npy**	Neuropeptide Y (Npy), mRNA.
1.1	Ghr	Growth hormone receptor (Ghr), transcript variant 1, mRNA.
0.9	Npy2r	Neuropeptide Y receptor Y2 (Npy2r), mRNA.
0.9	Calcr	Calcitonin receptor (Calcr), transcript variant a, mRNA.
0.9	Acvr1c	A receptor, type IC (Acvr1c), mRNA.
0.8	**4732456N10Rik**	RIKEN cDNA 4732456N10 gene (4732456N10Rik), mRNA.
0.6	LOC100047200	PREDICTED: Similar to T-box 3 protein (LOC100047200), mRNA.
0.5	Plagl1	Pleiomorphic adenoma gene-like 1 (Plagl1), mRNA.
0.3	Gpc4	Glypican 4 (Gpc4), mRNA.

Table 3-6: WT vs. Mutant FASTED state

FASTED GENE EXPRESSION DIFFERENCES		
Fasted IP WT/KO	**SYMBOL**	DEFINITION
14.6	*Cited1*	Cbp/p300-interacting transactivator with Glu/Asp-rich carboxy-terminal domain 1 (Cited1), mRNA.
12.3	*Foxq1*	Forkhead box Q1 (Foxq1), mRNA.
7.3	*Rrad*	Ras-related associated with diabetes
5.5	*Sdk2*	Sidekick homolog 2 (chicken) (Sdk2), mRNA.
3.7	*Rbp4*	Retinol binding protein 4, plasma (Rbp4), mRNA.
3.1	*Ghsr*	Growth hormone secretagogue receptor (Ghsr), mRNA.
2.4	*Vgf*	VGF nerve growth factor inducible (Vgf), mRNA.
2.0	*Ghsr*	Growth hormone secretagogue receptor (Ghsr), mRNA.
1.5	*Acvr1c*	A receptor, type IC (Acvr1c), mRNA.
1.3	*Zdhhc14*	Zinc finger, DHHC domain containing 14 (Zdhhc14), mRNA.
1.3	***4732456N10Rik***	RIKEN cDNA 4732456N10 gene (4732456N10Rik), mRNA.
1.1	*Ghr*	Growth hormone receptor (Ghr), transcript variant 1, mRNA.
0.8	***Npy***	Neuropeptide Y (Npy), mRNA.
0.8	***Agrp***	Agouti related protein (Agrp), mRNA.
Fasted IP KO/WT	**SYMBOL**	DEFINITION
6.0	*Lrrc29*	Leucine rich repeat containing 29 (Lrrc29), mRNA.
4.4	*Bclaf1*	BCL2-associated transcription factor 1 (Bclaf1), transcript variant 2, mRNA.
4.1	*Bclaf1*	BCL2-associated transcription factor 1 (Bclaf1), transcript variant 2, mRNA.
2.0	*Spnb1*	Spectrin beta 1 (Spnb1), mRNA.
1.9	*Serpina3n*	Serine (or cysteine) peptidase inhibitor, clade A, member 3N (Serpina3n), mRNA.
1.3	***Agrp***	Agouti related protein (Agrp), mRNA.
1.2	***Npy***	Neuropeptide Y (Npy), mRNA.
0.9	*Ghr*	Growth hormone receptor (Ghr), transcript variant 1, mRNA.
0.8	***4732456N10Rik***	RIKEN cDNA 4732456N10 gene (4732456N10Rik), mRNA.
0.7	*Acvr1c*	A receptor, type IC (Acvr1c), mRNA.
0.5	*Ghsr*	Growth hormone secretagogue receptor (Ghsr), mRNA.
0.5	*Ptprn*	Protein tyrosine phosphatase, receptor type, N
0.4	*Vgf*	VGF nerve growth factor inducible (Vgf), mRNA.
0.3	*Gpc4*	Glypican 4 (Gpc4), mRNA.
0.3	*Ghsr*	Growth hormone secretagogue receptor (Ghsr), mRNA.
0.2	*Dlk1*	Delta-like 1 homolog (Drosophila) (Dlk1), mRNA.

CHAPTER 4: APPLICATIONS OF RIBOTAG TECHNOLOGY

4.1 INTRODUCTION

Despite the mechanistic manipulations used to determine the function and relevance of a neuronal population, the determination of a population's full gene expression profile is rarely known. The ability to isolate the gene expression profile of a defined cell population present within a larger heterogeneous tissue has been a challenge for the scientific community. Procedures required to isolate the population of interest are often coarse and time-consuming.

The RiboTag technology allows rapid isolation of cell-specific transcripts by isolating tagged ribosomes by immunoprecipitation. The RiboTag transgenic mouse expresses a modified gene for *Rpl22*, a 60S ribosomal protein. The fourth and final exon for *Rpl22* is modified in two ways: (1) loxP sites are inserted flanking the wild-type exon 4 followed by (2) the insertion of a second modified exon 4 containing three hemagglutinin tags. Upon Cre-mediated recombination, the wild-type exon is excised and the tagged ribosomal protein is expressed (Sanz et al. 2009). Immunoprecipitation of the tagged polysome and its associated transcripts following gross dissection and homogenization is then possible and the entire translatome (polysome-associated mRNAs) may then be determined by microarray or RNA-sequencing. By crossing the RiboTag mouse to Cre-driver mice defining specific hypothalamic nuclei, further characterization of these populations is made possible.

RiboTag may be used to determine the full gene expression profile of the many neuronal populations during their basal state or in response to an intervention. Also, it may be used to determine alterations in gene expression in genetic deletion or mutation mouse models. This chapter documents three RiboTag experiments and their use in defining the gene expression profiles of the arcuate nucleus (ARC), the ventromedial hypothalamus (VMH), and the dentate gyrus (DG).

4.2 PROJECT 1: USE OF RIBOTAG TO DETERMINE CHANGES IN GENE EXPRESSION IN A KO MOUSE MODEL: THE POMC-EXPRESSING NEURONS IN THE RIIβ KO MOUSE

Introduction

The study of body weight regulation began with lesion studies linking the loss of a particular anatomically defined brain region to changes in glucose or body weight homeostasis. As lesion studies became more refined, regions began to be more narrowly defined. However, following the discovery of unique gene expression patterns, it became possible to further segregate a region into neuronal populations. Indeed, the characterization of two key populations expressing either the Agouti-related protein (*AgRP*) gene or the Pro-opiomelanocortin (*Pomc*) gene has expanded the body weight homeostasis field exponentially. By developing mice expressing Cre-recombinase driven by the promoters for these key genes, we have been able to further interrogate the functional roles of these narrowly defined populations.

The initial studies defining these AgRP and Pomc neuronal populations relied upon *in situ* hybridization (Brady et al. 1990; Broberger et al. 1998). *AgRP* and *Pomc* are key genes encoding proteins with key roles in the neurons they define. Other hypothalamic populations have also been identified based upon their expression of a specific gene. If a population of neurons expressed other specific genes comparable to these defining genes, they might also help clarify the functional value of a neuronal population. Indeed, other hypothalamic populations have been defined by genes that do not always further our understanding of the role of population in the adult mouse. The ventromedial hypothalamus is defined by its expression of the transcription factor, steroidogenic factor-1 (*Nr5a1* or *Sf-1*). Although SF-1 is important for the development of the mature hypothalamus (Kim et al. 2011), additional genes also specific for the population may provide greater understanding of the how the population functions in the adult hypothalamus.

The type II regulatory subunit of PKA, RIIβ, is highly expressed in brain, brown and white adipose tissue (Cummings et al. 1996). The targeted loss of RIIβ results in a lean phenotype with enhanced nocturnal locomotion(Newhall et al. 2005), reduced fat pads, resistance to diet-induced obesity (DIO), and highly reduced serum leptin (Cummings et al. 1996), an adipocyte-derived peripheral hormone known to cross the blood-brain barrier (Williams & Elmquist 2012). Initially, the lean RIIβKO phenotype was thought to be partly due to enhanced energy expenditure and augmented induction of uncoupling protein in fat stores (Cummings et al. 1996). However, additional work by our lab found that selective re-expression of RIIβ in adipose tissue did not rescue any of the body weight phenotypes due to compensation by RIα (Brandon et al. 1998; Cummings et al. 1996). Further studies found that increasingly selective neuronal re-expression did rescue aspects of the RIIβKO phenotype. The return of RIIβ to medium spiny neurons rescued the enhanced nocturnal locomotion phenotype while re-expression in hypothalamic gabaergic neurons rescued the body weight phenotype (Zheng et al. 2013).

The adipokine leptin, crosses the blood-brain barrier at circumventricular organs, such as the median eminence, and induces intracellular signaling pathways via the long isoform of the leptin receptor, leptin receptor-b, a member of the type I cytokine receptor family. Associated with this receptor are JAK2 tyrosine kinases known to phosphorylate additionally associated STAT3, inducing their dimerization and subsequent translocation to the nucleus. STAT3 is a transcription factor, inducing expressing of a negative feedback regulator of the leptin signaling pathway, suppressor of cytokine signaling-3 (*Socs3)*(Elmquist et al. 1999; Buettner et al. 2008; Aaronson & C. M. Horvath 2002). Focusing on the role of hypothalamic RIIβ, we found that, consistent with highly reduced serum leptin, the RIIβKO mouse demonstrated enhanced leptin sensitivity. Further, leptin signaling was significantly extended in the arcuate nucleus (Arc), dorsomedial (DMH) and ventromedial hypothalamus (VMH) (Yang & McKnight 2015). However, the interplay/crosstalk between PKA and hypothalamic leptin signaling is unclear.

Two key first order hypothalamic neuronal populations found in the Arc are regulated by leptin: the *Pomc*-expressing neurons and the *AgRP*-expressing neurons (Cone & Simerly 2011). AgRP neurons are exclusively gabaergic (Tong et al. 2008) and are inhibited by leptin, while Pomc-neurons demonstrate

both glutamatergic and gabaergic populations(Wittmann et al. 2013; Hentges et al. 2009) and are activated by leptin (Varela & T. L. Horvath 2012). Recently, it has been shown that the return of leptin signaling to populations with the Arc (Balthasar et al. 2005; Padilla et al. 2010) modestly rescues the obesity phenotype of *db/db* mice (Balthasar et al. 2004). Considering the extended duration of leptin signaling in the Arc of the RIIβKO mouse, presumably, transcriptional responses downstream from leptin signaling should also differ. To test this, isolated translatomes from neurons labeled by the same *Pomc*-Cre mouse utilized in the leptin receptor rescue study (Balthasar et al. 2004) crossed to the RiboTag mouse (Sanz et al. 2009) were tested for differences in their response to fasting and leptin when RIIβ is deleted. Pomc and AgRP neurons respond in an opposing manner to leptin. The lack of fidelity of the Cre driver does not allow us to dissect a clear gene expression profile for either. However, the extended duration of leptin signaling in the RIIβKO and compensatory behavior or of other PKA subunits for the loss of RIIβ (Clegg et al. 1987) may be teased from the microarray data.

Results

The RIIβKO mouse has a well-described lean phenotype and enhanced leptin sensitivity leading to extended activation of the transcription factor STAT3 (Cummings et al. 1996; Yang & McKnight 2015). The creation of a triple transgenic mouse, RiboTag$^{+/-}$;Cre$^{+/-}$;RIIβ$^{-/-}$, allows gene profiling of neuronal populations within the hypothalamus of the RIIβKO defined by the Cre driver mouse in response to feeding-related cues. Considering the enhanced leptin-signaling and sensitivity present in the RIIβKO mouse (Yang & McKnight 2015), presumably gene expression differences at a time-point when leptin signaling is terminated in the WT but still activated in the RIIβKO will provide insight into genes induced by leptin signaling.

The hypothalamus, considered the feeding center of the brain, is divided into a number of subregions based on anatomical and functional characteristics. Some of these populations remain generally defined by the expression of a specific marker. For example, the paraventricular nucleus (PVN) is generally defined by the expression of the transcription factor *Sim1* (single-minded homolog 1). However, ongoing research continues to challenge and refine our classification of these subpopulations(Krashes et al. 2014). Considering this, the initial goal for our array analysis was to validate enrichment for expected transcripts, and de-enrichment for markers known to define other hypothalamic regions. Indeed, our IP samples enriched for *AgRP*, *Npy*, and *Pomc*, as was expected from recent literature (Padilla et al. 2010), and de-enriched for markers for the PVN (*Pacap, Sim1*), lateral hypothalamus (LH) (*Hcrt*), and ventromedial hypothalamus (VMH) (*Cbln1, Nr5a1, Pacap*) (Figure 4-1).

Corroborating previous work by our lab, we found *Pomc* expression was enhanced in the RIIβKO mouse (Yang & McKnight 2015) (Figure 4-2A). Reductions in *AgRP* and *Npy* were seen in our RIIβKO+ leptin IP samples (Figure 4-2B). Presumably this is due to enhanced inhibition of the AgRP neurons at the six-hour time point (Yang & McKnight 2015).

Considering the enhanced leptin sensitivity of RIIβKO mice, transcript differences of key genes

comprising the leptin-signaling pathway were also investigated. Interestingly, *Jak2* expression was increased by leptin in the Wild-type (WT) IP samples, while this was abrogated in the RIIβKO (Figure 4-3). Compensatory upregulation of regulatory PKA isoforms and down-regulation of catalytic subunits has also been seen in the RIIβKO mouse (Brandon et al. 1998; Cummings et al. 1996). However, these alterations were not present at the message level (Figure 4-4) and presumably are due to enhanced stabilization of the compensatory regulatory PKA protein isoforms and reduced stabilization of the catalytic subunit proteins.

Differences in leptin-induced transcript profiles were also extracted from the microarray (Table 4-1) and differences in genes induced by fasting in the mutant vs. the WT were also extracted (Table 4-2).

Discussion

There were a number of issues with this array. The lack of specificity for the Cre could have been surmounted if not for the antagonistic nature of the two main neuronal populations labeled, *Pomc* and *AgRP*-expressing neurons. Additionally, later work by our lab found that the *Pomc*-Cre is also expressed in progenitors of *Kiss1*-expressing neurons (Sanz et al. 2015). There is still a great deal of value, considering the number of probes on the microarray, to compare the input samples between the WT and mutant. Additional work from our lab also found that the six-hour timepoint was post maximal induction of *Socs3*, the main transcriptional target of STAT3, in WT mice (Figure 4-5).

4.3 PROJECT 2: USE OF RIBOTAG TO CHARACTERIZE A NEURONAL POPULATION BY ADDITIONAL CELL-SPECIFIC MARKERS: SF1 NEURONS OF THE VMH

Introduction

The ventromedial hypothalamus (VMH) can be differentiated from the rest of the hypothalamus by its expression of the nuclear receptor, steroidogenic factor-1 (*Sf-1* or *Nr5a1*), the loss of which leads to vastly altered cellular distribution within the hypothalamus during development[10]. Early lesion studies found a role for the ventromedial hypothalamus (VMH) in hyperphagia, hypogonadism and obesity[1]. Predominantly populated by glutamatergic neurons[14], the VMH sends projections to the arcuate nucleus (ARC), the paraventricular nucleus of the hypothalamus (PVH), and the lateral hypothalamus (LH). The VMH expresses leptin and insulin receptors and responds directly to changes in leptin, insulin and circulating glucose[12], serving as a modulator of the phagic response circuitry[11]. Further, the loss of the leptin receptor from *Sf-1*-expressing neurons leads to increased fat deposition and lower activity levels[9]. However, *Sf-1*-expressing neuron-specific loss of suppressor of cytokine-3 (Socs3), a negative regulator of leptin signaling, improved leptin and glucose sensitivity and reduced food intake without a reduction in body weight, presumably due to a reduction in energy expenditure.

The VMH may be divided into smaller, overlapping nuclei defined by their expression of one of the following: estrogen receptor-alpha (*ERα*), brain-derived neurotrophic factor (*Bdnf*), glucokinase (*Gck*),

insulin or leptin receptor (*Insr*). Glucokinase expression is present in all VMH neurons (Kim et al. 2011). Beyond its role in body weight homeostasis, the VMH also has roles in reproduction and demonstrates sex differences in overall morphology and gene expression (Xu et al. 2012). Considering this, we queried the *Sf1*-expressing neuronal population for additional transcripts with comparable enrichment to *Sf1*, further characterizing genes expressed specifically within this population.

Results

Initial validation of the array found strong enrichment for *Sf-1* (*Nr5a1*) and de-enrichment for markers known to define other hypothalamic nuclei that do not overlap with the VMH (*Gad1*) and oligodendrocyte markers (*Cnp*) (Figure 4-6). In addition, changes in leptin receptor (*LepR*) expression were found, with enhanced expression during a fast (Figure 4-7).

The key point of the study was to determine other genes specifically co-expressed comparable to *Sf1/Nr5a1*. There were a large number of hits with equivalent expression enrichment (IP signal/Input signal) according to the microarray, including a number of kinases, an ion channel, synaptic proteins and another nuclear receptor, *Nr1d1*, which encodes the protein Rev-ErbAα (Figure 4-8 and Table 4-3).

Discussion

The large number of transcripts demonstrating comparable enrichment to Sf1/Nr5a1 was surprising. Validation of these hits was not performed and, considering the low n value (n=1/group), this is an important criticism. Further directions for this study would include validation of these hits, with particular focus on those that might have roles in body weight regulation. In particular, Nr1d1/Rev-ErbAa, a nuclear receptor that functions as a transcriptional repressor and has a possible role in circadian rhythym (Zhang et al. 2009) and is also expressed in the suprachiasmatic nucleus (Allen Brain in situ atlas).

4.4 PROJECT 3: USE OF RIBOTAG TO CHARACTERIZE INTERVENTION-INDUCED GENE EXPRESSION CHANGES: DENTATE GRANULE NEURONS RESPONSE TO KAINIC ACID

Introduction

Uncontrolled and synchronized electrical activity in the hippocampus leads to seizures. The excitability of dentate granule (DG) neurons, in particular, has a dominant role in the induction of a seizure (Seress et al. 2009). However, loss of inhibition, commonly by underlying genetic factor, can predispose dentate granule neurons to fire more often, synchronize and kindle a seizure. The DG neurons respond to a seizure by inducing genes that allow a cellular response to injury and enhanced plasticity, reorganizing the synaptic structures in both the mossy fiber axons projecting from the DG neurons and post-synaptic structures.

Expected gene expression changes underlying epileptogenesis include a group of immediate early genes (IEGs), a first wave of transcriptional response to activity. These IEGs include transcription

factors such as *cFOS*, *Fosb* (Okuno 2011), and *Zif268*, able to then induce their own complement of transcriptional products, and synaptic restructuring proteins such as the activity-dependent cytoskeletal associated protein (*Arc*) (Veyrac et al. 2013). Other genes induced by IEGs include growth and other trophic factors such as brain-derived neurotrophic factor (*Bdnf*) (Dong et al. 2006) and neuropeptides, such as Neuropeptide Y (*Npy*) (GRUBER et al. 1994). However, previous studies have only been able to probe a handful of genes whose expression is altered by KA. The studies were also time consuming and often dependent upon *in situ* hybridization to confirm their findings. The goal of our study was to discover new genes underlying kainic acid-induced activity within dentate granule neurons in response to a sub-seizure dose, preventing a cellular injury response. By stably express RiboTag in the majority of dentate granule neurons, we are able to determine the full complement of gene expression changes in this population in response to kainic acid.

Results

Previous studies have demonstrated activation of the majority of dentate granule cells following KA injection. However, these studies typically induced a full seizure. We decided to induce a sub-seizure level of activity to reduce co-morbidity complications and eliminate or reduce the cell injury gene response. To validate the use of a sub-seizure KA dose we required two criteria to be met: (1) the animals were closely monitored for lack of seizures symptoms according to the Racine scale, and (2) immunoprecipitated transcripts had to demonstrate the induction of known genes: cFOS and Arc, and the reduction in Desmoplakin (Dsp), a highly enriched and specific gene known to be reduced by KA seizures (Lein et al. 2004).

Animals were dosed with a series of KA concentrations peripherally and monitored for seizure symptoms according to the Racine scale.

We found increased immunoreactivity for cFOS throughout the DG at a 12.5 mg/kg KA dose, without associated seizure symptoms over a four-hour period (Figure 4-9A). However, although cFOS protein was present, gene transcription of *cFos* was not detected at four hours. A time-course of RiboTag IPs following a 20mg/kg KA dose found strong induction of *cFos* at 1-2 hours post KA that returned to baseline by four hours. Our additional checks for KA response by DG neurons included the reduction in Desmoplakin (*Dsp*) transcription and the induction of *Arc* (Figure 4-9C).

Microarray analysis of immunoprecipitated transcripts demonstrated intact enrichment for known DG-specific transcripts in both –KA and +KA samples. Transcripts for region CA1/3 and oligodendrocyte markers were de-enriched (Figure 4-9D). To validate our microarray results, we performed qRT-PCR and checked both for enrichment of DG-specific genes (Figure 4-10A). Validation of KA induction of gene expression changes included a panel of genes known to change in response to KA (Figure 4-10B).

While analyzing our array results, we discovered strong enrichment for phosphodiesterase 1b (*Pde1b*) that was highly attenuated following KA (Figure 4-10C). We investigated this result further and found it highly expressed in the DG compared to the rest of the hippocampus with localization in both pre

and post-synaptic regions of the DG neuron (Figure 4-10D). However, protein levels of PDE1b were unchanged four hours post-KA (Figure 4-10E).

Discussion

Our results strongly validated gene expression changes uncovered by previous literature. Our unique finding, the specific expression of PDE1b for dentate granule cells was intriguing. Also, its localization to the mossy fiber axons was unexpected.

PDEs have been known to anchor to A-Kinase anchoring proteins (AKAPs). Considering our previous work with AKAP7, we tested for delocalization of PDE1b in the AKAP7 KO. No delocalization was noted and it is possible that another AKAP might be localizing PDE1b to the presynaptic regions. In addition, PDE1b is activated by calmodulin/Ca^{2+}(Bender & Beavo 2006). The AKAP7 KO phenotype also included impaired forskolin-induced long term potentiation at the mossy fiber synapse (MF-LTP), a cAMP-dependent form of LTP. It is possible that part of our phenotype might be due to enhanced activation of PDE1b in the presynaptic mossy fiber projections perhaps by inhibiting activation of exchange protein activated by cAMP (EPAC) (Fernandes et al. 2015) due to enhanced degradation of cAMP by the phosphodiesterase. Or, possibly, considering its down-regulation following KA, it may have a role in reducing protein kinase A (PKA) activity until the synapse is activated, when it is down-regulated. PDE1b is also important for circadian rhythm, and its loss leads to dysregulation of cellular activity fluctuations regulated by accordingly (Zhang et al. 2009). The role of PDE1b in proper dentate granule cell function is an interesting subject for future studies.

4.4 EXPERIMENTAL PROCEDURES

Animal Care: All procedures were approved by the Institutional Animal Care and Use Committee (IACUC) of the University of Washington and conformed to NIH guidelines. Mice were group housed in a 12-hour light/dark cycle with ad libitum access to food and water. Both *Pomc*-Cre lines (Balthasar et al. 2004; McHugh et al. 2007) and *Sf1*-Cre (Klöckener et al. 2011) driver mice were generously donated by the laboratory of Dr. Bradford Lowell (Harvard). RIIβKO (Cummings et al. 1996) and RiboTag (Sanz et al. 2009) mice were generated previously by our lab. All mice were euthanized by CO2 overdose according to IACUC approval.

RIIβ$^{-/-}$;Pomc-Cre $^{Cre/+}$;RiboTag$^{+/-}$ mice RiboTag experiments: *RIIβ$^{-/-}$* mice were bred onto both RiboTag$^{+/+}$ and *Pomc-Cre*$^{Cre/+}$ backgrounds and resulting offspring from these crosses were then bred to obtain triple cross RIIβ$^{-/-}$;*Pomc-Cre*$^{Cre/+}$;RiboTag$^{+/-}$ mice. This did not allow *Pomc*$^{Cre/+}$;RiboTag$^{+/-}$ littermate controls. All animals were fasted for 24 hrs. Animals were either sacrificed at the end of the fast or received a single IP injection of 5mg/kg leptin and allowed to rest for 6 hours before being sacrificed.

Sf1-Cre$^{Cre/+}$;RiboTag$^{+/-}$ experiments: *Sf1*-Cre$^{Cre/+}$ mice were bred to homozygous RiboTag$^{+/+}$ mice to obtain desired offspring. Animals were segregated into male and female groups. Animals were either sacrificed at the end of the fast or received a single IP injection of 5mg/kg leptin and allowed to rest for 6 hours before being sacrificed.

Pomc-Cre$^{Cre/+}$;RiboTag$^{+/-}$ experiments: The more robust Pomc-Cre line (McHugh et al. 2007) bred to homozygous RiboTag$^{+/+}$ mice to obtain desired offspring. Dentate granule cell numbers are very high allowing us to perform an immunoprecipitation with a single animal. A male mouse and a female mouse were treated with each intervention. Animals were sacrificed at the end of four hours post a single subseizure dose of kainic acid (12.5 mg/kg) or saline. Validation of kainic acid induced gene expression changes was performed by qRT-PCR prior to continuing with experiment.

Feeding related interventions: For fasted groups, mice were rehoused in a clean cage starting at 9AM and fasted for 24-36 hrs. For the fasted plus leptin groups, mice were handled similarly but received a 5mg/kg intraperitoneal (IP) leptin (National Hormone & Peptide Program (NHPP), NIDDK, and Dr. Parlow) injection following the fast. Mice were sacrificed either at the termination of the fast or six hours post leptin injection, without food being returned to the cage.

RiboTag Immunoprecipitation: Mice were sacrificed and the hypothalamus was rapidly dissected and a 2mm punch made encompassing the hypothalamus. Samples were flash frozen. Two or four individual tissue samples were pooled and dounce homogenized in a buffer supplemented with RNase inhibitors. Polysomes were immunoprecipitated using antibodies to HA (Covance) and protein A/G-coupled magnetic beads (Pierce BioTechnologies). RNA was isolated from immunoprecipitate by RNeasy Micro Plus or Micro kit (Qiagen). Quantification of RNA in input and immunoprecipitate were quantitated by Quant-It RiboGreen assay (Life Technologies).

Validation of gene changes by qRT-PCR: Quantitative reverse transcriptase-PCR (qRT-PCR) was performed using SYBR green One-Step master mix (Agilent). Enrichment for a particular marker is defined as the ratio of expression in the immunoprecipitated (IP) sample to the input (I) sample, or total hypothalamic homogenate. Oligonucleotides selected using the PrimerBank database, except *Socs3*, a Taqman probe was utilized (Applied Biosystems).

Gene	Primers
Brain-derived neurotrophic factor (*Bdnf*)	*FOR:* 5'-TCATACTTCGGTTGCATGAAGG-3' *REV:* 5'-AGACCTCTCGAACCTGCCC-3'
FBJ osteosarcoma oncogene *(cFos)*	*FOR:* 5'-CGGGTTTCAACGCCGACTA-3' *REV:* 5'-TGGCACTAGAGACGGACAGAT-3'
2',3'-cyclic nucleotide 3' phosphodiesterase*C (Cnp)*	*FOR:* 5'-TTTACCCGCAAAAGCCACACA-3' *REV:* 5'-CACCGTGTCCTCATCTTGAAG-3'
Cerebellin 1 *(Cbln1)*	*FOR:* 5'-AACCCCACGTCTGACCCTA-3' *REV:* 5'-GGTGCGATTACTCATCTCGGA-3'
Desmoplakin *(Dsp)*	*FOR:* 5'-GGATTCTTCTAGGGAGACTCAGT-3' *REV:* 5'-TCCACTCGTATTCCGTCTGGG-3'
Glutamate decarboxylase 1 (*Gad1)*	*FOR:* 5'-TTCCAGCTAAGAACGGGGAG-3' *REV:* 5'-CAGCTAGGTGATGGTCAACCC-3'
Leptin receptor b *(Lepr)*	*FOR:* 5'-GTCTTCGGGGATGTGAATGTC-3' *REV:* 5'-ACCTAAGGGTGGATCGGGTTT-3'
Neuropeptide Y *(Npy)*	*FOR:* 5'-C TCCGCTCTGCGACACTAC-3' *REV:* 5'-AGGGTCTTCAAG CCTTGTTCT-3'
Steroidogenic factor-1 (*Nr5a1* or *Sf-1)*	*FOR:* 5'-GTAACTGAACTGGTCAAACCCC-3' *REV:* 5'-AAGCCTGGCTAGTGCATGTC-3'

Phosphodiesterase 1a *(Pde1a)*	*FOR:* 5'-CCGGGATTGGTTGGCTTCAA-3' *REV:* 5'-AATGCTGCGAAACTTTGGTTTT-3'
Phosphodiesterase 1b *(Pde1b)*	*FOR:* 5'-GATGCTGGAGTCGGATTGCC-3' *REV:* 5'-TTCAGTGTCTAGGATTTGCCTTG-3'
Proximal 1 *(Prox1)*	*FOR:* 5'-AGAAGGGTTGACATTGGAGTGA-3' *REV:* 5'-TGCGTGTTGCACCACAGAATA-3'
Proenkephalin *(Penk)*	*FOR:* 5'-GAGAGCACCAACAATGACGAA-3' *REV:* 5'-TCTTCTGGTAGTCCATCCACC-3'
Transferrin *(Trf)*	*FOR:* 5'-GCTGTCCCTGACAAAACGGT-3' *REV:* 5'-CGGAAGGACGGTCTTCATGTG-3'
Solute carrier family 30 (zinc transporter), member 3 (*Znt3)*	*FOR:* 5'-GAAGAGTCTTTTCACAGAGCCC-3' *REV:* 5'-TGTGTGCTAAATACCCACCAAC-3'

Microarray: Isolated RNA (7ng) was amplified using the Ovation Pico SL WTA V2 system (NuGEN) to produce ssDNA. The quality of the amplified ssDNA was confirmed by Bioanalyzer RNA 6000 Nano chips (Agilent Biotechnologies) and quantified by Nanodrop (Thermo Scientific). Prior to hybridization to microarray chip, amplified ssDNA was checked for proper amplification by qRT-PCR of key genes of known enrichment. The amplified ssDNA (2.5µg) was then biotinylated using the EncoreIL biotinylation kit (NuGEN). Biotinylated cDNA (750 ng) was hybridized at 48°C to MouseRef-8 v2 expression beadchips (Illumina) per accompanied procedural instructions. The signal generated was detected using a BeadArray Reader (Illumina). Data analysis was completed using GenomeStudio data analysis software (Illumina) and included average normalization, the Illumina custom error model, and multiple testing corrections.

Immunohistochemistry and Imaging: Brains were fixed and processed for standard immunohistochemistry. Citrate buffer antigen retrieval was required to recover PDE1b (generous gift from laboratory of Joseph Beavo) immunostaining. cFOS was visualized using a Goat-anti-cFOS antibody (Sant Cruz). Fluorescent secondary antibodies were utilized (Molecular Probes). Coverslips were mounted with ProLong Gold (Molecular Probes) with DAPI. Slides were imaged in the University of Washington Keck Microscopy Center on a Nikon Eclipse E600, Zeiss 510 META, or Leica SL confocal microscopes.

Racine scale for seizure scoring:

Animals were dosed with a series of KA concentrations peripherally and monitored for seizure symptoms according to the Racine scale: Stage 1:Normal behavior, Stage 2: Rigidity, whisker twitching, Stage 3: Reared, rigid posture and some automatisms (forelimb pawing, head bobbing, tail whipping), Stage 4:Intermittent rearing and falling with forelimb/jaw clonus, Stage 5:Continuous rearing and falling (>30sec) or continuous jumping, Stage 6:Tonic-clonic seizures, whole body involvement.

Chapter 4: FIGURES

Figure 4-1:

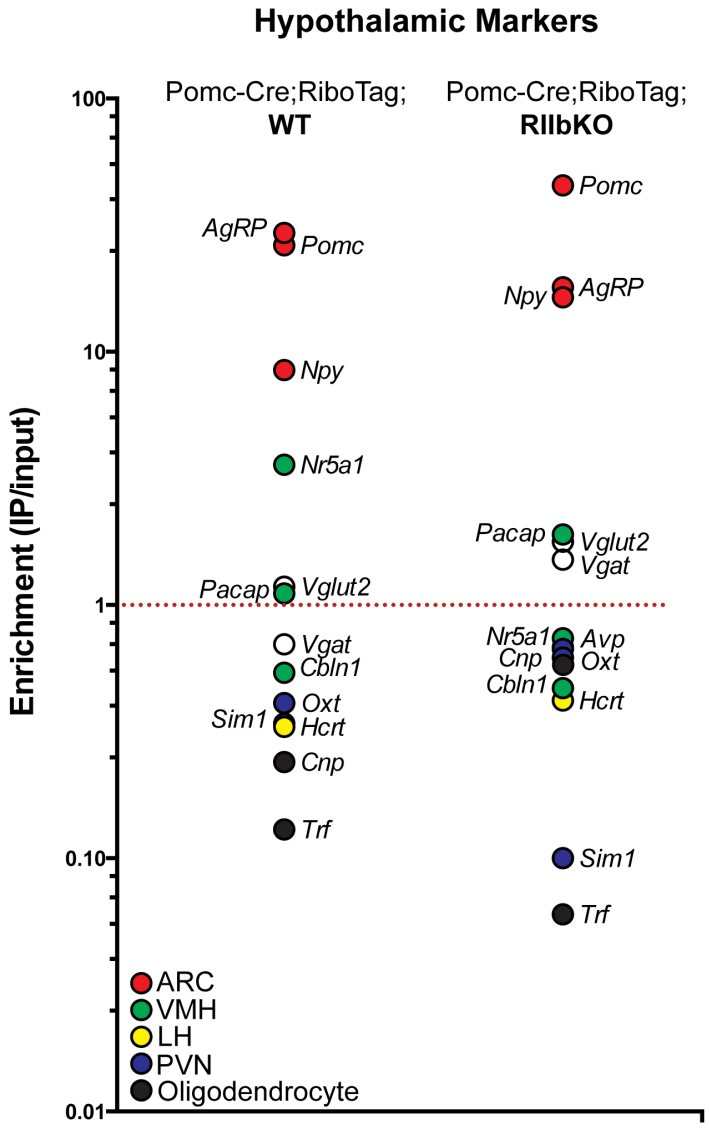

Figure 4-1 Legend: Specificity for POMC and AgRP neurons demonstrated by array. Microarray results presented as enrichment (immunoprecipitated transcript signal/total hypothalamic transcript signal). *AgRP*, *Pomc*, and *Npy* demonstrate strong enrichment. Well-characterized genetic markers for hypothalamic regions or neuronal populations in the ventromedial hypothalamus (VMH), *Nr5a1*: Steroidogenic factor-1 nuclear receptor, *Pacap*: Pituitary adenylate cyclase activating peptide, *Cbln1*: Cerebellin-1; lateral hypothalamus (LH), *Hrct*: Hypocretin/Orexin; paraventricular nucleus (PVN), *Oxt*: Oxytocin, *Sim1*: single-minded homolog 1, and oligodendrocyte markers, *Cnp*: 2',3'-cyclic nucleotide 3' phosphodiesterase, *Trf*; Transferrin, demonstrated de-enrichment or equivalent expression to background. Glutamatergic, *Vglut*: Vesicular glutamate transporter-2 and gabaergic marker, *Vgat*: Vesicular GABA transporter, were equivalently expressed.

Figure 4-2:

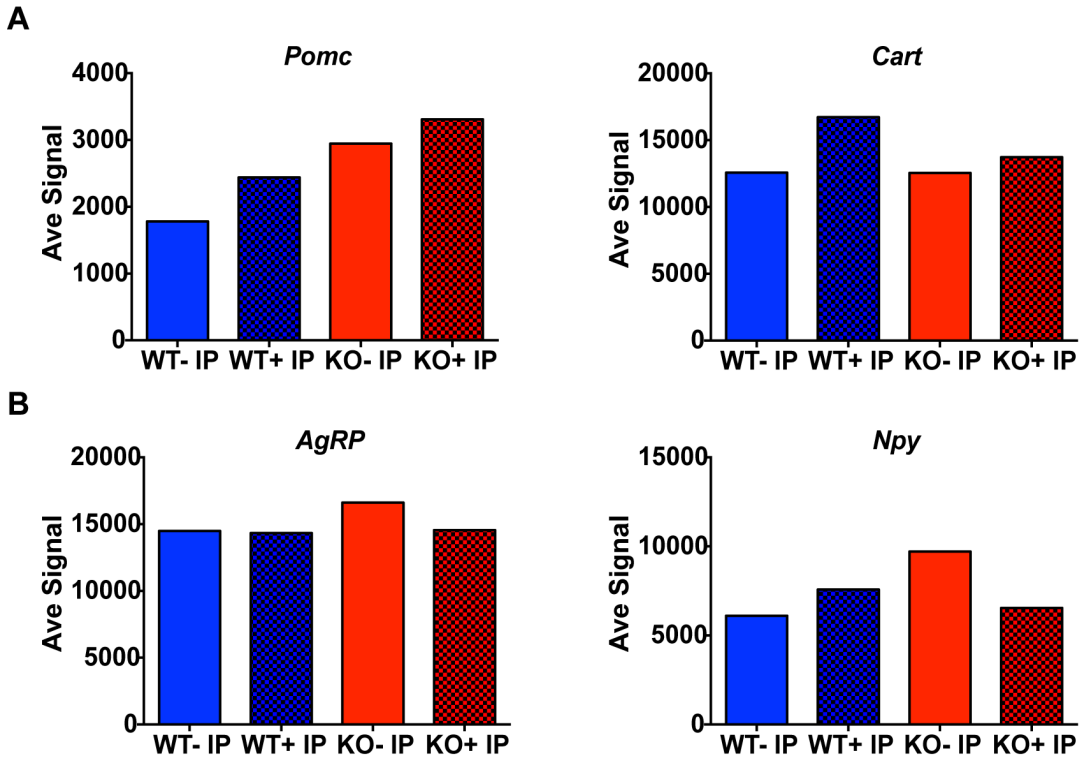

Figure 4-2 Legend: Microarray values for genetic markers specific for AgRP and Pomc neurons. (A) Microarray signal values for immunoprecipitated (IP) samples wild-type or RIIβKO with or without leptin. All four IP samples signal values for *Pomc*: Pro-opiomelanocortin and *Cart*: Cocaine- and amphetamine-regulated transcript, specific for Pomc-neurons. RIIβKO values are greater for Pomc message. (B) Microarray signal values for IP samples are comparable for AgRP neuron genetic markers, *AgRP*: Agouti-related protein and *Npy*: Neuropeptide Y.

Figure 4-3

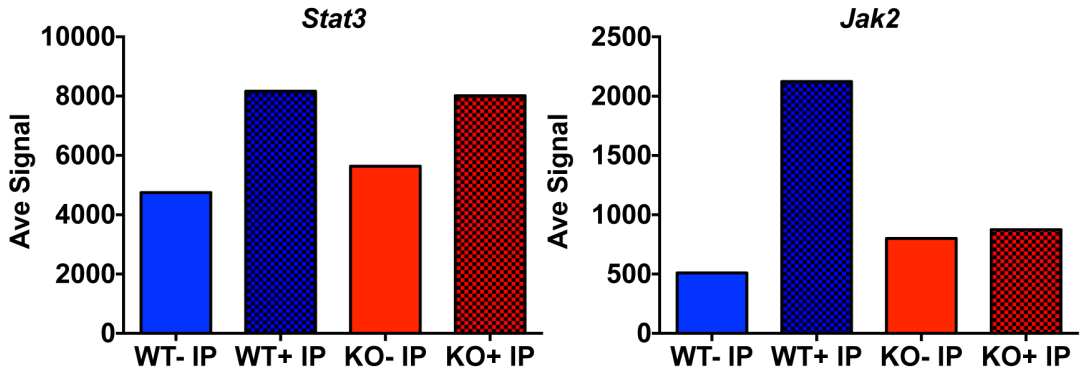

Figure 4-3 Legend: Leptin signaling pathway genes.
Transcripts for leptin receptor associated proteins, Janus kinase 2 (*Jak2)* and signal transducer and activator of transcription 3 (*Stat3). Jak2* is induced by leptin signaling in the wild-type mouse, but this is attenuated in the RIIβKO mouse.

Figure 4-4:

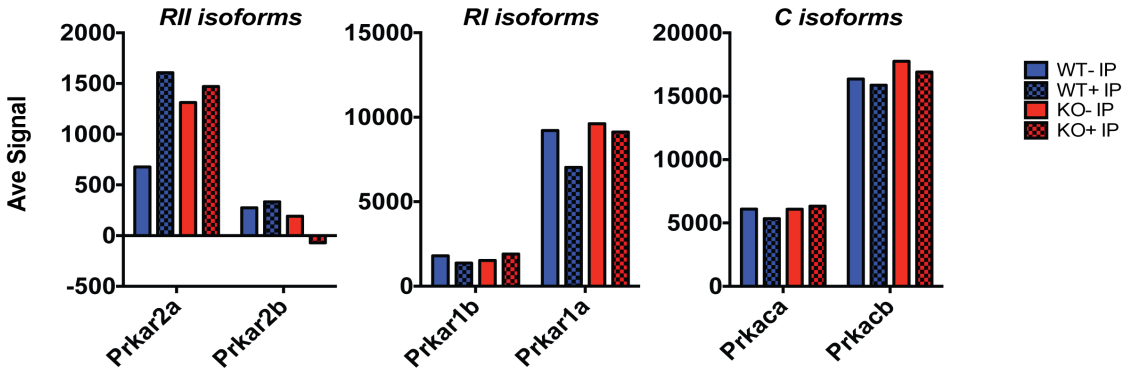

Figure 4-4 Legend: Compensation by other PKA isoforms for loss of RIIb not present at the message level.
Previous genetic deletion studies of PKA subunits found compensatory upregulation of other PKA isoforms to reduce aberrant activity. Microarray signal values for immunoprecipitated other PKA isoforms transcripts: protein kinase cAMP-dependent type II regulatory subunit alpha *(Prkar2a),* and beta (*Prkar2b*), type I regulatory subunit alpha (*Prkar1a*), and beta (*Prkar1b*) and catalytic subunits: protein kinase cAMP-dependent type catalytic subunit alpha (*Prkaca*) and beta (*Prkacb*).

Figure 4-5:

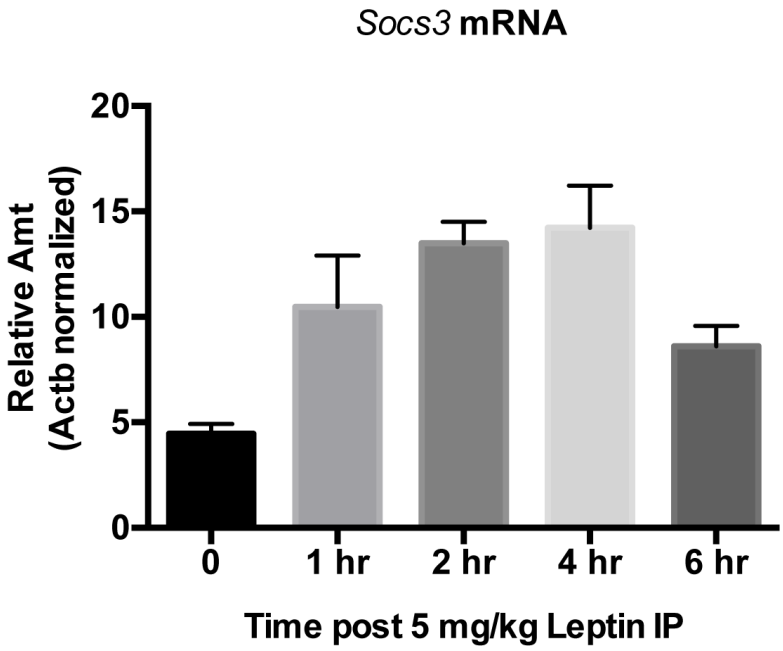

Figure 4-5 Legend: Induction of *Socs3* message post leptin injection.
A peripheral injection of leptin (5mg/kg) demonstrates maximum induction of suppressor of cytokine signaling 3 (*Socs3*), a gene product of leptin signaling, transcript by four hours, reduced by six hours.

Table 4-1: Induced in WT

IP WT/KO	SYMBOL	DEFINITION
5.06	*4832428D23Rik*	RIKEN cDNA 4832428D23 gene (4832428D23Rik), mRNA.
4.99	*Slc22a6*	Solute carrier family 22 (organic anion transporter), member 6 (Slc22a6), mRNA.
3.90	*Itm2a*	Integral membrane protein 2A (Itm2a), mRNA.
3.76	*Rph3al*	Rabphilin 3A-like (without C2 domains) (Rph3al), mRNA.
3.52	*LOC100044322*	Similar to UDP-glucose ceramide glucosyltransferase-like 1 (LOC100044322), mRNA.
3.13	*Traip*	TRAF-interacting protein (Traip), mRNA.
2.64	*Ndufab1*	NADH dehydrogenase (ubiquinone) 1, alpha/beta subcomplex, 1 (Ndufab1), mRNA.
2.48	*Tsc1*	Tuberous sclerosis 1 (Tsc1), mRNA.
2.28	*2610018G03Rik*	RIKEN cDNA 2610018G03 gene (2610018G03Rik), mRNA.
1.67	*Plekhm3*	Pleckstrin homology domain containing, family M, member 3 (Plekhm3), mRNA.
1.32	*Copg*	Coatomer protein complex, subunit gamma (Copg), transcript variant 2, mRNA.
1.21	*Flcn*	Folliculin (Flcn), mRNA.

Table 4-2: Fasting induction in RIIβKO vs. WT

IP KO/WT	SYMBOL	DEFINITION
10.50	*Ddx3y*	DEAD (Asp-Glu-Ala-Asp) box polypeptide 3, Y-linked (Ddx3y), mRNA.
5.66	*Neto1*	Neuropilin (NRP) and tolloid (TLL)-like 1 (Neto1), mRNA.
4.46	*LOC100047238*	PREDICTED: Similar to N-deacetylase/N-sulfotransferase 4 (LOC100047238), mRNA.
3.78	*Wnt5a*	Wingless-related MMTV integration site 5A (Wnt5a), mRNA.
3.72	*Asph*	Aspartate-beta-hydroxylase (Asph), transcript variant 2, mRNA.
3.71	*Zfp553*	Zinc finger protein 553 (Zfp553), mRNA.
3.71	*Rage*	Renal tumor antigen (Rage), mRNA.
3.57	*Znrf1*	Zinc and ring finger 1 (Znrf1), mRNA.
3.54	*Rusc2*	RUN and SH3 domain containing 2 (Rusc2), transcript variant 1, mRNA.
3.53	*Dars*	Aspartyl-tRNA synthetase (Dars), mRNA.
3.40	*Atp2a3*	ATPase, Ca++ transporting, ubiquitous (Atp2a3), mRNA.
3.35	*Fbxo42*	F-box protein 42 (Fbxo42), mRNA.
3.33	*Emd*	Emerin (Emd), mRNA.
3.28	*Vars2*	Valyl-tRNA synthetase 2, mitochondrial (putative) (Vars2), mRNA.
3.24	*Cdh13*	Cadherin 13 (Cdh13), mRNA.
3.22	*Tuba8*	Tubulin, alpha 8 (Tuba8), mRNA.
3.17	*Rbm11*	RNA binding motif protein 11 (Rbm11), mRNA.
3.16	*C630011I23*	Secisbp2l (SECIS binding protein 2-like), mRNA
3.13	*Atp13a4*	Mus musculus ATPase type 13A4 (Atp13a4), mRNA.
3.12	*Lrrc29*	Leucine rich repeat containing 29 (Lrrc29), mRNA.
3.11	*Adi1*	Acireductone dioxygenase 1 (Adi1), mRNA.
3.01	*5730453I16Rik*	RIKEN cDNA 5730453I16 gene (5730453I16Rik), mRNA.

Figure 4-6:

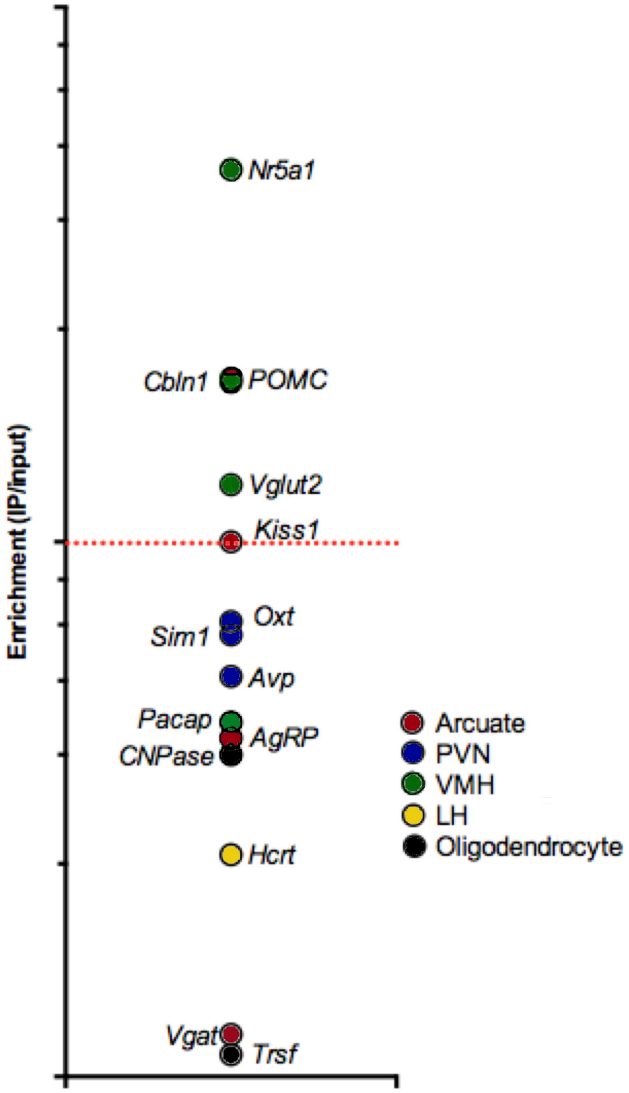

Figure 4-6 Legend: Ventromedial Hypothalamus Microarray Enrichment Check
Microarray results presented as enrichment (immunoprecipitated transcript signal/total hypothalamic transcript signal). Well-characterized genetic markers for hypothalamic regions or neuronal populations in the ventromedial hypothalamus (VMH), *Nr5a1*: Steroidogenic factor-1 nuclear receptor, *Pacap*: Pituitary adenylate cyclase activating peptide, *Cbln1*: Cerebellin-1; and, considering its predominant glutamatergic population, Glutamatergic, *Vglut*: Vesicular glutamate transporter-2 and gabaergic marker. Other hypothalamic gene markers demonstrated de-enrichement for lateral hypothalamus (LH), *Hrct*: Hypocretin/Orexin; paraventricular nucleus (PVN), *Oxt*: Oxytocin, *Sim1*: single-minded homolog 1, *Avp*: Arginine vasopressin; Arcuate nucleus (Arcuate): *AgRP*: Agouti-related peptide, *Pomc*: Pro-opiomelanocortin, *Kiss1*: Kisspeptin. Oligodendrocyte markers also demonstrated strong de-enrichment, *Cnp*: 2',3'-cyclic nucleotide 3' phosphodiesterase, *Trsf*; Transferrin, demonstrated de-enrichment or equivalent expression to background., *Vgat*: Vesicular GABA transporter, was highly de-enriched. *AgRP*, *Pomc*, and *Npy* demonstrate strong enrichment.

Figure 4-7

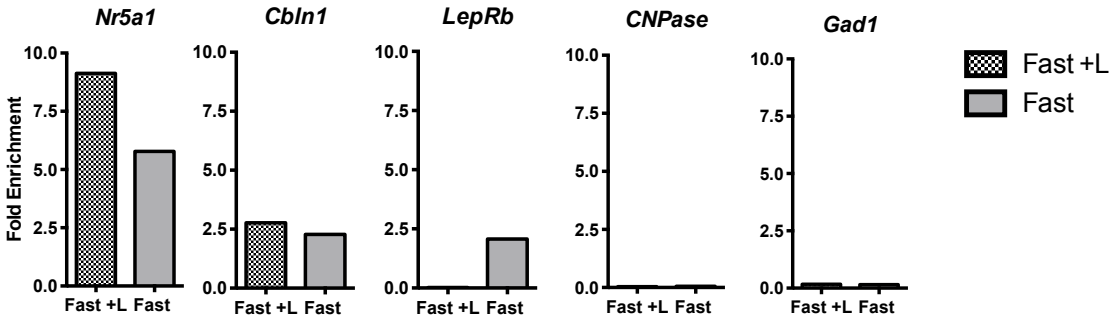

Figure 4-7 Legend: qRT-PCR validation of key genes from microarray
Validation of key genes was performed by qRT-PCR. Immunoprecipitated and Input samples were pooled to obscure sex differences. Key markers for the ventromedial hypothalamus included: *Nr5a1*: Steroidogenic Factor-1, *Cbln*: Cerebellin 1. Leptin receptor (*LepR*) expression was enriched in the VMH during the fast, but reduced post-six hours of leptin. De-enrichment markers included *CNPase*: 2',3'-cyclic nucleotide 3' phosphodiesterase and *Gad1*: glutamate decarboxylase 1.

Figure 4-8:

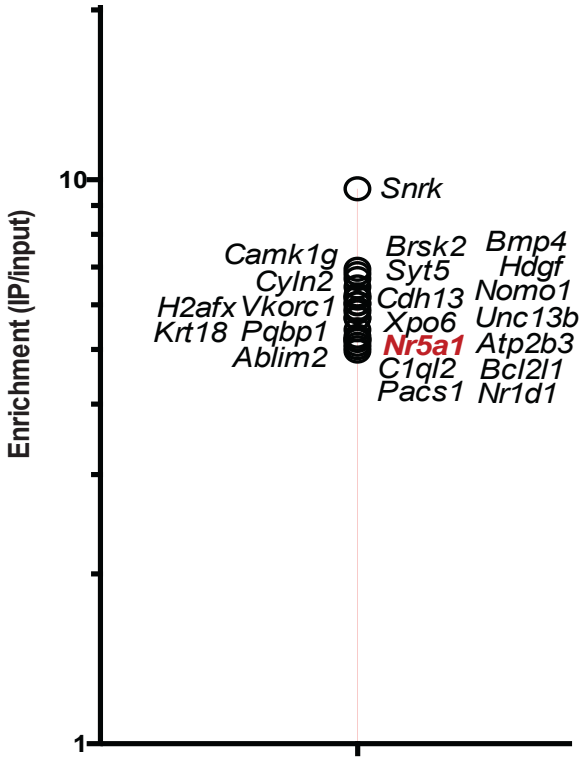

Figure 4-8 Legend: Microarray gene hits demonstrating equivalent enrichment to Nr5a1. Genes with comparable enrichment to Steroidogenic factor 1 (*Nr5a1/Sf1)* by microarray. (Enrichment = immunoprecipitated (IP) /Input signal after background subtraction and >200 Average signal in IP).

Table 4-3: Enrichment ratio of message demonstrating comparable enrichment to *Nr5a1/Sf1*.

IP/Input	*SYMBOL*	*DEFINITION*
9.64	*Snrk*	SNF related kinase
6.94	*Brsk2*	BR serine/threonine kinase 2
6.82	*Camk1g*	Calcium/calmodulin-dependent protein kinase I gamma
6.68	*Nomo1*	Nodal modulator 1
6.46	*Hdgf*	Hepatoma-derived growth factor
6.25	*Syt5*	Synaptotagmin V
6.19	*Bmp4*	Bone morphogenetic protein 4
6.17	*Cdh13*	Cadherin 13
6.04	*Unc13b*	Unc-13 homolog B (C. elegans)
5.90	*Vkorc1*	Vitamin K epoxide reductase complex, subunit 1
5.83	*Xpo6*	Exportin 6
5.69	*Pqbp1*	Polyglutamine binding protein 1
5.68	*C1ql2*	Complement component 1, q subcomponent-like 2
5.42	*Bcl2l1*	BCL2-like 1, nuclear gene encoding mitochondrial protein
5.41	*Dyrk3*	Dual-specificity tyrosine-(Y)-phosphorylation regulated kinase 3
5.28	*Atp2b3*	ATPase, Ca++ transporting, plasma membrane 3
5.22	*H2afx*	H2A histone family, member X
5.20	*Nr1d1*	Nuclear receptor subfamily 1, group D, member 1
5.11	*Krt18*	Keratin 18
4.97	*Nr5a1*	Nuclear receptor subfamily 5, group A, member 1 (SF1)

Figure 4-9:

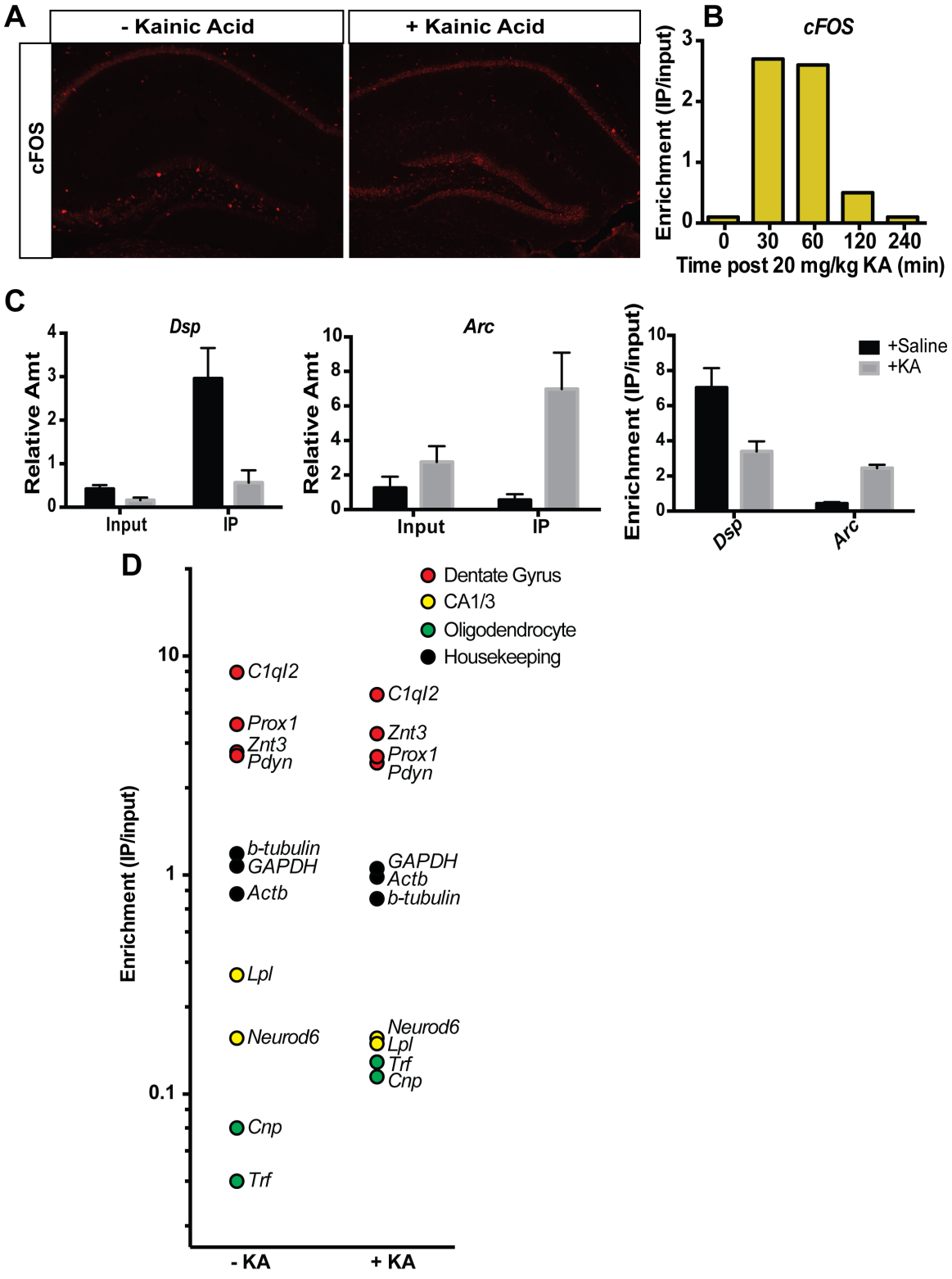
A
- Kainic Acid
+ Kainic Acid
cFOS
B
cFOS
Enrichment (IP/input)
Time post 20 mg/kg KA (min)
0
30
60
120
240
C
Dsp
Arc
Relative Amt
Input
IP
Enrichment (IP/input)
+Saline
+KA
D
Dentate Gyrus
CA1/3
Oligodendrocyte
Housekeeping
C1ql2
Prox1
Znt3
Pdyn
b-tubulin
GAPDH
Actb
Lpl
Neurod6
Cnp
Trf
- KA
+ KA

Figure 4-9 Legend: Validation of Kainic Acid model and specificity of RiboTag for DG neurons. (A) Immunohistochemistry of cFOS in hippocampal section from mice after four hours of either saline (control) or kainic acid (KA). (B) Lack of cFos gene expression at the four hour time-point does not correlate with lack of KA activity. cFOS is rapidly induced within the first hour and returned to baseline by four hours. (C) Validation of KA was performed by qRT-PCR validation of known gene expression changes following KA dosing at four hours: Desmoplakin (*Dsp*) expression is highly attenuated by KA and activity-regulated cytoskeleton-associated protein (Arc) is highly induced. (D) The specificity RiboTag expression in dentate granule neurons was validated by enrichment of dentate gyrus specific genes and de-enrichment of region CA1/3 and oligodendrocyte-specific transcripts. Enrichment = immunoprecipitated (IP) /Input signal after background subtraction and >200 Average signal in IP.

Figure 4-10:

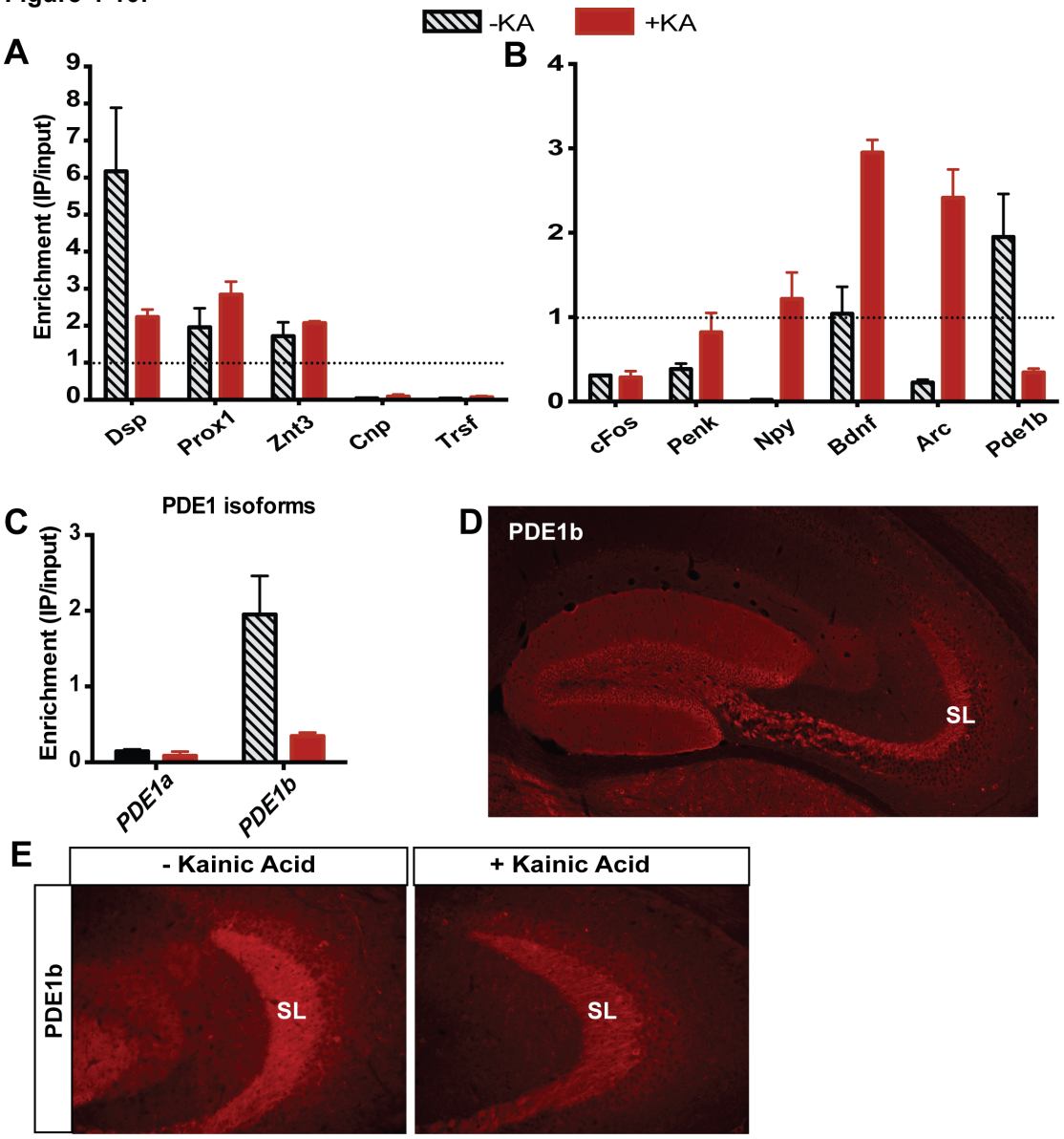

Figure 4-10

Legend: Validation of Microarray results by qRT-PCR. *PDE1b* is specific for dentate gyrus. (A-B) Specificity for dentate gyrus and kainic acid (KA)-induced transcript changes were validated by qRT-PCR. (C) *Pde1b* expression is highly reduced by KA at four hours. Immunohistochemical analysis of PDE1b protein level in the hippocampus found strong staining throughout dentate gyrus molecular layer and localization in stratum lucidum. Despite reduction of *Pde1b* expression at four hours post KA, reductions in PDE1b by immunohistochemistry at four hours were not found.
Desmplakin (*Dsp*), Proximal 1 (*Prox1*), solute carrier family 30, member 3 (*Znt3*), 2',3'-cyclic nucleotide 3' phosphodiesterase (*Cnp*), Transferrin (*Trsf*), FBJ osteosarcoma oncogene (*cFos*), Pro-enkephalin (*Penk*), Neuropeptide Y (*Npy*), Brain-derived neurotrophic factor (*Bdnf*), Activity-regulated cytoskeleton-associated protein (*Arc*).

CHAPTER 5: ADDITIONAL PHENOTYPES ASSOCIATED WITH LOSS OF AKAP7

5.1 INTRODUCTION

AKAP7 is highly expressed in the brain, with the short isoform being dominantly expressed (Jones et al. 2012). Considering this, it is not surprising that other neural regions were impacted by the loss of AKAP7. While investigating the AKAP7 KO mouse, additional phenotypes were discovered. This section provides documentation of these phenotypes. This chapter will describe each phenotype with an accompanying discussion and a general methods section.

5.2 PROJECT 1: AKAP7 ANCHORS PRESYNAPTIC PKA-RIIβ IN NEUROHYPOPHYSIS

Results

The pituitary is divided into three distinct structural and functional regions: the anterior, or adenohypophysis, the intermediate, and posterior, or neurohypophysis (NP). The NP is largely composed of axonal projections from magnocellular neurons originating in the paraventricular nucleus (PVH) and the supraoptic nucleus (SON) of the hypothalamus. Additional small support/glial cells, known as pituicytes, are also present. The two main neuropeptides released from the NP are arginine vasopressin (AVP) and oxytocin (OXT) (Dayanithi et al. 2008; Hatton 1988). The two hormones are released in response to changes in osmolarity, parturition, and lactation. We found strong AKAP7 and PKA-RIIβ staining localized to the NP. When AKAP7 is genetically deleted, PKA-RIIβ staining is lost in the NP and delocalized back to the soma of neurons in PVH (Figure 5-1A and B). We did not test for delocalization back to the SON.

Discussion

How the loss of AKAP7 impacts the function of AVP and OXT neurons within the NP is unknown. Functionally, the NP releases its two main neuropeptides, AVP and OXT, in a calcium-dependent manner, with excitation at the soma leading to increases in intracellular calcium, and, by mechanisms not fully understood, the release of neuropeptide-containing dense core vesicles (Hatton 1988). If AKAP7 is anchoring PKA near calcium channels and providing a functional potentiation of calcium influx, it is possible that AVP and OXT release might be impaired if potentiation is impaired. Further, the bulbous axons within the NP make numerous *en passant* contacts with the surrounding lamina, allowing for multiple sites of release that may be enhanced by frequency facilitation (Dayanithi et al. 2008) as each of these sites is capable of neuropeptide release upon excitation. It is possible that AKAP7's localization of PKA is important for proper facilitation of neuropeptide release. Performing pituitary function testing for AVP and OXT content in serum both basally and following water restriction could test deficits in peripheral effects of AKAP7 loss.

The AVP and OXT neurons demonstrate different firing patterns, with AVP-neurons displaying a consistent burst-firing pattern while OXT neurons fire far less frequently and do not exhibit burst firing (Dayanithi et al. 2008). This is an important point to consider when querying mechanistic changes due to

the loss of AKAP7, as the identity of the neurons in the NP expressing AKAP7 was not determined. However, the staining for AKAP7 was present equivalently across the NP and its role being unique to one population over the other seems unlikely. Electrophysiological testing would be required to determine alterations in firing patterns. Immunohistochemistry to validate co-localization of AVP and OXT with AKAP7 would be an obvious first experiment. Finally, although we typically focus on the peripheral effects of AVP and OXT release, central dysfunction of these neurons after loss of AKAP7 is also possible as PVH and SON axons extend numerous collateral projections prior to entering the NP. The role of these projections, whether or not they also release these key neuropeptides and their impact on other hypothalamic populations is unknown.

5.3 PROJECT 2: THE LOSS OF AKAP7 ENHANCES AND DYSREGULATES ACOUSTIC STARTLE RESPONSE

Introduction

Deficits in pattern separation, similar to those we observed in the AKAP7 KO (Figure 2-5 and 2-7), have been linked by multiple studies to deficits in adult neurogenesis within the hippocampal subgranular zone (Aimone et al. 2011). Although we found no deficit in adult hippocampal neurogenesis in the AKAP7 KO, we decided to test other behaviors linked to deficits in adult neurogenesis. One such behavior is the acoustic startle response (ASR), an intense and sudden contraction of facial and skeletal muscles in response to an acoustic stimulus (Koch 1999). Previous animal studies induced deficits in adult neurogenesis by irradiation and found that this significantly enhanced the ASR (Mickley & Ferguson 1989; Blaszczyk et al. 1999).

The ASR is a reflexive response mediated by a simple sensorimotor circuit beginning in cochlear nuclei which sends the signal on to the caudal pontine reticular nucleus, which then signals to the motor neurons (Koch & Schnitzler 1997). The ASR is proportional to the strength of the stimulus provided and testing includes a startle curve of a range of acoustic startles from null (70dB) to 120dB, considered the maximum. Despite the simplicity of the circuit underlying the ASR, it may be enhanced or attenuated in response to external stimuli, nicotine, ethanol (Lewis & Gould 2003), cocaine (Malave 2014), morphine (Meng et al. 2010), or by the release of stress hormones, including cortisol (Grillon et al. 2005) and corticotropin releasing hormone (Y. Lee & Davis 1997). Further, modulation provided by multiple neural regions including the hippocampus (Caine et al. 1992), amygdala (Jovanovic et al. 2010; Liang et al. 1992), cerebellum (Leaton & Supple 1986), and bed nucleus of the stria terminalis (Y. Lee & Davis 1997) have a significant effect on the ASR (Koch 1999).

Although most of the experiments underlying these findings have been performed in animals, human psychological disorders, including anxiety and early stage post-traumatic stress disorder, present with enhanced ASRs. In addition, certain psychological disorders are classically linked by a particular deficit in sensorimotor gating: prepulse inhibition (PPI). PPI is the brain's ability to inhibit a startle

response if it is preceded by a weaker pre-stimulus (pre-pulse).

We found interesting differences between the wild-type and AKAP7 KO animals in their responses to an acoustic startle, with enhanced and erratic responses at all stimuli presented.

Results

In testing the AKAP7 KO animals for baseline ASR and PPI, we found interesting differences between wildtype and AKAP7 KO mice. An intact baseline startle response curve was obtained to ensure each animal startled to the range of startle stimuli from null (75dB) to 120dB, as the background C57Bl6 strain has a high incidence of hearing loss(Bowl & Dawson 2015). The acoustic startle curve test demonstrated an enhanced and leftward shifted startle response for the AKAP7 KO animals (Figure 5-2C). Further, when dissecting the ten trials of startle curve presentation, the first and last startle curves were highly erratic in the AKAP7 KO, while the wild-type curves were remarkably similar (Figure 5-2A-B). Although the AKAP7 KO animals had normal pre-pulse inhibition (Figure 5-2D), their maximum acoustic startle response was significantly enhanced in the pre-pulse inhibition testing (Figure 5-2E), when the stimuli were presented pseudorandomly. However, when the stimuli were presented sequentially, as in the acoustic startle curves, the maximum startle response is equivalent, possibly presenting enhanced habituation to the acoustic startle.

Discussion

The AKAP7 KO presents a clearly dysfunctional reflexive response to startling acoustic stimuli. We found enhanced responses in the AKAP7KO at 80, 90, and 100dB stimuli that drew no response from wild-type mice. In addition, the acoustic startle curves of the AKAP7 KO mice were erratic in nature, presenting reduced responses at the highest stimuli (120dB) compared to the more moderate (105dB) stimuli. Finally, when viewing the responses of the KO at the maximal stimuli (120dB), how the stimuli were preceded may affect the response. Indeed, the stimuli were presented pseudo-randomly in the PPI testing and a significantly higher response was found. In the baseline acoustic startle curves, preceding stimuli were presented in sequential order and the ASR at 120dB was equivalent between wild-type and KO.

Although this study was initiated by considering the involvement of the hippocampus, it is not exactly clear how the hippocampus mechanistically modulates the ASR (Y. Lee & Davis 1997). Previous behavioral lesion studies of the amygdala found it also modulates the acoustic startle response in a manner similar to the AKAP7 KO phenotype. The neonatal lesion of the amygdala led to a loss of fear-potentiated startle. However, they also found enhancements in the startle response at all stimuli presented without fear potentiation, similar to our phenotype (Kazama et al. 2012). Another brain region that could be underlying this phenotype is the circuit between the lateral parabrachial nucleus (lPBN) and the amygdala. The circuit demonstrates presynaptic PKA-dependent LTP (Fourcaudot et al. 2008), similar to our dentate gyrus phenotype and the lPBN is implicated in freezing behavior (Han et al. 2015).

The discrepancy between the startle response at 120dB obtained during the baseline startle curve testing and the one obtained during the pre-pulse inhibition must be addressed. Theories behind habituation include the dual process theory (Groves & Thompson 1970), which describes the outcome of a response as the summation of enhancing and dampening, or sensitization and habituation. The presentation order of the stimuli differ between the two behavioral assays. In the PPI assay, the stimuli are presented in a pseudo-random order. In the startle curves, they are presented in increasing sequential order. By presenting the stimuli in increasing order, both first and last startle curves in the AKAP7 KO show a reduction in the startle response at 120dB compared to lower stimuli. It is possible the AKAP7 KO mice have enhanced habituation.

Finally, it is possible that the differences we are seeing in the ASR are due to a dysfunction in a peripheral system, possibly motor. AKAP7 was initially discovered in rabbit skeletal muscle associating with L-type calcium channels and regulated its potentiation by PKA (Gray et al. 1997). Although there were no deficits in rotarod performance between wild-type and KO in our AKAP7 dentate gyrus study (S Figure 2-4), the instantaneous nature of the startle response might be able to bring out deficits in skeletal muscle performance not seen in the Rotarod. To continue to investigate this phenotype would require dissection of cell populations possibly responsible for the phenotype.

5.4 EXPERIMENTAL PROCEDURES

Animal Care: Mice were given access to food pellets and water ad libitum, and maintained on a 12:12-hr light/dark cycle. For all experiments, the experimenter All procedures conformed to Animal Care and Use Committee of the University of Washington and NIH guidelines. For all experiments, the experimenter was blind to genotype and un-blinded after completing data analysis.

Immunohistochemistry and Imaging: Brains were fixed and processed for standard immunohistochemistry. Citrate buffer antigen retrieval was required to recover AKAP7 (Proteintech) immunostaining. PKA subunits were visualized using anti-PKA-RIIβ (BD Biosciences). Fluorescent secondary antibodies were utilized (Molecular Probes). Coverslips were mounted with ProLong Gold (Molecular Probes) or Fluoromount G (Electron Microscopy Sciences) with or without DAPI. Slides were imaged in the University of Washington Keck Microscopy Center on a Nikon Eclipse E600, Zeiss 510 META, or Leica SL confocal microscopes.

Behavioral Assays:

Acoustic Startle Response (ASR): Mice were handled for two days prior to the initiation of the assay. Following a 5-minute habituation period in the startle chamber, mice were presented with ten trials of acoustic startle increasing from null (75dB) to 120dB, 40 ms in duration with an intertrial interval of 30 sec for a total of 70 trials. Trials were averaged.

Pre-pulse-inhibition (PPI): On day 2, following a 5-min habituation period in the startle chamber, mice were presented with pseudo-random presentation of the maximal acoustic stimulus, 120dB, or one of 3 possible pre-pulse trials, 5, 10 or 15dB above background which preceded the acoustic stimulus by

100ms. Intertrial intervals were 20 sec. PPI was calculated as the percent reduction in maximum acoustic startle response.

Chapter 5: FIGURES

Figure 5-1:

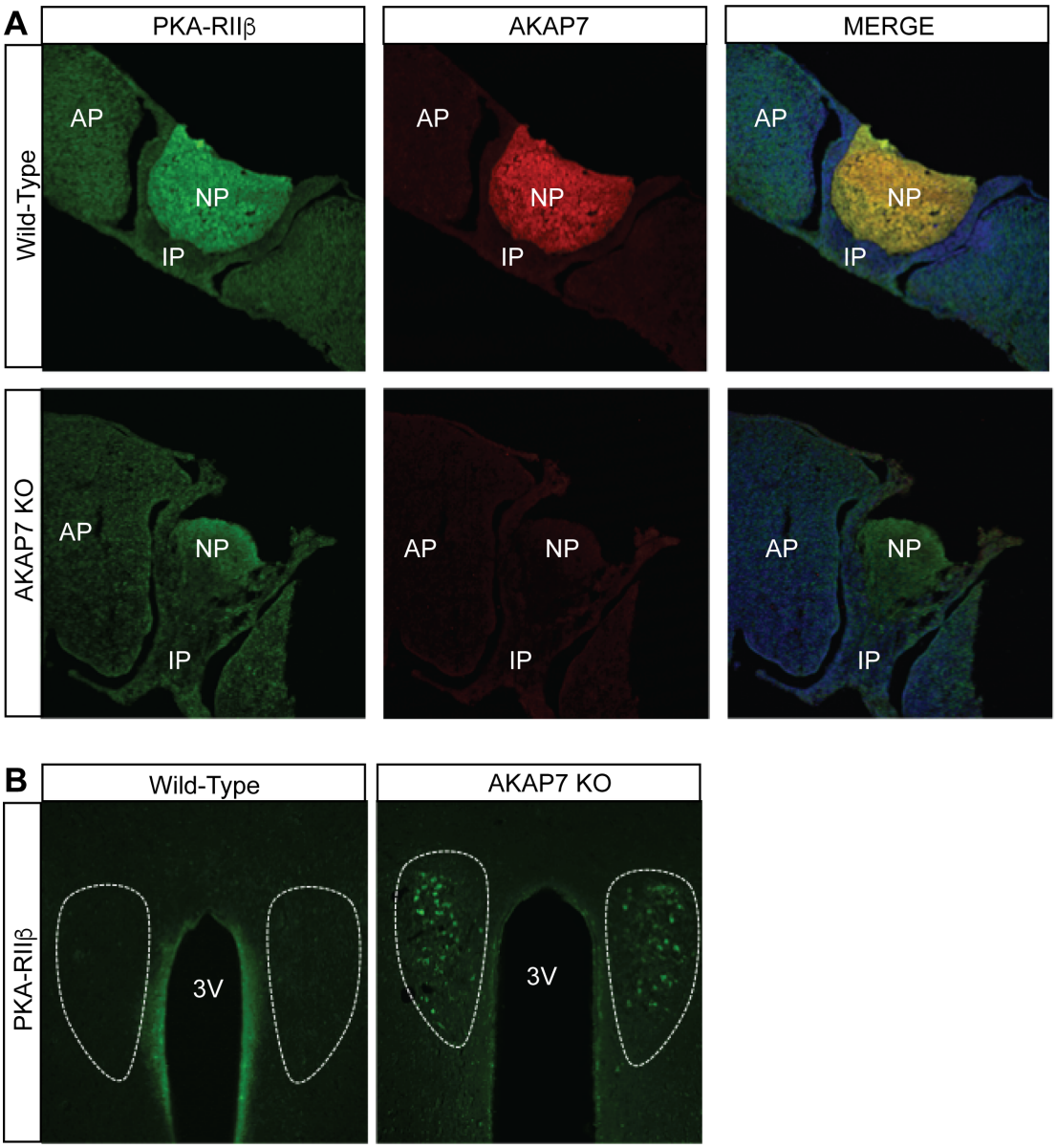

Figure 5-1 Legend: Akap7 Presynaptically Anchors PKA-RIIβ In Neurohypophysis
(A) Immunohistochemistry of pituitary sections using anti-PKA-RIIβ and anti-AKAP7 antibodies. Merged wild-type image shows the presence of both AKAP7 and PKA-RIIβ selectively localized to neurohypophysis. In the AKAP7 KO sections, AKAP7 staining and PKA-RIIβ staining are absent. (B) Immunohistochemisty of wild-type and AKAP7KO hypothalamic sections. Outline denotes paraventricular nucleus of the hypothalamus. AKAP7 KO sections demonstrate strong staining for delocalized PKA-RIIβ in soma of neurons localized to the paraventricular nucleus, not present in wild-type sections.

Figure 5-2:

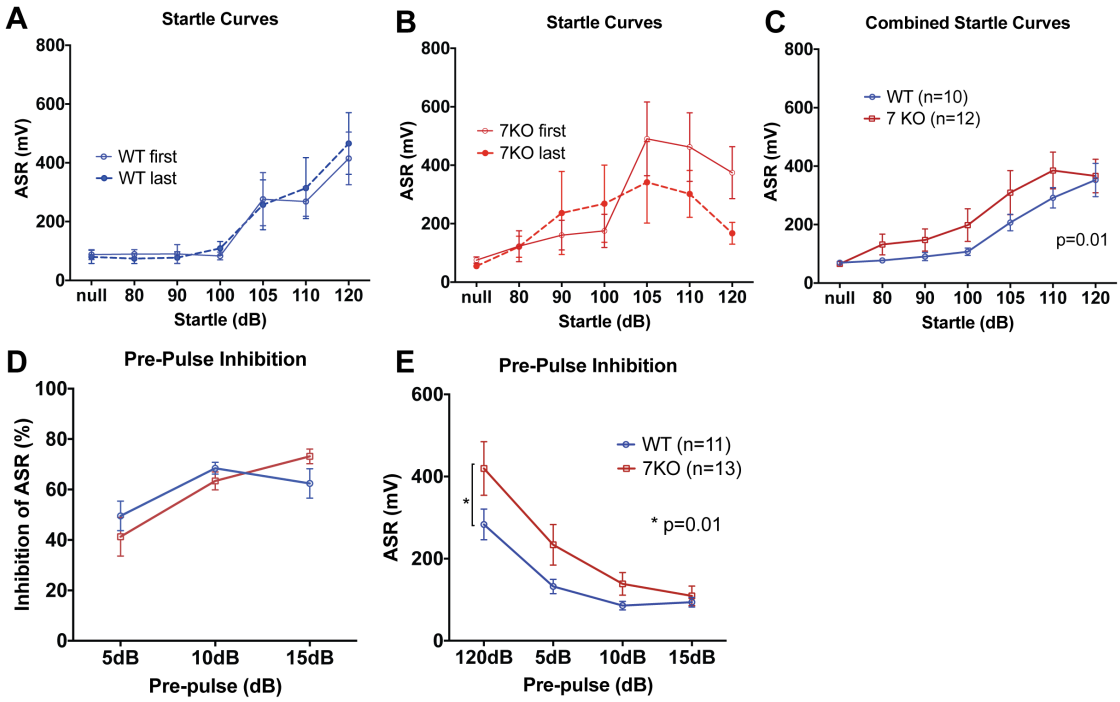

Figure 5-2 Legend: The Loss Of Akap7 Enhances Acoustic Startle Response
The basal acoustic startle response testing included the presentation of sequential acoustic startles for ten total trials. (A) First and tenth acoustic startle curves for the wild-type mice (n=10). (B) First and tenth acoustic startle curve for AKAP7 KO mice (n=13). (C) Averaged acoustic startle curves for wild-type and AKAP7 KO mice (wild-type, n=10; knockout n=13; 2-way ANOVA, p=0.01). (D) Percent inhibition achieved by presentation of a pre-pulse was comparable between wild-type and AKAP7 KO mice. Pre-pulse= 75dB + value on x-axis. (wild-type, n=10; knockout n=13). (E) Maximal acoustic startle (120dB) was significantly enhanced in AKAP7 KO mice. Pre-pulse inhibition testing included ten trials of pseudo-randomized presentation of 120dB acoustic startle with or without pseudo-randomized prepulse; pre-pulse= 75dB + value on x-axis (wild-type, n=10; knockout n=13; multiple t-tests, p=0.01 at 120dB acoustic startle without pre-pulse). Error bars represent s.e.m.

REFERENCES

Aaronson, D.S. & Horvath, C.M., 2002. A road map for those who don't know JAK-STAT. *Science*, 296(5573), pp.1653–1655.

Aimone, J.B., Deng, W. & Gage, F.H., 2011. Resolving New Memories: A Critical Look at the Dentate Gyrus, Adult Neurogenesis, and Pattern Separation. *Neuron*, 70(4), pp.589–596.

Altarejos, J.Y. & Montminy, M., 2011. CREB and the CRTC co-activators: sensors for hormonal and metabolic signals. *Nature Reviews Molecular Cell Biology*, 12(3), pp.141–151.

Altarejos, J.Y. et al., 2008. The Creb1 coactivator Crtc1 is required for energy balance and fertility. *Nature Medicine*, 14(10), pp.1112–1117.

Amieux, P.S. & McKnight, G.S., 2002. The essential role of RI alpha in the maintenance of regulated PKA activity. *Annals of the New York Academy of Sciences*, 968, pp.75–95.

Amieux, P.S. et al., 2002. Increased Basal cAMP-dependent Protein Kinase Activity Inhibits the Formation of Mesoderm-derived Structures in the Developing Mouse Embryo. *Journal of Biological Chemistry*, 277(30), pp.27294–27304.

Aponte, Y., Atasoy, D. & Sternson, S.M., 2010. AGRP neurons are sufficient to orchestrate feeding behavior rapidly and without training. *Nature Publishing Group*, 14(3), pp.351–356.

Atasoy, D. et al., 2012. Deconstruction of a neural circuit for hunger. *Nature*, 488(7410), pp.172–177. Available at: http://eutils.ncbi.nlm.nih.gov/entrez/eutils/elink.fcgi?dbfrom=pubmed&id=22801496&retmode=ref&cmd=prlinks.

Balland, E. & Cowley, M.A., 2015. New insights in leptin resistance mechanisms in mice. *Frontiers in Neuroendocrinology*, 39, pp.59–65.

Balthasar, N. et al., 2005. Divergence of Melanocortin Pathways in the Control of Food Intake and Energy Expenditure. *Cell*, 123(3), pp.493–505.

Balthasar, N. et al., 2004. Leptin receptor signaling in POMC neurons is required for normal body weight homeostasis. *Neuron*, 42(6), pp.983–991.

Banday, A.R. et al., 2013. Computational prediction and characterisation of ubiquitously expressed new splice variant of Prkaca gene in mouse. *Cell Biology International*, 37(7), pp.687–693.

Baver, S.B. et al., 2014. Leptin Modulates the Intrinsic Excitability of AgRP/NPY Neurons in the Arcuate Nucleus of the Hypothalamus. *Journal of Neuroscience*, 34(16), pp.5486–5496.

Beebe, S.J. et al., 1992. The C gamma subunit is a unique isozyme of the cAMP-dependent protein kinase. *The Journal of biological chemistry*, 267(35), pp.25505–25512.

Belgardt, B.F., Okamura, T. & Brüning, J.C., 2009. Hormone and glucose signalling in POMC and AgRP neurons. *The Journal of Physiology*, 587(22), pp.5305–5314.

Bender, A.T. & Beavo, J.A., 2006. Cyclic nucleotide phosphodiesterases: molecular regulation to clinical use. *Pharmacological reviews*, 58(3), pp.488–520.

Bengrine, A., Li, J. & Awayda, M.S., 2007. The A-kinase anchoring protein 15 regulates feedback inhibition of the epithelial Na+ channel. *The FASEB Journal*, 21(4), pp.1189–1201.

Beuschlein, F. et al., 2014. Constitutive Activation of PKA Catalytic Subunit in Adrenal Cushing's Syndrome. *New England Journal of Medicine*, 370(11), pp.1019–1028.

Blaszczyk, J. et al., 1999. Changes of the acoustic startle reflex in rats with radiation-induced hippocampal lesion. *Acta neurobiologiae experimentalis*, (59), pp.171–176.

Bowl, M.R. & Dawson, S.J., 2015. The mouse as a model for age-related hearing loss - a mini-review. *Gerontology*, 61(2), pp.149–157.

Brady, L.S. et al., 1990. Altered expression of hypothalamic neuropeptide mRNAs in food-restricted and food-deprived rats. *Neuroendocrinology*, 52(5), pp.441–447.

Brandon, E.P. et al., 1998. Defective motor behavior and neural gene expression in RIIbeta-protein kinase A mutant mice. *The Journal of neuroscience : the official journal of the Society for Neuroscience*, 18(10), pp.3639–3649.

Brandon, E.P. et al., 1995. Hippocampal long-term depression and depotentiation are defective in mice carrying a targeted disruption of the gene encoding the RI beta subunit of cAMP-dependent protein kinase. *Proceedings of the National Academy of Sciences of the United States of America*, 92(19), pp.8851–8855.

Brandon, E.P., Idzerda, R.L. & McKnight, G.S., 1997. PKA isoforms, neural pathways, and behaviour: making the connection. *Current Opinion in Neurobiology*, 7(3), pp.397–403.

Broberger, C. et al., 1998. The neuropeptide Y/agouti gene-related protein (AGRP) brain circuitry in normal, anorectic, and monosodium glutamate-treated mice. *Proceedings of the National Academy of Sciences of the United States of America*, 95(25), pp.15043–15048.

Brown, R.L. et al., 2003. AKAP7gamma is a nuclear RI-binding AKAP. *Biochemical and Biophysical Research Communications*, 306(2), pp.394–401.

Buettner, C. et al., 2008. Leptin controls adipose tissue lipogenesis via central, STAT3–independent mechanisms. *Nature Medicine*, 14(6), pp.667–675.

Burton, K.A. et al., 1999. Deletion of Type II Regulatory Subunit Delocalizes Protein Kinase A in Mouse Sperm without Affecting Motility or Fertilization. *JBC*, 274(34), pp.24131–24136.

Burton, K.A. et al., 1997. Type II regulatory subunits are not required for the anchoring-dependent modulation of Ca2+ channel activity by cAMP-dependent protein kinase. *Proceedings of the National Academy of Sciences of the United States of America*, 94(20), pp.11067–11072.

Cadd, G. & McKnight, G.S., 1989. Distinct patterns of cAMP-dependent protein kinase gene expression in mouse brain. *Neuron*, 3(1), pp.71–79.

Caine, S.B., Geyer, M.A. & Swerdlow, N.R., 1992. Hippocampal modulation of acoustic startle and prepulse inhibition in the rat. *Pharmacology, biochemistry, and behavior*, 43(4), pp.1201–1208.

Carr, D.W. et al., 1992. Localization of the cAMP-dependent protein kinase to the postsynaptic densities by A-kinase anchoring proteins. Characterization of AKAP 79. *The Journal of biological chemistry*, 267(24), pp.16816–16823.

Castillo, P.E., 2012. Presynaptic LTP and LTD of Excitatory and Inhibitory Synapses. *Cold Spring Harbor perspectives in biology*, 4(2), pp.–.

Catterall, W.A., 2010. Signaling complexes of voltage-gated sodium and calcium channels. *Neuroscience Letters*, 486(2), pp.107–116.

Ch'ng, T.H. et al., 2012. Activity-Dependent Transportof the Transcriptional Coactivator CRTC1 from Synapse to Nucleus. *Cell*, 150(1), pp.207–221.

Chen, Y. et al., 2015. Sensory Detection of Food Rapidly Modulates Arcuate Feeding Circuits. *Cell*, 160(5), pp.829–841.

Cheung, J. et al., 2015. Structural insights into mis-regulation of protein kinase A in human tumors. *Proceedings of the National Academy of Sciences*, 112(5), pp.1374–1379.

Choi, E.J. et al., 1993. The regulatory diversity of the mammalian adenylyl cyclases. *Current Opinion in Cell Biology*, 5(2), pp.269–273.

Clegg, C.H. et al., 1987. Inhibition of intracellular cAMP-dependent protein kinase using mutant genes of the regulatory type I subunit. *The Journal of biological chemistry*, 262(27), pp.13111–13119.

Clegg, C.H., Cadd, G.G. & McKnight, G.S., 1988. Genetic characterization of a brain-specific form of the type I regulatory subunit of cAMP-dependent protein kinase. *Proceedings of the National Academy of Sciences of the United States of America*, 85(11), pp.3703–3707.

Cone, R.D. & Simerly, R.B., 2011. Leptin Grows Up and Gets a Neural Network. *Neuron*, 71(1), pp.4–6.

Corbin, J.D. et al., 1977. Compartmentalization of adenosine 3':5'-monophosphate and adenosine 3“:5-”monophosphate-dependent protein kinase in heart tissue. *The Journal of biological chemistry*, 252(11), pp.3854–3861.

Cowley, M.A. et al., 2003. The distribution and mechanism of action of ghrelin in the CNS demonstrates a novel hypothalamic circuit regulating energy homeostasis. *Neuron*, 37(4), pp.649–661.

Cummings, D.E. et al., 1996. Genetically lean mice result from targeted disruption of the RII beta subunit of protein kinase A. *Nature*, 382(6592), pp.622–626.

Czyzyk, T.A. et al., 2008. Disruption of the RIIbeta subunit of PKA reverses the obesity syndrome of Agouti lethal yellow mice. *Proceedings of the National Academy of Sciences*, 105(1), pp.276–281.

Dayanithi, G., Viero, C. & Shibuya, I., 2008. The role of calcium in the action and release of vasopressin and oxytocin from CNS neurones/terminals to the heart. *Journal of physiology and pharmacology : an official journal of the Polish Physiological Society*, 59 Suppl 8, pp.7–26.

Di Benedetto, G. et al., 2008. Protein Kinase A Type I and Type II Define Distinct Intracellular Signaling Compartments. *Circulation Research*, 103(8), pp.836–844.

Djouder, N. et al., 2009. PKA phosphorylates and inactivates AMPK. *The EMBO journal*, 29(2), pp.1–13.

Dong, M. et al., 2006. c-fos modulates brain-derived neurotrophic factor mRNA expression in mouse hippocampal CA3 and dentate gyrus neurons. *Neuroscience Letters*, 400(1-2), pp.177–180.

Drane, L. et al., 2014. A transgenic mouse line for collecting ribosome-bound mRNA using the tetracycline transactivator system. *Frontiers in molecular neuroscience*, 7, p.82.

Eisenhaure, B., 2010. TetTag Technology. pp.1–1.

Ekstrand, M.I. et al., 2014. Molecular Profiling of Neurons Based on Connectivity. *Cell*, 157(5), pp.1230–1242.

Ellacott, K.L.J. et al., 2010. Perspective. *Cell Metabolism*, 12(1), pp.10–17.

Elmquist, J.K., Elias, C.F. & Saper, C.B., 1999. From lesions to leptin: hypothalamic control of food intake and body weight. *Neuron*, 22(2), pp.221–232.

Emmert-Buck, M.R. et al., 1996. Laser capture microdissection. *Science*, 274(5289), pp.998–1001.

Enns, L.C. et al., 2009. Attenuation of Age-Related Metabolic Dysfunction in Mice With a Targeted Disruption of the C Subunit of Protein Kinase A. *The Journals of Gerontology Series A: Biological Sciences and Medical Sciences*, 64A(12), pp.1221–1231.

Esseltine, J.L. & Scott, J.D., 2013. AKAP signaling complexes: pointing towards the next generation of therapeutic targets? *Trends in Pharmacological Sciences*, pp.1–8.

Fernandes, H.B. et al., 2015. Epac2 Mediates cAMP-Dependent Potentiation of Neurotransmission in the Hippocampus. *Journal of Neuroscience*, 35(16), pp.6544–6553.

Fourcaudot, E. et al., 2008. cAMP/PKA signaling and RIM1alpha mediate presynaptic LTP in the lateral amygdala. *Proceedings of the National Academy of Sciences*, 105(39), pp.15130–15135.

Fraser, I.D. & Scott, J.D., 1999. Modulation of ion channels: a “current” view of AKAPs. *Neuron*, 23(3), pp.423–426.

Fraser, I.D. et al., 1998. A novel lipid-anchored A-kinase Anchoring Protein facilitates cAMP-responsive membrane events. *The EMBO journal*, 17(8), pp.2261–2272.

Fukuda, M. et al., 2011. Short Article. *Cell Metabolism*, 13(3), pp.331–339.

Fulwyler, M.J., 1965. Electronic separation of biological cells by volume. *Science*, 150(3698), pp.910–911.

Gilbert, M.L. et al., 2015. Expression of a dominant negative PKA mutation in the kidney elicits a diabetes insipidus phenotype. *American Journal of Physiology - Renal Physiology*, 308(6), pp.F627–F638.

Gilbert, P.E., Kesner, R.P. & Lee, I., 2001. Dissociating hippocampal subregions: A double dissociation between dentate gyrus and CA1. *Hippocampus*, 11(6), pp.626–636.

Gray, P.C. et al., 1997. Identification of a 15-kDa cAMP-dependent protein kinase-anchoring protein associated with skeletal muscle L-type calcium channels. *The Journal of biological chemistry*, 272(10), pp.6297–6302.

Grillon, C. et al., 2005. Cortisol and DHEA-S are associated with startle potentiation during aversive conditioning in humans. *Psychopharmacology*, 186(3), pp.434–441.

Groves, P.M. & Thompson, R.F., 1970. Habituation: a dual-process theory. *Psychological review*.

GRUBER, B. et al., 1994. Differential Npy Messenger-Rna Expression in Granule Cells and Interneurons of the Rat Dentate Gyrus After Kainic Acid Injection. *Hippocampus*, 4(4), pp.474–482.

Gusho, E. et al., 2014. Murine AKAP7 has a 2“,5-”phosphodiesterase domain that can complement an inactive murine coronavirus ns2 gene. *mBio*, 5(4), pp.e01312–14.

Hall, D.D. et al., 2007. Critical Role of cAMP-Dependent Protein Kinase Anchoring to the L-Type Calcium Channel Ca v1.2 via A-Kinase Anchor Protein 150 in Neurons †. *Biochemistry*, 46(6), pp.1635–1646.

Han, S. et al., 2015. Elucidating an Affective Pain Circuit that Creates a Threat Memory. *Cell*, 162(2), pp.363–374.

Hatton, G.I., 1988. Pituicytes, glia and control of terminal secretion. *The Journal of experimental biology*, 139, pp.67–79.

Hehnly, H. et al., 2015. A mitotic kinase scaffold depleted in testicular seminomas impacts spindle orientation in germ line stem cells. *eLife*, 4, p.e09384.

Heiman, M. et al., 2008. A Translational Profiling Approach for the Molecular Characterization of CNS Cell Types. *Cell*, 135(4), pp.738–748.

Henry, F.E. et al., 2015. Cell type-specific transcriptomics of hypothalamic energy-sensing neuron responses to weight-loss. *eLife*, 4.

Hensch, T.K. et al., 1998. Comparison of plasticity in vivo and in vitro in the developing visual cortex of normal and protein kinase A RIbeta-deficient mice. *The Journal of neuroscience : the official journal*

of the Society for Neuroscience, 18(6), pp.2108–2117.

Hentges, S.T. et al., 2009. Proopiomelanocortin Expression in both GABA and Glutamate Neurons. *Journal of Neuroscience*, 29(43), pp.13684–13690.

Herberg, F.W. et al., 2000. Analysis of A-kinase anchoring protein (AKAP) interaction with protein kinase A (PKA) regulatory subunits: PKA isoform specificity in AKAP binding. *Journal of Molecular Biology*, 298(2), pp.329–339.

Herberg, F.W., Taylor, S.S. & Dostmann, W.R., 1996. Active site mutations define the pathway for the cooperative activation of cAMP-dependent protein kinase. *Biochemistry*, 35(9), pp.2934–2942.

Howe, D.G. et al., 2006. Inhibition of protein kinase A in murine enteric neurons causes lethal intestinal pseudo-obstruction. *Journal of Neurobiology*, 66(3), pp.256–272.

Howe, D.G., Wiley, J.C. & McKnight, G.S., 2002. Molecular and behavioral effects of a null mutation in all PKA C beta isoforms. *Molecular and cellular neurosciences*, 20(3), pp.515–524.

Huang, Y., Roelink, H. & McKnight, G.S., 2002. Protein kinase A deficiency causes axially localized neural tube defects in mice. *The Journal of biological chemistry*, 277(22), pp.19889–19896.

Huang, Y.Y. et al., 1995. A genetic test of the effects of mutations in PKA on mossy fiber LTP and its relation to spatial and contextual learning. *Cell*, 83(7), pp.1211–1222.

Hulme, J.T. et al., 2002. A novel leucine zipper targets AKAP15 and cyclic AMP-dependent protein kinase to the C terminus of the skeletal muscle Ca2+ channel and modulates its function. *The Journal of biological chemistry*, 277(6), pp.4079–4087.

Johannessen, M., Delghandi, M.P. & Moens, U., 2004. What turns CREB on? *Cellular Signalling*, 16(11), pp.1211–1227.

Johnson, D.A. et al., 2001. Dynamics of cAMP-Dependent Protein Kinase. *Chemical Reviews*, 101(8), pp.2243–2270.

Jones, B.W. et al., 2012. Cardiomyocytes from AKAP7 knockout mice respond normally to adrenergic stimulation. *Proceedings of the National Academy of Sciences of the United States of America*, 109(42), pp.17099–17104.

Jovanovic, T. et al., 2010. Fear potentiation is associated with hypothalamic-pituitary-adrenal axis function in PTSD. *Psychoneuroendocrinology*, 35(6), pp.846–857.

Kandel, E.R., Dudai, Y. & Mayford, M.R., 2014. The Molecular and Systems Biology of Memory. *Cell*, 157(1), pp.163–186.

Kasper, L.H. et al., 2010. CBP/p300 double null cells reveal effect of coactivator level and diversity on CREB transactivation. *The EMBO journal*, 29(21), pp.3660–3672.

Kazama, A.M. et al., 2012. Effects of neonatal amygdala lesions on fear learning, conditioned inhibition, and extinction in adult macaques. *Behavioral neuroscience*, 126(3), pp.392–403.

Keil, M.F., Briassoulis, G. & Stratakis, C.A., 2016. The Role of Protein Kinase A in Anxiety Behaviors. *Neuroendocrinology*.

Kim, K.-W. et al., 2011. SF-1 in the ventral medial hypothalamic nucleus: A key regulator of homeostasis. *Molecular and Cellular Endocrinology*, 336(1-2), pp.219–223.

Klöckener, T. et al., 2011. High-fat feeding promotes obesity via insulin receptor/PI3K-dependent inhibition of SF-1 VMH neurons. *Nature Publishing Group*, 14(7), pp.911–918.

Knight, Z.A. et al., 2012. Molecular Profiling of Activated Neurons by Phosphorylated Ribosome Capture. *Cell*, 151(5), pp.1126–1137.

Koch, M., 1999. The neurobiology of startle. *Progress in Neurobiology*, 59(2), pp.107–128.

Koch, M. & Schnitzler, H.U., 1997. The acoustic startle response in rats--circuits mediating evocation, inhibition and potentiation. *Behavioural Brain Research*, 89(1-2), pp.35–49.

Kohno, D. et al., 2003. Ghrelin directly interacts with neuropeptide-Y-containing neurons in the rat arcuate nucleus: Ca2+ signaling via protein kinase A and N-type channel-dependent mechanisms and cross-talk with leptin and orexin. *Diabetes*, 52(4), pp.948–956.

Kojima, M. et al., 1999. Ghrelin is a growth-hormone-releasing acylated peptide from stomach. *Nature*, 402(6762), pp.656–660.

Krashes, M.J. et al., 2014. An excitatory paraventricular nucleus to AgRP neuron circuit that drives hunger. *Nature*, 507(7491), pp.238–242. Available at: http://www.nature.com/doifinder/10.1038/nature12956.

Kritzer, M.D. et al., 2012. AKAPs: The architectural underpinnings of local cAMP signaling. *Journal of molecular and cellular cardiology*, 52(2), pp.351–358.

Kumon, A., Yamamura, H. & Nishizuka, Y., 1970. Mode of action of adenosine 3“,5-”cyclic phosphate on protein kinase from rat liver. *Biochemical and Biophysical Research Communications*, 41(5), pp.1290–1297.

Langeberg, L.K. & Scott, J.D., 2015. Signalling scaffolds and localorganization of cellular behaviour. *Nature Reviews Molecular Cell Biology*, 16(4), pp.232–244.

Leaton, R. & Supple, W., 1986. Cerebellar vermis: essential for long-term habituation of the acoustic startle response. *Science*, 232(4749), pp.513–515.

Lee, D.C. et al., 1983. Isolation of a cDNA clone for the type I regulatory subunit of bovine cAMP-dependent protein kinase. *Proceedings of the National Academy of Sciences of the United States of America*, 80(12), pp.3608–3612.

Lee, Y. & Davis, M., 1997. Role of the hippocampus, the bed nucleus of the stria terminalis, and the amygdala in the excitatory effect of corticotropin-releasing hormone on the acoustic startle reflex. *The Journal of neuroscience : the official journal of the Society for Neuroscience*, 17(16), pp.6434–6446.

Lein, E.S., Zhao, X. & Gage, F.H., 2004. Defining a molecular atlas of the hippocampus using DNA microarrays and high-throughput in situ hybridization. *Journal of Neuroscience*, 24(15), pp.3879–3889.

Lerner, R.G. et al., 2009. scientific report. *EMBO reports*, 10(10), pp.1175–1181.

Lewis, M.C. & Gould, T.J., 2003. Nicotine and ethanol enhancements of acoustic startle reflex are mediated in part by dopamine in C57BL/6J mice. *Pharmacology, biochemistry, and behavior*, 76(1), pp.179–186.

Liang, K.C. et al., 1992. Lesions of the central nucleus of the amygdala, but not the paraventricular

nucleus of the hypothalamus, block the excitatory effects of corticotropin-releasing factor on the acoustic startle reflex. *The Journal of neuroscience : the official journal of the Society for Neuroscience*, 12(6), pp.2313–2320.

Liu, T. et al., 2012. Fasting Activation of AgRP Neurons Requires NMDA Receptors and Involves Spinogenesis and Increased Excitatory Tone. *Neuron*, 73(3), pp.511–522.

López Soto, E.J. et al., 2015. Constitutive and ghrelin-dependent GHSR1a activation impairs CaV2.1 and CaV2.2 currents in hypothalamic neurons. *The Journal of general physiology*, 146(3), pp.205–219.

Malave, L.B., 2014. Caffeine's attenuation of cocaine-induced deficiency in acoustic startle response by inhibition of adenosine in a sex and dose dependent manner.

Mardis, E.R., 2008. The impact of next-generation sequencing technology on genetics. *Trends in Genetics*, 24(3), pp.133–141.

Margulies, M. et al., 2005. Genome sequencing in microfabricated high-density picolitre reactors. *Nature cell biology*.

Martin, B.R. et al., 2007. Isoform-Specific PKA Dynamics Revealed by Dye-Triggered Aggregation and DAKAP1α-Mediated Localization in Living Cells. *Chemistry & Biology*, 14(9), pp.1031–1042.

McHugh, T.J. et al., 2007. Dentate Gyrus NMDA Receptors Mediate Rapid Pattern Separation in the Hippocampal Network. *Science*, 317(5834), pp.94–99.

Mear, Y., Enjalbert, A. & Thirion, S., 2013. GHS-R1a constitutive activity and its physiological relevance. *Frontiers in neuroscience*, 7, p.87.

Meng, Z. et al., 2010. Chronic morphine treatment decreases acoustic startle response and prepulse inhibition in rats. *Science China Life Sciences*, 53(11), pp.1356–1360.

Mickley, G.A. & Ferguson, J.L., 1989. Enhanced acoustic startle responding in rats with radiation-induced hippocampal granule cell hypoplasia. *Experimental brain research. Experimentelle Hirnforschung. Expérimentation cérébrale*, 75(1), pp.28–34.

Murphy, J.G. et al., 2014. AKAP-Anchored PKA Maintains Neuronal L-type Calcium Channel Activity and NFAT Transcriptional Signaling. *CellReports*, 7(5), pp.1577–1588.

Nakajima, K.-I. et al., 2016. Gs-coupled GPCR signalling in AgRP neurons triggers sustained increase in food intake. *Nature communications*, 7, p.10268.

Newhall, K.J. et al., 2005. Deletion of the RIIβ-Subunit of Protein Kinase A Decreases Body Weight and Increases Energy Expenditure in the Obese, Leptin-Deficient ob/obMouse. *Molecular Endocrinology*, 19(4), pp.982–991.

Nolan, M.A., Babcock, D.F., et al., 2004. Sperm-specific protein kinase A catalytic subunit Calpha2 orchestrates cAMP signaling for male fertility. *Proceedings of the National Academy of Sciences of the United States of America*, 101(37), pp.13483–13488.

Nolan, M.A., Sikorski, M.A. & McKnight, G.S., 2004. The Role of Uncoupling Protein 1 in the Metabolism and Adiposity of RIIβ-Protein Kinase A-Deficient Mice. *Molecular Endocrinology*, 18(9), pp.2302–2311.

Nuñez, J.L. & McCarthy, M.M., 2007. Evidence for an extended duration of GABA-mediated excitation in the developing male versus female hippocampus. *Developmental Neurobiology*, 67(14), pp.1879–

1890.

Ogreid, D. et al., 1989. Comparison of the two classes of binding sites (A and B) of type I and type II cyclic-AMP-dependent protein kinases by using cyclic nucleotide analogs. *European journal of biochemistry / FEBS*, 181(1), pp.19–31.

Okuno, H., 2011. Regulation and function of immediate-early genes in the brain: Beyond neuronal activity markers. *Neuroscience Research*, 69(3), pp.175–186.

Oliveria, S.F., Dell'Acqua, M.L. & Sather, W.A., 2007. AKAP79/150 Anchoring of Calcineurin Controls Neuronal L-Type Ca2+ Channel Activity and Nuclear Signaling. *Neuron*, 55(2), pp.261–275.

Padilla, S.L. et al., 2016. Agouti-related peptide neural circuits mediate adaptive behaviors in the starved state. *Nature Neuroscience*, 19(5), pp.734–741.

Padilla, S.L., Carmody, J.S. & Zeltser, L.M., 2010. Pomc-expressing progenitors give rise to antagonistic neuronal populations in hypothalamic feeding circuits. *Nature Medicine*, 16(4), pp.403–405.

Patel, H.R. et al., 2006. Neuropeptide Y deficiency attenuates responses to fasting and high-fat diet in obesity-prone mice. *Diabetes*, 55(11), pp.3091–3098.

Pidoux, G. & Taskén, K., 2010. Specificity and spatial dynamics of protein kinase A signaling organized by A-kinase-anchoring proteins. *Journal of molecular endocrinology*, 44(5), pp.271–284.

Planas, J.V. et al., 1999. Mutation of the RII Subunit of Protein Kinase A Differentially Affects Lipolysis but Not Gene Induction in White Adipose Tissue. *JBC*, 274(51), pp.1–8.

Poisbeau, P. et al., 1999. Modulation of synaptic GABAA receptor function by PKA and PKC in adult hippocampal neurons. *The Journal of neuroscience : the official journal of the Society for Neuroscience*, 19(2), pp.674–683.

Qi, M. et al., 1996. Impaired hippocampal plasticity in mice lacking the Cbeta1 catalytic subunit of cAMP-dependent protein kinase. *Proceedings of the National Academy of Sciences of the United States of America*, 93(4), pp.1571–1576.

Rao, Y. et al., 2004. Reduced ocular dominance plasticity and long-term potentiation in the developing visual cortex of protein kinase A RIIalpha mutant mice. *European Journal of Neuroscience*, 20(3), pp.837–842.

Redden, J. et al., 2012. Spatiotemporal Regulation of PKC via Interactions with AKAP7 Isoforms. *Biochemical Journal*.

Reimann, E.M., Brostrom, C.O., et al., 1971. Separation of regulatory and catalytic subunits of the cyclic 3",5-"adenosine monophosphate-dependent protein kinase(s) of rabbit skeletal muscle. *Biochemical and Biophysical Research Communications*, 42(2), pp.187–194.

Reimann, E.M., Walsh, D.A. & Krebs, E.G., 1971. Purification and properties of rabbit skeletal muscle adenosine 3",5-"monophosphate-dependent protein kinases. *The Journal of biological chemistry*, 246(7), pp.1986–1995.

Reinton, N. et al., 1998. The gene encoding the C gamma catalytic subunit of cAMP-dependent protein kinase is a transcribed retroposon. *Genomics*, 49(2), pp.290–297.

Salmon, D. et al., 2012. Adenylate cyclases of Trypanosoma brucei inhibit the innate immune response of the host. *Science*, 337(6093), pp.463–466.

Sanz, E. et al., 2009. Cell-type-specific isolation of ribosome-associated mRNA from complex tissues. *Proceedings of the National Academy of Sciences of the United States of America*, 106(33), pp.13939–13944.

Sanz, E. et al., 2015. Fertility-Regulating Kiss1 Neurons Arise from Hypothalamic Pomc-Expressing Progenitors. *Journal of Neuroscience*, 35(14), pp.5549–5556.

Saper, C.B. & Lowell, B.B., 2014. The hypothalamus. *CURBIO*, 24(23), pp.R1111–R1116.

Schreyer, S.A. et al., 2001. Subunit of Protein Kinase APrevents Diet-Induced Insulin Resistance andDyslipidemia in Mice. *Diabetes*, 50, pp.1–8.

Schuster, S.C., 2007. Next-generation sequencing transforms today's biology. *Nature Methods*, 5(1), pp.16–18.

Scott, J.D. et al., 1987. The molecular cloning of a type II regulatory subunit of the cAMP-dependent protein kinase from rat skeletal muscle and mouse brain. *Proceedings of the National Academy of Sciences of the United States of America*, 84(15), pp.5192–5196.

Scott, J.D., Dessauer, C.W. & Taskén, K., 2013. Creating Order from Chaos: Cellular Regulation by Kinase Anchoring. *Annual Review of Pharmacology and Toxicology*, 53(1), pp.187–210.

Screaton, R.A. et al., 2004. The CREB coactivator TORC2 functions as a calcium- and cAMP-sensitive coincidence detector. *Cell*, 119(1), pp.61–74.

Segal, J.P., 2005. Use of Laser-Capture Microdissection for the Identification of Marker Genes for the Ventromedial Hypothalamic Nucleus. *Journal of Neuroscience*, 25(16), pp.4181–4188.

Seress, L. et al., 2009. Survival of mossy cells of the hippocampal dentate gyrus in humans with mesial temporal lobe epilepsy. *Journal of neurosurgery*, 111(6), pp.1237–1247.

Shi, G. et al., 2006. The Transcriptional Activity of CITED1 Is Regulated by Phosphorylation in a Cell Cycle-dependent Manner. *Journal of Biological Chemistry*, 281(37), pp.27426–27435.

Skålhegg, B.S. & Taskén, K., 2000. Specificity in the cAMP/PKA signaling pathway. Differential expression,regulation, and subcellular localization of subunits of PKA. *Frontiers in bioscience : a journal and virtual library*, 5, pp.D678–93.

Skålhegg, B.S. et al., 2002. Mutation of the Calpha subunit of PKA leads to growth retardation and sperm dysfunction. *Molecular endocrinology (Baltimore, Md.)*, 16(3), pp.630–639.

Sternson, S.M. & Atasoy, D., 2014. AGRP Neuron Circuits that Regulate Appetite. *Neuroendocrinology*.

Sutherland, E.W. & Rall, W.A., 1958. Fractionation and characterization of a cyclic adenine ribonucleotide formed by tissue particles. *The Journal of biological chemistry*, 232(2), pp.1077–1091.

Taskén, K. & Aandahl, E.M., 2004. Localized effects of cAMP mediated by distinct routes of protein kinase A. *Physiological Reviews*, 84(1), pp.137–167.

Tavalin, S.J. et al., 2002. Regulation of GluR1 by the A-kinase anchoring protein 79 (AKAP79) signaling complex shares properties with long-term depression. *Journal of Neuroscience*, 22(8), pp.3044–3051.

Taylor, S.S. et al., 2012. Assembly of allosteric macromolecular switches: lessons from PKA. *Nature Reviews Molecular Cell Biology*, 13(10), pp.646–658.

Taylor, S.S. et al., 2013. Biochimica et Biophysica Acta. *BBA - Proteins and Proteomics*, 1834(7), pp.1271–1278.

Taylor, S.S. et al., 2004. PKA: a portrait of protein kinase dynamics. *Biochimica et Biophysica Acta (BBA) - Proteins and Proteomics*, 1697(1-2), pp.259–269.

Terunuma, M., Pangalos, M.N. & Moss, S.J., 2010. Functional Modulation of GABAB Receptors by Protein Kinases and Receptor Trafficking. In *Advances in Pharmacology*. Advances in Pharmacology. Elsevier, pp. 113–122.

Theurkauf, W.E. & Vallee, R.B., 1982. Molecular characterization of the cAMP-dependent protein kinase bound to microtubule-associated protein 2. *The Journal of biological chemistry*, 257(6), pp.3284–3290.

Tian, L. et al., 2003. Leucine zipper domain targets cAMP-dependent protein kinase to mammalian BK channels. *The Journal of biological chemistry*, 278(10), pp.8669–8677.

Tibbs, V.C. et al., 1998. AKAP15 anchors cAMP-dependent protein kinase to brain sodium channels. *The Journal of biological chemistry*, 273(40), pp.25783–25788.

Tong, Q. et al., 2008. Synaptic release of GABA by AgRP neurons is required for normal regulation of energy balance. *Nature Neuroscience*, 11(9), pp.998–1000.

Townsend, K.L., Lorenzi, M.M. & Widmaier, E.P., 2008. High-fat diet-induced changes in body mass and hypothalamic gene expression in wild-type and leptin-deficient mice. *Endocrine*, 33(2), pp.176–188.

Trotter, K.W. et al., 1999. Alternative splicing regulates the subcellular localization of A-kinase anchoring protein 18 isoforms. *The Journal of cell biology*, 147(7), pp.1481–1492.

Tsien, J.Z., Huerta, P.T. & Tonegawa, S., 1996. The essential role of hippocampal CA1 NMDA receptor-dependent synaptic plasticity in spatial memory. *Cell*, 87(7), pp.1327–1338.

Ubersax, J.A. & Ferrell, J.E., Jr, 2007. Mechanisms of specificity in protein phosphorylation. *Nature Reviews Molecular Cell Biology*, 8(7), pp.530–541.

Uhler, M.D., Carmichael, D.F., et al., 1986. Isolation of cDNA clones coding for the catalytic subunit of mouse cAMP-dependent protein kinase. *Proceedings of the National Academy of Sciences of the United States of America*, 83(5), pp.1300–1304.

Uhler, M.D., Chrivia, J.C. & McKnight, G.S., 1986. Evidence for a second isoform of the catalytic subunit of cAMP-dependent protein kinase. *The Journal of biological chemistry*, 261(33), pp.15360–15363.

Valjent, E. et al., 2011. Haloperidol Regulates the State of Phosphorylation of Ribosomal Protein S6 via Activation of PKA and Phosphorylation of DARPP-32. *Neuropsychopharmacology*, 36(12), pp.2561–2570.

Varela, L. & Horvath, T.L., 2012. Leptin and insulin pathways in POMC and AgRP neurons that modulate energy balance and glucose homeostasis. *EMBO reports*, 13(12), pp.1079–1086.

Veugelers, M. et al., 2004. Comparative PRKAR1A genotype-phenotype analyses in humans with Carney complex and prkar1a haploinsufficient mice. *Proceedings of the National Academy of Sciences of the United States of America*, 101(39), pp.14222–14227.

Veyrac, A. et al., 2013. Zif268/egr1 gene controls the selection, maturation and functional integration of adult hippocampal newborn neurons by learning. *Proceedings of the National Academy of Sciences*,

110(17), pp.7062–7067.

Vong, L. et al., 2011. Leptin Action on GABAergic Neurons Prevents Obesity and Reduces Inhibitory Tone to POMC Neurons. *Neuron*, 71(1), pp.142–154.

Walsh, D.A., Perkins, J.P. & Krebs, E.G., 1968. An adenosine 3“, 5-”monophosphate-dependant protein kinase from rabbit skeletal muscle. *Journal of Biological Chemistry*.

Wang, Q. et al., 2014. Arcuate AgRP neurons mediate orexigenic and glucoregulatory actions of ghrelin. *Molecular Metabolism*, 3(1), pp.64–72.

Welch, E.J., Jones, B.W. & Scott, J.D., 2010. Networking with AKAPs: context-dependent regulation of anchored enzymes. *Molecular interventions*, 10(2), pp.86–97.

Williams, K.W. & Elmquist, J.K., 2012. From neuroanatomy to behavior: central integration of peripheral signals regulating feeding behavior. *Nature Publishing Group*, 15(10), pp.1350–1355.

Willis, B.S. et al., 2011. Cell-Type Specific Expression of a Dominant Negative PKA Mutation in Mice L. Mei, ed. *PLoS ONE*, 6(4), p.e18772.

Wittmann, G., Hrabovszky, E. & Lechan, R.M., 2013. Distinct glutamatergic and GABAergic subsets of hypothalamic pro-opiomelanocortin neurons revealed by in situ hybridization in male rats and mice. *The Journal of Comparative Neurology*, 521(14), pp.3287–3302.

Woodford, T.A. et al., 1989. Expression and characterization of mutant forms of the type I regulatory subunit of cAMP-dependent protein kinase. The effect of defective cAMP binding on holoenzyme activation. *The Journal of biological chemistry*, 264(22), pp.13321–13328.

Xing, J. et al., 1998. Nerve growth factor activates extracellular signal-regulated kinase and p38 mitogen-activated protein kinase pathways to stimulate CREB serine 133 phosphorylation. *Molecular and Cellular Biology*, 18(4), pp.1946–1955.

Xu, X. et al., 2012. Modular Genetic Control of Sexually Dimorphic Behaviors. *Cell*, 148(3), pp.596–607.

Yang, L. & McKnight, G.S., 2015. Hypothalamic PKA regulates leptin sensitivity and adiposity. *Nature communications*, 6, p.8237.

Yang, L. et al., 2014. Selective Expression of a Dominant-Negative Type I PKA Regulatory Subunit in Striatal Medium Spiny Neurons Impairs Gene Expression and Leads to Reduced Feeding and Locomotor Activity. *Journal of Neuroscience*, 34(14), pp.4896–4904.

Yin, Y., Li, Y. & Zhang, W., 2014. The Growth Hormone Secretagogue Receptor: Its Intracellular Signaling and Regulation. *International Journal of Molecular Sciences*, 15(3), pp.4837–4855.

Yu, B. et al., 2012. Protein Kinase A Alterations in Endocrine Tumors. *Hormone and Metabolic Research*, 44(10), pp.741–748.

Zhan, C. et al., 2013. Acute and Long-Term Suppression of Feeding Behavior by POMC Neurons in the Brainstem and Hypothalamus, Respectively. *Journal of Neuroscience*, 33(8), pp.3624–3632.

Zhang, E.E. et al., 2009. A Genome-wide RNAi Screenfor Modifiers of the Circadian Clock in Human Cells. *Cell*, 139(1), pp.199–210.

Zheng, R. et al., 2013. Deficiency of the RIIβ subunit of PKA affects locomotor activity and energy homeostasis in distinct neuronal populations. *Proceedings of the National Academy of Sciences*,

110(17), pp.E1631–40.